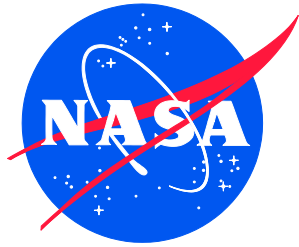


NASA/TM-20240002004
NESC-RP-21-01678



Agency Additive Manufacturing (AM) Certification Support Team (AACT) Risk Reduction – Safe Life Category: *Fracture Control Framework for Un-inspectable Fracture Critical AM Parts*

*Alison M. Park/NESC
Langley Research Center, Hampton, Virginia*

*William G. Tilson and Douglas N. Wells
Marshall Space Flight Center, Huntsville, Alabama*

*Christopher G. Lang
Langley Research Center, Hampton, Virginia*

*Christopher A. Kantzos
Glenn Research Center, Cleveland, Ohio*

NASA STI Program Report Series

Since its founding, NASA has been dedicated to the advancement of aeronautics and space science. The NASA scientific and technical information (STI) program plays a key part in helping NASA maintain this important role.

The NASA STI program operates under the auspices of the Agency Chief Information Officer. It collects, organizes, provides for archiving, and disseminates NASA's STI. The NASA STI program provides access to the NTRS Registered and its public interface, the NASA Technical Reports Server, thus providing one of the largest collections of aeronautical and space science STI in the world. Results are published in both non-NASA channels and by NASA in the NASA STI Report Series, which includes the following report types:

- **TECHNICAL PUBLICATION.** Reports of completed research or a major significant phase of research that present the results of NASA Programs and include extensive data or theoretical analysis. Includes compilations of significant scientific and technical data and information deemed to be of continuing reference value. NASA counterpart of peer-reviewed formal professional papers but has less stringent limitations on manuscript length and extent of graphic presentations.
- **TECHNICAL MEMORANDUM.** Scientific and technical findings that are preliminary or of specialized interest, e.g., quick release reports, working papers, and bibliographies that contain minimal annotation. Does not contain extensive analysis.
- **CONTRACTOR REPORT.** Scientific and technical findings by NASA-sponsored contractors and grantees.

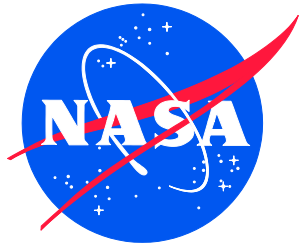
- **CONFERENCE PUBLICATION.** Collected papers from scientific and technical conferences, symposia, seminars, or other meetings sponsored or co-sponsored by NASA.
- **SPECIAL PUBLICATION.** Scientific, technical, or historical information from NASA programs, projects, and missions, often concerned with subjects having substantial public interest.
- **TECHNICAL TRANSLATION.** English-language translations of foreign scientific and technical material pertinent to NASA's mission.

Specialized services also include organizing and publishing research results, distributing specialized research announcements and feeds, providing information desk and personal search support, and enabling data exchange services.

For more information about the NASA STI program, see the following:

- Access the NASA STI program home page at <http://www.sti.nasa.gov>
- Help desk contact information: <https://www.sti.nasa.gov/sti-contact-form/> and select the "General" help request type.

NASA/TM-20240002004
NESC-RP-21-01678



Agency Additive Manufacturing (AM) Certification Support Team (AACT) Risk Reduction – Safe Life Category: *Fracture Control Framework for Un-inspectable Fracture Critical AM Parts*

*Alison M. Park/NESC
Langley Research Center, Hampton, Virginia*

*William G. Tilson and Douglas N. Wells
Marshall Space Flight Center, Huntsville, Alabama*

*Christopher G. Lang
Langley Research Center, Hampton, Virginia*

*Christopher A. Kantzos
Glenn Research Center, Cleveland, Ohio*

National Aeronautics and
Space Administration

Langley Research Center
Hampton, Virginia 23681-2199

February 2024

Acknowledgments

The final report authors would like to thank Chris Kantzos and Chris Lang for their contributions to this final report, Colton Katsarelis for providing metallographic images and examples of AM flaws, and Erin Lanigan for providing radiographic images.

The assessment team would also like to thank the following peer reviewers for their insightful comments: Andrew Glendening, Bryan McEnerney, Eric Burke, Joachim Beek, Elliott Cramer, Andrew Chaloupka, Joel Sills, Sara Wilson, and Michael Gorelik (Federal Aviation Administration (FAA)).

The use of trademarks or names of manufacturers in the report is for accurate reporting and does not constitute an official endorsement, either expressed or implied, of such products or manufacturers by the National Aeronautics and Space Administration.

Available from:

NASA STI Program / Mail Stop 148
NASA Langley Research Center
Hampton, VA 23681-2199
Fax: 757-864-6500



**NASA Engineering and Safety Center
Technical Assessment Report**

**Agency Additive Manufacturing (AM) Certification Support Team
(AACT) Risk Reduction – Safe Life Category: *Fracture Control*
*Framework for Un-inspectable Fracture Critical AM Parts***

TI-21-01678

**Alison Park, NESC Lead
Will Tilson, Technical Lead
January 18, 2024**

Report Approval and Revision History

NOTE: This document was approved at the January 18, 2024, NRB.

Approved: TIMMY WILSON  Digitally signed by TIMMY WILSON Date: 2024.02.09 16:30:47 -05'00'
NESCS Director

Version	Description of Revision	Office of Primary Responsibility	Effective Date
1.0	Initial Release	Alison M. Park, Deputy NASA Technical Fellow for Materials, LaRC	1/18/2024

Table of Contents

1.0	Notification and Authorization	6
2.0	Signatures	7
3.0	Team Members	8
3.1	Acknowledgments	8
4.0	Executive Summary	9
5.0	Assessment Plan	11
6.0	Problem Description and Background.....	11
6.1	Foundations of Fracture Control for AM Materials.....	13
6.2	AM Challenges to Traditional Fracture Control Approaches.....	14
6.2.1	Inspectability Challenges.....	15
6.2.2	Material Quality.....	16
6.2.3	Flaws.....	16
6.2.4	Heritage.....	17
6.3	Tools for Fracture Control for Un-inspectable AM Hardware	17
7.0	Analysis.....	18
7.1	Categorization of Flaws	19
7.1.1	Terminology.....	19
7.1.2	AM Flaw Categories.....	20
7.1.3	Integration with NASA-STD-6030.....	23
7.2	Use of AM Flaw Information in Fracture Control.....	24
7.2.1	Application of Flaw State to Fracture Control Assessments	24
7.2.2	AM Process Assessments	25
7.2.3	Component-Level Assessments.....	26
7.2.4	Risk Scenarios.....	28
7.2.5	Zone-based Assessment.....	31
7.2.6	Flaw Location Dependence.....	34
7.2.7	Implementation of Probabilistic Damage Tolerance Analysis (PDTA)	34
7.2.8	Role of Specialized Inspection Techniques	38
7.2.9	Design for Inspectability.....	41
7.2.10	Detected Flaws.....	41
7.2.11	Additional Considerations	42
7.2.12	Future Work.....	44
7.3	Flaw Types.....	47
7.3.1	Porosity	47
7.3.2	Other Flaw Types.....	50
7.3.3	Process Escape Flaws	52
7.4	Effect of AM Flaws	53
7.4.1	Material Properties.....	53
7.4.2	Tensile.....	53
7.4.3	Fracture Toughness.....	54
7.4.4	Creep.....	56
7.4.5	Fatigue	56
7.4.6	Fatigue Crack Growth Rate	57
7.4.7	Factors affecting Flaw Severity	57
7.5	Characterization Methods for AM Flaws	58
7.5.1	Nondestructive Evaluation (NDE).....	58
7.5.2	Destructive Methods	65
7.5.3	<i>In-situ</i> Monitoring.....	67

7.5.4	Flaw Descriptors and Distributions	69
7.6	Procedures for Representative Inherent Flaw State Characterization.....	70
7.6.1	Evolution of Flaw Population Data.....	71
7.6.2	Process Equivalence	71
7.6.3	Flaw Distributions.....	72
7.6.4	Influence of AM Build Thermal History on Flaw State	73
7.6.5	Thermal History Studies	74
7.7	Conclusions.....	77
8.0	Findings, Observations, and NESC Recommendations.....	78
8.1	Findings	78
8.2	Observations	79
8.3	NESC Recommendations	79
9.0	Alternate Technical Opinion(s)	79
10.0	Other Deliverables	79
11.0	Recommendations for the NASA Lessons Learned Database	79
12.0	Recommendations for NASA Standards, Specifications, Handbooks, and Procedures	80
13.0	Definition of Terms.....	80
14.0	Acronyms and Nomenclature List.....	82
15.0	References.....	83
	Appendix A. NASA 5 Challenge Geometries Final Report.....	89

List of Figures

Figure 6.0-1.	Examples of Engine Hardware Produced via AM.....	12
Figure 6.0-2.	Test Stand Failure of AM Combustion Chamber	12
Figure 7.1.2.2-1.	Notional AM Flaw Distributions.....	23
Figure 7.2.1-1.	Notional AM Flaw Distributions with CIFS Overlays	25
Figure 7.2.3-1.	Example of Component-level Assessments.....	27
Figure 7.2.4.1-1.	Illustration of Risk Scenario 1, where CIFS is within Inherent Flaw Distribution.....	29
Figure 7.2.4.2-1.	Illustration of Risk Scenario 2, where CIFS is below Detection Capability but above Inherent Flaw Distribution	30
Figure 7.2.4.3-1.	Illustration of Risk Scenario 3, with CIFS Larger Than Detection Limit	31
Figure 7.2.5-1.	Example of Part-zoning Approach	32
Figure 7.2.7-1.	Example Flaw Distributions of AM GrCop42 Manufactured with Different Specimen Thicknesses	34
Figure 7.2.7.3-1.	Example Results from DARWIN Tool.....	36
Figure 7.3.1.1-1.	Examples of Flaws in L-PBF Materials.....	48
Figure 7.3.1.1-2.	Collapsed LoF Flaw in L-PBF Alloy 718 Post Hot Isostatic Press	48
Figure 7.3.1.3-1.	L-PBF Alloy 718 showing Small Entrapped Gas Porosity.....	50
Figure 7.3.2.1-1.	Embedded Spatter Particle with Associated LoF Flaw	51
Figure 7.3.2.2-1.	Titanium Nitride Inclusion in L-PBF Alloy 718 produced at MSFC	51
Figure 7.3.3-1.	Residual Stress Crack in L-PBF Alloy 625 Component.....	52
Figure 7.3.3-2.	Skipped Layer Flaw	53
Figure 7.4.2-1.	Stress-strain Curves from L-PBF Alloy 718	54
Figure 7.4.3-1.	Fracture Toughness Tests from L-PBF Alloy 718 with Different Flaw States	55

Figure 7.4.3-2.	Fracture Surface of L-PBF Alloy 718 Specimen showing Significant Population of LoF Flaws.....	55
Figure 7.5.1.1-1.	Radiographs of L-PBF Test Specimens.....	59
Figure 7.5.1.2-1.	Example Source/Detector Arrangement for X-ray CT.....	60
Figure 7.5.1.2-2.	Cross-section Image taken from X-ray CT Scan of Part with Varying Flaw Sizes.....	60
Figure 7.5.1.2-3.	CT Renderings of Powder Particles and Section from Part.....	61
Figure 7.5.1.3-1.	Dye Penetrant Inspection on a BP-DED Part showing Several Flaws.....	62
Figure 7.5.1.4-1.	Ultrasonic Inspection Results for Two Locations in a Part.....	63
Figure 7.5.1.5-1.	Examples of Eddy Current Inspection of Holes on AM Component.....	64
Figure 7.5.1.5-2.	Schematic of Induced Electric Fields in Part With and without Flaw.....	64
Figure 7.5.1.6-1.	Processed Thermography Images of AM Component with Intentional Defects, Imaged using Pulsed Thermography and Stepped Thermography.....	65
Figure 7.5.2.1-1.	Optical Montage from Alloy 718 Sample Made with Reused Powder.....	66
Figure 7.5.2.1-2.	Optical Image of Alloy 718 Sample Made with Reused Powder.....	66
Figure 7.5.2.2-1.	3D Visualization of Pores Collected using 3D Serial Sectioning.....	67
Figure 7.5.3.1-1.	Image of Powder Spreading Defects Segmented using Machine Learning Application.....	68
Figure 7.5.3.2-1.	Images of Single Part where Layer is increasing in the Columns.....	69
Figure 7.6.3.1-1.	Variation in Flaw State for AM GRCo-42 Manufactured with Different Specimen Thicknesses.....	73
Figure 7.6.5-1.	Identification and Dimensions for Five Challenge Geometries.....	75
Figure 7.6.5-2.	Example Geometry showing Locations of High Pixel Intensity Registered to Build Geometry.....	76
Figure 7.6.5-3.	Comparison of Interpass Temperature for Cone from Thermal Imaging Camera and Process Simulation.....	76

List of Tables

Table 6.2-1.	Comparison of AM and Wrought Materials.....	14
Table 7.5.4.2-1.	Notable Features that can lead to Porosity Formation in LPBF.....	70

List of Appendices

Appendix A. NASA 5 Challenge Geometries Final Report.....	89
--	-----------

Technical Assessment Report

1.0 Notification and Authorization

The NASA Engineering and Safety Center (NESC) was requested to support the development of a governing philosophy to provide a consistent and systematic approach for fracture control certification of additive manufacturing (AM) hardware that cannot be reliably inspected. Such “un-inspectable” hardware represents fracture critical AM components that cannot be adequately screened for critical defects through post-production nondestructive evaluation (NDE), proof testing, or other methods. The overall goal of the assessment was to make progress toward a framework for general certification of un-inspectable fracture critical AM hardware and toward approaches for evaluating risks associated with these components.

Ms. Alison Park (Additive Manufacturing) was selected to lead this assessment, and Mr. Will Tilson (Damage Tolerance) was selected as the technical lead. Key stakeholders for this assessment include the Agency AM Certification Team (AACT), the NASA Fracture Control Methodology Panel, the Office of the Chief Engineer (OCE), the Office of Safety and Mission Assurance (OSMA), the Exploration Systems Development Mission Directorate, and the NESC.

2.0 Signatures

Submitted by: NESC Lead

Alison Park Digitally signed by Alison Park
Date: 2024.02.09 10:45:58
-08'00'

Ms. Alison M. Park

Significant Contributors:

William Tilson Digitally signed by William Tilson
Date: 2024.02.07 07:21:29 -06'00'

Mr. William G. Tilson

Signatories declare the findings, observations, and NESC recommendations compiled in the report are factually based from data extracted from program/project documents, contractor reports, and open literature, and/or generated from independently conducted tests, analyses, and inspections.

3.0 Team Members

Name	Discipline	Organization
Core Team		
Alison Park	NESC Lead	LaRC
Will Tilson	Technical Lead	MSFC
Doug Wells	AACT	MSFC
Brian West	AACT	MSFC
Sarah Luna	Materials & Processes (M&P)	JSC
Chris Kantzos	Damage Tolerance	GRC
Chris Williams	M&P	KSC
Chris Lang	Thermal	LaRC
Consultants		
Eric Burke	OSMA NDE	LaRC
Steve Gentz	NESC Chief Engineer for MSFC	MSFC
Ed Glaessgen	Materials	LaRC
Kausar Imtiaz	NASA Technical Fellow for Structures (former)	JSC, retired
Bryan McEnerney	NASA Technical Fellow for Materials	JPL
Bill Prosser	NASA Technical Fellow for NDE	LaRC
Rick Russell	NASA Technical Fellow for Materials (former)	KSC, retired
Business Management		
Lisa Hall	Program Analyst	LaRC/MTSO
Assessment Support		
Melissa Strickland	Project Coordinator	LaRC/AMA
Linda Burgess	Planning and Control Analyst	LaRC/AMA
Jonay Campbell	Technical Editor	LaRC/AS&M

3.1 Acknowledgments

The final report authors would like to thank Chris Kantzos and Chris Lang for their contributions to this final report, Colton Katsarelis for providing metallographic images and examples of AM flaws, and Erin Lanigan for providing radiographic images.

The assessment team would also like to thank the following peer reviewers for their insightful comments: Andrew Glendening, Bryan McEnerney, Eric Burke, Joachim Beek, Elliott Cramer, Andrew Chaloupka, Joel Sills, Sara Wilson, and Michael Gorelik (Federal Aviation Administration (FAA)).

4.0 Executive Summary

Additive manufacturing (AM) is increasingly being used to manufacture spaceflight hardware. Some of these components will be fracture critical, for which the consequences of part failures may be catastrophic. The design flexibility afforded by AM processes can result in designs that are highly efficient but contain regions that cannot be fully inspected for flaws and defects. Coupled with the lack of heritage experience with AM materials and the comparably high average occurrence rate of flaws that arise as a natural result of AM build operations, the risk of failure due to an undetected crack or defect associated with the use of fracture critical, un-inspectable AM components has the potential to be high.

A governing philosophy is needed to support the fracture control certification and risk acceptance for the use of fracture critical un-inspectable components in human-rated applications. Due to the inspection challenges, these components will not meet NASA fracture control requirements as written. Thus, for these parts to be certified, an alternative approach must be approved by the responsible Fracture Control Board, or an elevated risk must be accepted by the affected program. A consistent approach for assessing the risks associated with these components needs to be developed.

This report provides an initial framework for assessing un-inspectable fracture critical AM components. The approach focuses on understanding the flaws that are inherent to an AM process and those that arise because of an AM process escape. *Inherent flaws*, which are those flaws that are representative of the characterized nominal operation of a qualified AM process, should be understood and characterized for a particular AM process on a per-machine basis. Relevant characteristics of this inherent flaw distribution are compared with critical initial flaw sizes (CIFS) and nondestructive evaluation (NDE) detection capabilities to ensure tolerance of the design to inherent flaws. Then, the risk of the component containing a process escape flaw should be evaluated. *Process escape flaws* are those that are not part of the characterized nominal operation of the AM process and arise due to an error within the AM process.

Following discussion of the framework, this report provides additional information regarding inherent flaws. Several types of flaws common to the laser powder bed fusion (L-PBF) AM process category are discussed in the context of the inherent and process escape flaw categories. A brief discussion of the potential effects of inherent flaws on material properties is provided, followed by an overview of common NDE and destructive evaluation techniques and their capabilities for inherent flaw detection and characterization. Finally, approaches for appropriately evaluating the inherent flaw state in an AM process are discussed.

The L-PBF AM process category is currently the most advanced for production of critical hardware. Thus, the scope of the discussion in this report is focused on L-PBF processes, although many of the conclusions will be broadly applicable to other AM process categories (e.g., directed energy deposition (DED)).

In summary, fracture critical un-inspectable AM components require new approaches for evaluating risks for these components and assessing compliance with NASA requirements. These approaches must necessarily rely on material controls, including robust process development, material characterization, and process controls. A framework is presented for assessing risks associated with these components through understanding of the inherent flaw state of the AM material. However, additional development is needed to fully define approaches for flaw characterization and damage tolerance analysis for un-inspectable fracture critical AM components.

5.0 Assessment Plan

AM parts are being used by active and emerging NASA programs. These AM parts and processes need to be qualified and certified for safety and mission success. For human-rated applications, this hardware must meet NASA requirements for fracture control to minimize the risk associated with component failure due to an undetected crack or defect. Full inspection using standard NDE, which is commonly used for flaw and defect screening, is not possible for some of these parts. Typically, these inspections are used to confirm that no detrimental flaws are present in a critical part. A governing philosophy is needed to provide a consistent and systematic approach for fracture control certification of un-inspectable fracture critical AM parts.

The objectives of this assessment were to:

- Establish the foundation of a framework for the assessment of un-inspectable fracture critical AM components.
- Catalog the causes and characteristics of AM flaws inherent to the L-PBF process category.
- Assess methodologies for characterizing the distributions of these inherent flaws in AM materials.
- Investigate approaches for appropriately evaluating the inherent flaw state of a particular AM process.

Development of such a framework is a significant undertaking and should be approached incrementally without expectation of a “clean and final” answer. Continuing development of AM will potentially require further evolution and adaptation of the framework.

6.0 Problem Description and Background

AM is the process of joining materials to make parts from three-dimensional (3D) model data, usually layer upon layer, as opposed to subtractive manufacturing (e.g., milling) and formative manufacturing (e.g., forging) methodologies [ISO/ASTM 52900]. AM technologies enable a wide variety of previously impractical or impossible designs and are increasingly being adopted for spaceflight applications. Many spaceflight applications require manufacturing of small quantities of complex components, a use case for which AM is ideally suited.

AM techniques are increasingly being adopted for the most critical spaceflight applications. Recent examples include AM components on the E-2 engine manufactured by Launcher Space¹, structural and propulsive elements on the Terran R and Terran 1 rockets manufactured by Relativity Space², and next-generation RS-25 engines produced by Aerojet Rocketdyne, which will be used on the Space Launch System³. Figure 6.0-1 shows example engine hardware produced via AM. Like all materials, AM materials can contain flaws or defects that can cause hardware failures. An example is shown in Figure 6.0-2, where an AM combustion chamber failed during hot-fire testing at Marshall Space Flight Center (MSFC).

For human-rated NASA applications, critical components are subject to rigorous standards to ensure safety and performance. For example, NASA standard NASA-STD-5019, “Fracture

¹ <https://www.launcherspace.com/light>

² <https://www.relativityspace.com/rockets>

³ <https://www.rocket.com/space/liquid-engines/rs-25-engine>

Control Requirements for Spaceflight Hardware,” is intended to protect against component failure due to an undetected crack or defect. Components associated with a catastrophic consequence of failure due to the propagation of a crack or defect are classified as fracture critical and are subject to a range of requirements intended to reduce the risk of catastrophic failure due to the presence of an undetected crack or defect [NASA-STD-5019].



Figure 6.0-1. Examples of Engine Hardware Produced via AM [adapted from Gradl, 2022b]



Figure 6.0-2. Test Stand Failure of AM Combustion Chamber [Gradl, 2022b]

Standard approaches to fracture control rely on NDE to inspect for flaws or other material damage. These inspections are intended to assess the full surface and volume of the component.

The design flexibility afforded by AM processes allows for component designs that cannot be reliably inspected for flaws or material damage with the level of rigor required for fracture critical hardware. As a consequence, some AM hardware will contain regions that are un-inspectable relative to the inspection requirements defined in NASA-STD-5019 and NASA-STD-5009 “Nondestructive Evaluation Requirements for Fracture Critical Metallic Components.” For the purposes of this report, the category of un-inspectable AM hardware includes any component for which full volumetric and surface inspection is not possible, which includes both parts for which no inspection capability exists and parts for which some amount of inspection is possible.

Fracture critical AM components will be used on future NASA programs, and a subset of those components will fall into the un-inspectable category. Fracture control rationale and approaches to evaluating and approving the use of un-inspectable AM components must evolve and develop while maintaining the same level of technical rigor and safety focus established by standard fracture control approaches. Such un-inspectable AM components present a potentially significant risk to the missions on which they are used. This NESC assessment was undertaken to begin development of a consistent and systematic approach for certifying un-inspectable fracture critical AM components and evaluating risk associated with these components.

Numerous AM process categories exist, including DED, powder bed fusion, material extrusion, binder jetting, and others. In the context of fracture control, few AM process categories have reached sufficient maturity to produce fracture critical spaceflight components. These process categories are metallic L-PBF, metallic wire directed energy deposition (W-DED), and metallic blown powder directed energy deposition (BP-DED). The process category restrictions for fracture critical components are codified in NASA-STD-6030, “Additive Manufacturing Requirements for Spaceflight Systems.” Of these, L-PBF is currently the most advanced for production of critical hardware. Thus, the scope of the discussion in this report is focused on the L-PBF process category, although many of the conclusions will be broadly applicable to other AM processes categories (e.g., DED).

6.1 Foundations of Fracture Control for AM Materials

Fracture control activities are intended to increase the safety of human-rated spaceflight applications by reducing the risk associated with component failures due to undetected cracks, voids, material defects, or other flaws. Typically, fracture control is implemented through a combination of appropriate component design, strength and fracture mechanics analyses, material and component testing, and NDE. When integrated, these activities help demonstrate that a component is damage tolerant, which is a design concept whereby an undetected flaw or material damage is assumed to exist and is shown by analysis or test not to grow to failure during the period equal to the service life of the component times a safety factor.

At a fundamental level, the fracture control approach is supported by several underlying assumptions, including:

- Components are produced from quality materials controlled by government and/or aerospace specifications.
- Relevant material properties of component materials are well characterized or conservatively bounded.

- The loads and environments to which a component will be subjected are well understood or conservatively bounded.
- NDE inspections are reliable and have appropriate or conservatively bounded detection capabilities.

These foundational assumptions support the use of analysis- or test-based rationale for demonstrating damage tolerance of a component.

When used in NASA applications, AM materials are subject to the requirements in NASA-STD-6030. This standard defines requirements for establishing robust process controls on AM production processes and defining material property design values for AM materials. From a fracture control perspective, the assumptions regarding aerospace quality material are valid when an AM process is compliant with NASA-STD-6030 or an equivalent standard. Material properties for an AM process are defined when that data meet the requirements in NASA-STD-6030 for a material property suite (MPS), which is a collection of AM material property data from which design values and build acceptance criteria are derived and documented. Reliable NDE inspections are governed by NASA-STD-5009, which defines requirements for NDE inspections of metallic fracture critical hardware, including establishing appropriate flaw detection limits, inspector training, and standard flaw sizes for use in damage tolerance analysis. Together, these requirements support the use of AM materials in critical applications.

6.2 AM Challenges to Traditional Fracture Control Approaches

The unique nature of AM processes challenges the standard approach to fracture control in several ways. First, AM processes allow for part geometries that may or may not be inspectable using NDE, per NASA-STD-5009. Second, the quality of an AM material is process sensitive, and assumptions regarding material quality and performance cannot necessarily be transferred across AM processes, vendors, or from AM machine to AM machine. Third, AM processes generate relatively high counts of material flaws that may or may not be detrimental to the final component. Finally, AM materials lack the heritage associated with more traditional materials, especially for alloy systems designed specifically for AM. Table 6.2-1 summarizes each of these challenges compared with a more traditionally manufactured material.

Table 6.2-1. Comparison of AM and Wrought Materials

	Wrought Materials	AM Materials
Inspectability	Raw stock is commonly fully inspectable; parts generally have high inspectability.	Inspectability varies based on component geometry; inspection techniques still under development.
Material Quality	More consistent quality due to a limited number of dedicated production mills with extensive experience.	Highly process-dependent material quality; variation from AM system to AM system.
Flaws	Flaws are typically rare.	Flaws are intrinsic to the process and can vary with the level of process refinement and user experience.
Heritage	Decades of experience.	Little to no experience for critical applications; rapid technological development and evolution.

6.2.1 Inspectability Challenges

Inspectability for AM components presents a significant challenge to standard damage tolerance approaches. Standard deterministic damage tolerance approaches assume the presence of an initial flaw, position that assumed flaw at the worst-case location and orientation for the component, and analytically propagate that flaw through the expected service life. Few designs are tolerant to a flaw of arbitrary size and location, so NDE inspections are used to bound the plausible initial flaw size. Inspections performed within the requirements of NASA-STD-5009 demonstrate a capability to detect flaws above a specified size with a high level of certainty. Such inspections are said to be “quantitative,” in that the flaw size associated with the detection capability is known. Frequently, damage tolerance assessments use the flaw sizes associated with reliable NDE detection limits to set the initial flaw sizes in the analysis based on the logic that larger flaws would be reliably detected, thus preventing the part from going into service. This paradigm breaks down in the absence of reliable quantitative inspection techniques with established flaw detectability assessments.

AM components with complex geometries, integrated internal features, and unimproved surfaces can challenge standard NDE techniques (e.g., penetrant inspection, eddy current, radiography, and ultrasonic inspections) as defined by NASA-STD-5009. These same features can challenge special inspection techniques (e.g., X-ray computed tomography (CT)) [Todorov et al., 2014]. Penetrant inspections are limited to surfaces with line of sight and cannot be used for internal features. Additionally, as-built surfaces can trap penetrant fluid, leading to reduced detection reliability. Eddy current and ultrasonic inspections work best on smooth, continuous surfaces that must be accessible, which limits the applicability of these techniques for complex geometries. Radiography and CT are challenged by part size and material density, which limits X-ray penetration. Additionally, radiography is challenged by geometric complexity, which complicates the interpretation of the radiograph images. AM part designs with these challenging features result in regions within the component for which full NDE coverage at the reliability required by NASA-STD-5009 is not possible.

These AM-related challenges generally preclude application of the standard detectable flaw sizes established for these traditional NDE techniques (per NASA-STD-5009), and detection capability must be assessed. (Quantitative NDE for AM parts is considered “special NDE” per NASA-STD-6030 and NASA-STD-5009.) Full coverage by reliable, quantitative NDE inspections that meet NASA-STD-5009 requirements may not be possible for a particular AM component design.

While NDE inspections are often used to ensure flaws or damage are detected if they develop during component manufacturing, inspections play a critical role in assessing part safety and quality throughout a part’s lifetime. For aerospace components, inspections may be performed following proof or qualification testing, during development testing, or at intermediate points in the service life as part of life-extension efforts. Un-inspectable AM components will lead to challenges in each of these areas.

For un-inspectable AM hardware, the approach must necessarily shift from a focus on the flaws that can be detected (“What flaws *can be found* in the part?”) toward what flaws might be produced during the AM process (“What flaws *might* be in the part?”). Current AM process can generate high numbers of flaws even when the process is operating nominally, which complicates that approach. These flaws may or may not be detrimental to the component,

depending on their size, location, and morphology. Additionally, the service conditions and material properties of the component influence the sensitivity of the part to AM process-induced flaws. Understanding, assessing, and characterizing these inherent AM flaws is a key building block of fracture control rationale for un-inspectable AM components.

Traditional manufacturing techniques based on subtractive material machining and joining techniques are more accommodating to NDE, as critical areas (e.g., welds) are typically more accessible to NDE. However, inspectability challenges arise with components manufactured using traditional alloy product forms (wrought and cast), and alternative rationale has been developed for such cases. For components produced with wrought materials, alternative rationale often relies in part on intermediate raw stock inspections to verify material quality (e.g., ultrasonic inspection after plate rolling) and on manufacturing process controls intended to minimize defect occurrence. For castings, the risks are addressed through process controls and designs that reduce defect formation, leveraging heritage experience with casting defects and knowledge of solidification physics. For AM materials, the intermediate raw stock inspection is not possible, and the mechanisms for material flaw formation are not fully understood or controllable. New approaches will be needed for AM materials. Hardware manufactured using AM will have to rely on appropriately performed NDE screening to the extent possible and alternative rationale beyond that.

6.2.2 Material Quality

The assumption that components are manufactured from high-quality materials is foundational for fracture control. This assumption supports the use of handbook values for material properties and confidence that material specifications are sufficient to control material quality to an acceptable degree. This has generally been reasonable, as the use of traditional materials is supported by decades of user experience, industry-standard material specifications, and extensive material characterization. Additionally, many materials are produced by a small number of material producers with significant investment and expertise in that material's production.

In contrast, AM materials are process sensitive. The final material quality is dependent on the chemistry and morphology of the feedstock material, the operation of the AM machine, and the appropriate application of post-build processing steps (e.g., powder removal or heat treatment). These factors vary across AM processes, and controls may not transfer directly between AM systems. Coupled with the high number of individual AM systems and operators, the capability to consistently produce AM materials of aerospace quality has not been established across the AM industry, although some operators rise to this standard. These factors drive the process-dependent qualification approach defined by NASA-STD-6030.

6.2.3 Flaws

At the current state of development, AM processes generate some amount of material flaws during the production of a part. Although these flaws are typically small, the number of these flaws within a given volume of material can be orders of magnitude higher than for wrought materials. The frequency, size, and morphology of these flaws is affected by variability within the AM process, with aspects such as feedstock quality, build parameters, and built part geometries (e.g., thin walls) affecting the flaw state of the material. Additionally, AM processes have unique failure modes that can result in flaws (e.g., interactions between the energy source and combustion byproducts or errors in the powder deposition process). See Section 7.1 for further discussion of AM flaws.

6.2.4 Heritage

Traditional materials have been used in critical applications for decades, supported by robust characterization efforts to understand the performance of the material in demanding environments. For example, Alloy 718, a nickel-based superalloy used for high strength in high-temperature environments, was first developed in 1959. Alloy 718 comprised over 50% by weight of the Space Shuttle Main Engine (SSME). The use of Alloy 718 in the SSME was supported by extensive development to refine manufacturing processes, optimization of alloy chemistry and heat treatments, and characterization of material properties, particularly performance in gaseous hydrogen environments [Paulonis and Schirra, 2001; Jewett and Halchak, 1991].

As AM materials replace traditional materials in these critical applications, it will take time to develop the experience base that exists for traditional materials. AM has the advantage of high production rates that facilitate testing and using significant quantities of hardware, which could accelerate the learning curve for the use of these materials in critical applications. AM has the advantage of building upon existing knowledge of traditional alloy chemistries that are commonly used for AM (e.g., Alloy 718 and Ti-6Al-4V). However, as new alloy chemistries designed specifically for AM are developed, understanding of the material must be developed through characterization.

6.3 Tools for Fracture Control for Un-inspectable AM Hardware

Alternative inspection approaches are in development to alleviate challenges with AM component inspectability. Efforts are underway to develop reliable *in-situ* inspection approaches. *In-situ* monitoring encompasses the use of a variety of sensors and technologies to monitor the AM build and record the quality of the AM material as the build progresses. However, at present, *in-situ* inspection techniques are not sufficiently developed for use as reliable flaw detection compared with traditional NDE [Williams et al., 2023]. Additionally, specialized NDE methods (e.g., X-ray CT) are being evaluated for appropriate flaw detection capabilities in AM materials. However, standardized approaches for assessing probability of flaw detection have not been established for CT, although several methodologies have been proposed (e.g., inspections of intentionally introduced defects that are installed into inspection holders to mimic embedded flaws [Kim et al., 2019]). Methodologies based on representative image quality indicators (i.e., artifacts with intentionally introduced flaws) have been used to demonstrate detection capability for specific flaws in specific applications [ASTM E1817] but do not include a quantitative accounting of probability of detection. While *in-situ* monitoring and CT inspections do not currently meet the flaw detection reliability required by NASA standards, they provide useful engineering information that can be leveraged to develop rationale for un-inspectable AM components.

Another tool for assessing the risk associated with material flaws for damage-tolerant components is probabilistic damage tolerance analysis (PDTA). This method builds upon traditional deterministic damage tolerance analyses (e.g., crack propagation prediction using NASGRO®) by accounting for the distribution of potential flaw sizes and the probability of a flaw being present in the component. The analysis results in an overall component risk assessment in the form of a probability of failure as a function of service life. Because the probability of failure is strongly influenced by the distribution of potential initial flaw sizes, PDTA generally results in a less conservative but more representative evaluation of service life

in the presence of random flaws as compared with a deterministic approach that assumes all worst-case conditions occur simultaneously. PDTA differs from more traditional deterministic damage tolerance analysis in that results are given in the form of probabilities of failure rather than as a number of safe service lives.

Probabilistic assessments require one or more analysis variables to be provided in the form of statistical distributions. Typically, the random variable is a distribution of flaws characterized by flaw size and frequency of occurrence, which may be location specific. Other random variables might include loads or probabilities of detection from NDE inspections. PDTA approaches are used in several specialized applications. For example, PDTA has been successfully employed for aircraft certification, where rare material defects that can be below the NDE detection capability arise in fracture critical titanium engine components [Rotor Integrity Sub-Committee, 1997]. The probabilistic approach lends itself to the un-inspectable AM component problem by providing a means to bound the probability of failure associated with an undetected AM flaw.

7.0 Analysis

The scope of this NESC assessment included development of a framework for certifying un-inspectable fracture critical AM components and evaluating risk associated with these components. Fundamentally, the framework is based on understanding the relationships between the CIFS, the minimum detectable flaw size (when available), and the inherent flaw distribution. The relationships between these parameters define the risk scenario for a component and the appropriate approach toward a fracture control rationale. Scenarios where the CIFS is larger than the minimum detectable flaw size follow standard approaches. In scenarios where the CIFS cannot be reliably detected but is larger than the majority of the inherent flaw distribution, a damage tolerance rationale can be pursued using an appropriate analysis to evaluate the remaining risk due to process escape flaws and large inherent flaws. Finally, some components may have CIFS that are within the inherent flaw size distribution. In such cases, a damage tolerance rationale is not possible, and risk reduction activities should be considered.

The following topics are discussed in this section:

- Categorization of AM flaws, including discussions of relevant terminology and the introduction of two AM flaw categories: *inherent flaws* and *process escape flaws*.
- Discussion of approaches for integrating inherent flaw information into the development of fracture control rationales.
- Descriptions of common types of AM flaws in metallic L-PBF processes in the context of inherent and process escape flaw categorization.
- Discussion of the effects of common inherent flaws on the structural integrity of metallic L-PBF components.
- Assessments of inspection methodologies as they are applied to AM materials and their application to detecting and characterizing inherent flaws.
- Approaches for assessing the inherent flaw state of material produced by a metallic L-PBF process.

7.1 Categorization of Flaws

7.1.1 Terminology

Colloquially, many terms (e.g., *flaw*, *defect*, and *anomaly*) are used synonymously to refer to material imperfections or damage. For example, in the damage tolerance discipline generally and in NASA-STD-5019 specifically, *defect*, *flaw*, and *damage* are used interchangeably to mean a material condition that might adversely affect the structural integrity of a component. Certain segments of the aviation industry use *anomaly* to mean a flaw or defect. The AM community typically uses *flaw* and *defect* to describe imperfections in an AM material.

However, in the NDE discipline, *flaw* and *defect* have distinct meanings and implications. ASTM Standard E1316-22a “Standard Terminology for Nondestructive Examinations” [ASTM E1316] defines a *flaw* as an imperfection or discontinuity in a material. A *defect* is a flaw that is rejectable per a specified acceptance criterion. Thus, the term *defect* refers to a subset of flaws that have been assessed to be unacceptable for some application.

For the purposes of this report, the following terminology is adopted from ASTM E1316-22a:

- **Defect:** one or more flaws whose aggregate size, shape, orientation, location, or properties do not meet specified acceptance criteria and are rejectable.
- **Flaw:** an imperfection or discontinuity that may be detectable by NDE and is not necessarily rejectable.
- **Indication:** the response or evidence from a nondestructive examination.
- **Imperfection:** a departure of a quality characteristic from its intended condition.

Additionally, the following terms will be used in this report:

- **Anomaly:** a flaw.
- **Flaw state:** general term for the frequency, number, size distribution, and morphology of flaws generated in an AM material.

While *flaw* or *defect* can be used to refer to geometric or surface roughness features of AM components (e.g., out-of-tolerance features), the focus of this report will be on physical discontinuities in the material (e.g., voids, cracks, porosity, etc.) that have the potential to affect the structural integrity of a component.

Many AM flaws that arise as a natural aspect of the AM process are relatively small and, individually, are likely to have limited or no impact on structural integrity. Such flaws generally do not constitute a rejectable condition. Therefore, using the term *flaw* to refer to the generalized set of AM material imperfections, in alignment with ASTM E1316, is appropriate. This terminology serves to clarify that not all AM flaws represent a detrimental condition and, in many cases, AM material containing flaws will be acceptable for structural applications.

The distinction between flaws and defects in terms of acceptability for purpose represents a departure from the use of these terms in NASA standards documentation. For example, NASA-STD-5019A defines *flaw* as a defect for metallic materials and uses the two terms interchangeably throughout the document. NASA-STD-5009 does not use the term *defect*, preferring to use *flaw*. NASA-STD-6016C and NASA-STD-6030 use *flaw* and *defect* interchangeably. There is no consensus definition for *flaw* or *defect* within the AM community, but many AM users refer to these imperfections as *defects* in technical literature. The term *flaw*

was deliberately chosen for this report to avoid the connotation of unacceptability associated with the term *defect*. However, this choice means that use of the term *flaw* in this report must be read to mean imperfections that may or may not be impactful on the for-purpose use of an AM component, which may be incongruous to some readers.

F-1. Terminology related to AM material imperfections (e.g., *flaw*, *defect*, *anomaly*, etc.) is not consistent within the AM community, and NASA materials standards (e.g., NASA-STD-6016, NASA-STD-6030, etc.) do not distinguish between *flaws* and *defects*.

R-1. The OCE should update NASA-STD-6030 to adopt consistent terminologies for AM material imperfections. (*F-1*)

R-2. The OCE should update NASA-STD-5019, NASA-STD-5009, and NASA-STD-6016 to standardize terminology related to flaws, defects, and material imperfections. (*F-1*)

7.1.2 AM Flaw Categories

AM flaws arise from a multitude of conditions, some of which are currently unavoidable during the AM process. When assessing the damage tolerance of a particular component, it is useful to distinguish between those flaws that arise as a natural consequence of the AM build operation within its nominal conditions and those that do not. Within the scope of AM flaws, two flaw categories are proposed: *inherent flaws* and *process escape flaws*.

Defining two categories of AM flaws allows the development of targeted rationale to address the risks associated with each category. AM materials are expected to contain inherent flaws, likely at some relatively high average occurrence rate, and components produced via AM should be designed to account for this inherent flaw state. A different approach is required for process escape flaws, which might be mitigated by component inspections, AM process controls, and/or *in-situ* monitoring.

F-2. Distinguishing between AM flaws that arise during nominal AM build operation (i.e., inherent flaws) and those that occur due to a process escape (i.e., process escape flaws) allows for targeted approaches toward damage tolerance rationale for each flaw category.

7.1.2.1 Inherent Flaws

An *inherent flaw* is a flaw that is representative of the characterized nominal operation of a qualified AM process. Such flaws arise as a natural consequence of the operation of an in-control AM process and are currently unavoidable in nominally performing AM processes.

The inherent flaw definition implies that the nominal flaw state has been assessed through a characterization effort (see Section 7.6). Inherent flaws are expected to be common enough that direct characterization is possible. The characterization of the inherent flaw state should include assessment of flaw size and frequency of occurrence. Ideally, the characterization should account for influence factors that might affect flaw states, such as variations in thermal history, part geometry (thin walls), and/or changes to build parameters. This would include all aspects of the component processing leading to the final material condition, including hot isostatic pressing or surface finishing techniques (e.g., machining, chemical milling, etc.). Inherent flaw

characterization may include investigations of specific flaw types and of spatial variability of flaw state.

Appropriate characterization of the inherent flaw distribution is a critical part of the fracture control rationale. In addition to representing the nominal process, a robust inherent flaw state characterization should include material that reflects the edges of the “process box,” meaning that the flaw state characterization represents the process working at any state within its acceptable limits. This allows for conservative estimates of the inherent flaw state and improves coupon-to-part transferability by covering potential flaw state variations arising from a particular build geometry. However, characterization of the inherent flaw distribution is not intended to account for deficiencies in the development and qualification of an AM process. That is, AM processes used for spaceflight hardware should be controlled and capable of consistent material quality production. Inherent flaw characterization should not be used to justify the use of an inconsistent or poorly characterized AM process.

The definition of inherent flaw implies that the inherent flaw state is associated with a qualified AM process, so that a nominal material condition is defined and controlled. For NASA applications, *qualified* implies that the AM process meets the requirements of NASA-STD-6030 (or equivalent), including the associated process controls, traceability, and material characterization requirements. A qualified process is necessary for the definition of an inherent flaw state so that a consistent material quality baseline is established.

The baseline for flaw state is not likely to be consistent across all AM processes or materials. For example, some alloys may be more tolerant to inherent flaws than others, so the degree of process refinement necessary to obtain an acceptable flaw state may be reduced for such alloys. Additionally, tradeoffs between material performance, investment in process refinement, and build efficiency (speed) may result in AM material processes that produce different flaw states. For example, an AM process with high throughput at the expense of a relatively high inherent flaw density may be acceptable for components with minimal structural demand. The key is that the inherent flaw state is characterized to an appropriate degree and the process sufficiently controlled so that the material flaw state remains consistent.

Since the inherent flaw state represents the nominal material condition produced by an AM process, the effect of the inherent flaws on material properties (e.g., tensile, fatigue, thermal conductivity, etc.) is expected to be accounted for within the material characterization performed as part of process qualification. NASA AM requirements [NASA-STD-6030] are intended to ensure consistency in the AM process, which implies that properties are generated on material that is representative of the nominal process flaw state. Thus, it may be reasonably assumed that material characterization data, used to support component designs and assessments, reflect the impact of the inherent flaw state, particularly if influence factors that might cause variability between coupon-level material assessments and AM components have been appropriately considered.

7.1.2.2 Process Escape Flaws

Process escape flaws are flaws that are not representative of the characterized nominal operation of a qualified AM process. Process escape flaws are the result of a deviation from the nominal operation of the AM process.

The categorization of process escape flaws is not based on flaw type (i.e., keyhole pores or lack of fusion (LoF); see Section 7.3 for further discussion) but by the cause of those flaws. However, some flaw types might more commonly be inherent (e.g., small gas entrapped porosity), while other flaw types might only be formed as the result of a process escape (e.g., layer delamination). Some flaw types might be appropriately categorized in both the inherent and process escape flaw categories, depending on the flaw formation mechanism. For example, low densities of LoF flaws might be inherent, but periodic or large LoF flaws might be associated with some process escape. Flaws that are inherent for one AM process category may be considered process escape flaws in other AM process categories (e.g., L-PBF versus BP-DED).

Process escape flaws may or may not be rare. However, a controlled AM process is expected to have a low frequency of process escape flaws. The qualification state of processes that produce high frequencies of process escape flaws should be questioned and evaluated. Insufficiently developed or controlled AM processes may result in systematic process escapes that could lead to process escape flaws common enough to be captured by the inherent flaw distribution characterization. This should not be construed as a means to compensate for deficiencies in AM process control or process development. Such process escape flaws should be minimized to the degree possible.

Process escape flaws may be of any size. Flaw size is not a factor in the distinction between inherent and process escape flaws, although typical inherent flaws are anticipated to be relatively small. Process escape flaws would generally be expected to be larger than inherent flaws, but that is not a necessary condition. The size of some process escape flaws might be commensurate with common inherent flaw sizes. The size of the process escape flaw will be dependent on the process escape leading to the generation of the process escape flaw.

Process escape flaws may or may not be impactful on the structural integrity of an AM component (i.e., they are not necessarily defects). Process escape flaws may or may not be detectable.

The term *rogue flaw* is commonly used within the damage tolerance community to refer to an exceedingly rare flaw with severe impacts on the component's structural integrity. An alternative term was chosen for process escape flaws to avoid the connotation associated with rogue flaws regarding rarity and severity. Notional distributions of frequency of occurrence versus size for inherent and process escape flaws are shown in Figure 7.1.2.2-1. Measured flaw distributions may be different than these notional representations, based on the specifics of the AM process. For example, in a developed, controlled AM process, the occurrence rate of process escape flaws may be so low relative to the inherent flaw distribution as to be negligible when plotted on the same scale (as is done in the example). However, there is likely some trend between flaw count and flaw size for process escape flaws, although the specifics of these trends have not been determined. The relationships between these distributions, the critical flaw size for a particular component, and the size associated with the NDE detection capability will be discussed in later sections.

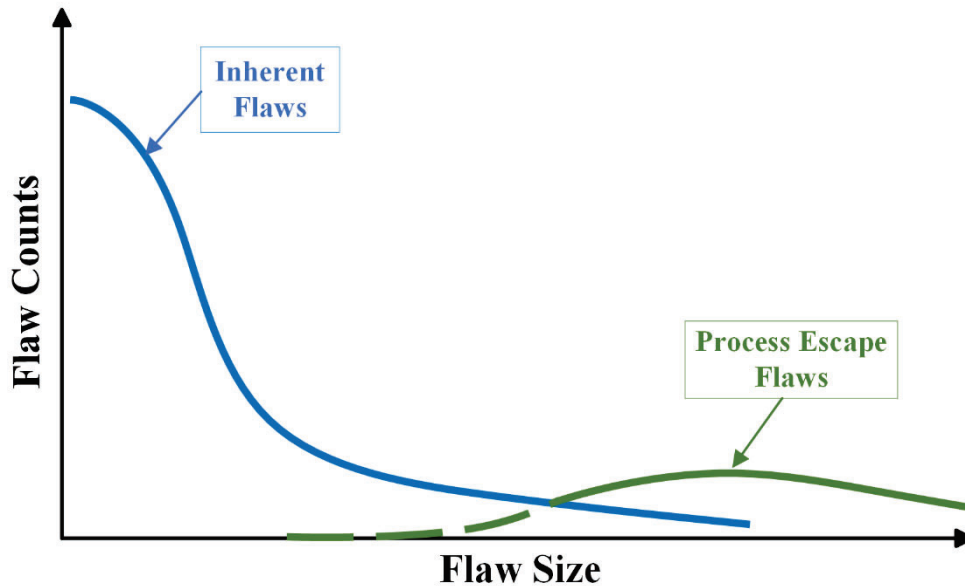


Figure 7.1.2.2-1. Notional AM Flaw Distributions

7.1.3 Integration with NASA-STD-6030

The concept of the inherent flaw state aligns with NASA-STD-6030 requirements regarding the characterization of material microstructures and the definition of microstructural acceptance criteria. NASA-STD-6030 requires that as-built materials be evaluated for detrimental flaws, with attention paid to consistency throughout the build area and thermal history extremes, among other influence factors. Inherent flaw characterization can be viewed as a refined version of the required foundational microstructural quality evaluations that define statistical metrics for the flaw state.

The baseline for the inherent flaw state characterization comes from the process qualification approach involved in developing a Qualified Material Process (QMP) per NASA-STD-6030, and the QMP provides a convenient location to document the inherent flaw state definition. Thus, the inherent flaw state can act as an additional material equivalence baseline for comparing AM processes for fracture critical components (e.g., for machine requalification or MPS registration).

To be useful for engineering assessments, the inherent flaw state for an AM process should be reasonably consistent and reflect the material state of the application, including all relevant post-processing (e.g., final heat treatments or surface finishing). This may require flaw state characterization to be performed on a per-machine basis. Consistency in the process supports applying the assumed inherent flaw state to develop component structural integrity rationale. The process control approaches established by NASA-STD-6030 (e.g., process definition in a QMP, statistical process control approaches through build witnessing and periodic sub-QMP builds, and component registration through first article inspections) help to ensure that flaw state metrics remain applicable for the AM process over time.

The AM process classification defined by NASA-STD-6030 reflects the need for inherent flaw state characterization. A comprehensive inherent flaw state characterization is not required for an AM process controlled by NASA-STD-6030. However, the inherent flaw state characterization may support the rationale for fracture critical components, which correspond to Class A AM

components (i.e., associated with a catastrophic consequence of failure) per NASA-STD-6030. Consequently, flaw state characterization would be performed for QMP-A processes in the interest of supporting rationale for fracture control requirements. An inherent flaw state characterization may support rationale for Class B (i.e., non-catastrophic consequence of failure) components, but the level of rigor required in such a scenario would likely be reduced commensurate with the reduced criticality of these components. Inherent flaw state characterization is likely not necessary for Class C or exempt AM components.

7.2 Use of AM Flaw Information in Fracture Control

Un-inspectable AM parts must rely on characterized inherent flaw information to support fracture control rationale. The flaw state generated by the AM process is compared with the structural integrity requirements for the component. Such an approach represents one partial solution to the un-inspectable AM component problem. Importantly, an approach based on characterized inherent flaw populations should not be viewed as a replacement for standard fracture control activities bounded by appropriate NDE inspections. There is no expectation that the approach outlined will meet the intent of existing fracture control requirements. Instead, the goal is to understand the fracture control-related risks associated with un-inspectable AM components and reduce those risks to a tolerable level.

7.2.1 Application of Flaw State to Fracture Control Assessments

Comparisons between the inherent flaw distribution generated by the AM process, the CIFS established by the structural demand on the component, and the NDE detection capability (as applicable) provide a foundation for rationale for un-inspectable fracture critical AM components. As an illustration, assume a complex AM component is produced using a qualified AM process. During development of the part inspection plan, it is discovered that the part cannot be reliably inspected. A flaw state characterization study (see Section 7.6) is performed to characterize the inherent flaw state of the AM process (on that machine), if such a study were not performed as part of the AM process qualification. As part of the fracture control rationale, critical locations in the component are identified, and, for each location, fracture analysis is performed to determine a CIFS. Comparisons between the NDE detection capability, the CIFS, and the expected inherent flaw state define the subsequent approach.

At one extreme, the majority of the inherent flaw population might be appropriately deemed non-relevant for parts with a CIFS that is sufficiently above the inherent flaw distribution, as illustrated by the “Large CIFS” line in Figure 7.2.1-1. In such cases, the effects of inherent flaws could be appropriately considered to have been accounted for in the property characterization. In such a scenario, analysis for structural margins would be sufficient to show robustness against inherent flaws, although checks for damage tolerance against the extreme value flaw sizes represented by the inherent distribution are appropriate. Process escape flaws for all scenarios must be evaluated.

At the other extreme, if the calculated CIFS is within the inherent flaw distribution (the “Small CIFS” line in Figure 7.2.1-1), then a significant risk arises as these inherent flaws are likely to be present. Such a scenario will not result in a robust flight rationale for a fracture critical component, and a design change to increase the CIFS or further refinement to the AM material process to reduce the inherent flaw size would be necessary.

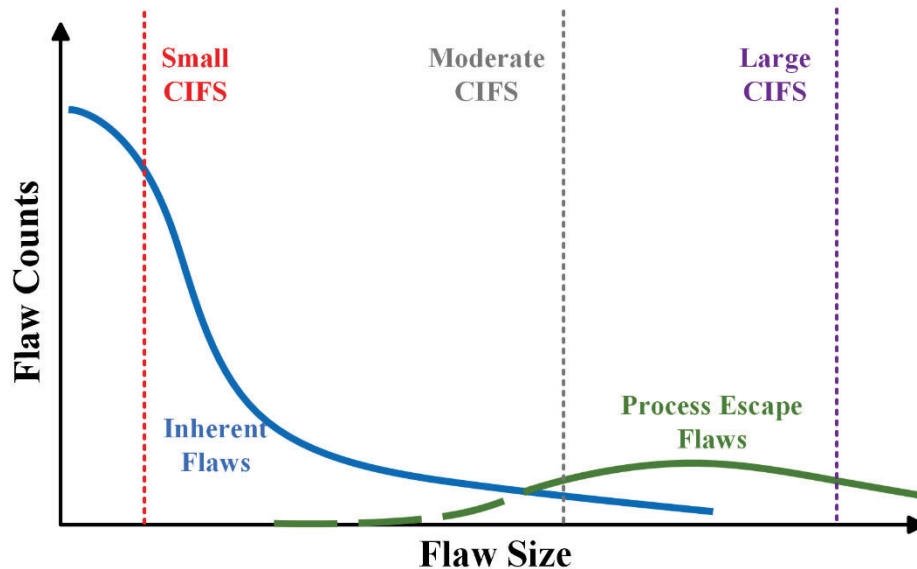


Figure 7.2.1-1. Notional AM Flaw Distributions with CIFS Overlays

In between these two extremes (the “Moderate CIFS” line in Figure 7.2.1-1), the inherent flaw distribution provides a quantitative input into damage tolerance analysis by demonstrating that the probability of a critical defect is acceptably low, or, more robustly, by providing an anomaly exceedance curve as a PDTA input. By employing such approaches, the risk associated with inherent defects can be assessed and quantified.

The approach described assumes that the AM components are produced with a process that meets the NASA-STD-6030 requirements (or equivalent) for Class A components, including characterization of fracture properties (i.e., toughness and fatigue crack growth rate). Robust process controls and characterized material properties are prerequisites to the use of fracture critical AM hardware, regardless of inspectability, but become even more important when component inspectability is limited.

The approach assumes an evaluation of material flaw state to a sufficient degree that variability within the build process is understood. Deterministic damage tolerance analyses are reliant on a postulated initial flaw size, typically bounded by the minimally detectable flaw size for the applied NDE inspection. When reliable NDE inspectability cannot be achieved, appropriately assessed flaw population data provide a bound on credible flaw sizes that is otherwise unavailable.

7.2.2 AM Process Assessments

Since flaws are currently unavoidable in metal AM processes, a purposeful approach to defining, characterizing, and controlling for flaws is the basis for an AM process-level assessment that can be used as a foundation for developing a fracture control rationale for un-inspectable components.

7.2.2.1 Inherent Flaws

As discussed in Section 7.1.1, the inherent flaw state is representative of the characterized nominal operation of a qualified AM process. The general effect of inherent flaw state on material properties may be reasonably assumed to be characterized as part of the material and

metallurgical assessment of the AM process as part of QMP development. In this paradigm, the effects of the inherent flaws are included in the material properties as a source of variability, analogous to within-specification variation in chemistry or heat-treatment temperatures for wrought materials. Thus, the primary concerns from a fracture control perspective are demonstrating that the component CIFS is sufficiently larger than the flaw sizes associated with the inherent flaw population and controlling the AM process such that the material produced remains within the characterized inherent flaw state.

7.2.2.2 Process Escape Flaws

Whereas inherent flaws are expected to be common enough for direct characterization, process escape flaws are expected to be rare or uncommon enough to preclude direct characterization. As a result, screening for process escape flaws requires understanding the potential sources of those flaws, which requires understanding the types of potential process escapes associated with the AM process. Tools for process assessment are well established in manufacturing; for example, process failure modes and effects analyses (PFMEAs) are commonly used to systematically evaluate manufacturing processes to identify and address manufacturing risks.

In the context of fracture control for AM, the PFMEA provides a framework to methodically assess the AM process, identify the potential process escapes that can lead to process escape flaws, and identify potential mitigations to address the risks associated with process escape flaws. This evaluation of the AM process informs development of specific preventive measures to preclude flaws from each type of potential process escape. For some types of process escapes, high detectability or low likelihood of process escape flaw generation might be sufficient rationale to deem resulting process escape flaws as non-credible. An example would be a process escape that causes a build crash. In this scenario, the process escape is highly detectable (i.e., the build crashed), and the part would be scrapped. For others, physics-based rationales might be used to conservatively bound the size and occurrence rate of the potential resulting process escape flaw. One example would be entrapped porosity, which is unlikely to be larger than the width of the melt pool. In cases where flaws may be credible and no reliable bounds on size and occurrence are possible, assessments of the flaw probabilities may be developed to support PDTA.

In the absence of reliable flaw detection (i.e., NDE), prevention or detection of process escapes becomes the primary means for screening for process escape flaws. A thorough understanding of the AM process is required, and the PFMEA provides an effective tool for rigorous assessment of the AM process. However, such approaches are inherently limited, as prevention or detection strategies supported by PFMEA address only known or postulated process escapes. AM process failure modes that are currently unknown may arise as experience with AM materials increases, current AM processes mature, and new AM processes are developed.

F-3. Prevention or detection of process escapes is the primary means to screen for process escape flaws in un-inspectable AM components.

7.2.3 Component-Level Assessments

Once the AM process-level assessments of flaw state distributions are defined, the fracture control rationale can be informed by component-specific assessments regarding CIFS and flaw detection capabilities. Figure 7.2.3-1 shows an overlay of notional CIFS and NDE capability on the notional flaw distributions. The CIFS is expected to shift based on what any given design can

tolerate, and the NDE detectable flaw size is driven by the capabilities of the inspection technique(s).

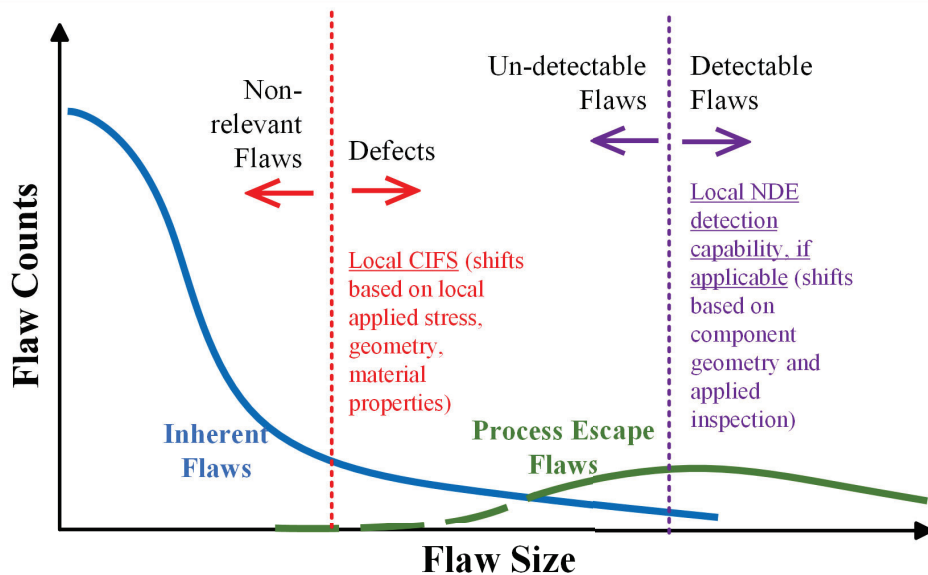


Figure 7.2.3-1. Example of Component-level Assessments

7.2.3.1 Critical Initial Flaw Size (CIFS)

The CIFS is the largest initial flaw predicted to survive the mission life without failure, with an appropriate factor of safety applied to the service life (e.g., four times the service life [NASA-STD-5019]). Flaws larger than the CIFS (i.e., defects) can be expected to lead to a higher risk of component failure during service. Flaws smaller than the CIFS might be expected to be benign and are considered non-relevant.

CIFS analysis is commonly performed for fracture critical components using established damage tolerance assessment tools (e.g., NASGRO). Typically, a bounding CIFS that represents the smallest CIFS present in the component is used for assessments. Multiple locations within a part may need to be analyzed to determine the bounding CIFS. CIFS assessments for AM materials follow fundamentally the same approach as for traditionally manufactured materials but may need to account for factors unique to AM product forms (e.g., local variability in geometry, surface finish, and/or material properties).

The CIFS varies throughout a component, driven primarily by applied stress and the component geometry, although local variability in material properties (including flaw state) may be relevant for AM materials. For AM applications, a more localized evaluation of CIFS at multiple points in the component might be necessary, particularly to support comparison with localized NDE detection capabilities or to account for material property or flaw state variability.

The identification of control points for CIFS calculations should account for features of the component design and features associated with the AM process, as appropriate. For example, highly stressed areas or areas of stress concentration are commonly identified for damage tolerance analysis, based on these locations providing a potential “worst case” location for a possible crack to propagate. For AM components, critical locations may be influenced by AM surface finish, variations in flaw state (e.g., differences between near-surface and bulk material

flaw states), and local material property changes (e.g., those associated with thin-wall geometries). Due to the number of potential influence factors, an intuitive identification of the worst-case flaw location may not be practical. Identification and assessment of multiple control points is prudent to ensure the damage tolerance of the component is appropriately bounded, particularly if a zone-based approach is adopted (see Section 7.2.5). Automated or probabilistic analysis tools may be necessary to account for the potential sources of variability that might affect CIFS calculations for AM components.

7.2.3.2 Minimum Detectable Flaw Size

Some inspections may be possible for AM components that are otherwise un-inspectable. Some regions of a component may be able to be inspected, and inspections should be performed wherever feasible to reduce the overall risk of the component. For regions that are inspectable, the minimum detectable flaw size is the smallest flaw size that can be detected with NDE with a sufficient degree of reliability. Typically, this flaw size is defined as the flaw size that can be detected 90% of the time with a 95% confidence [NASA-STD-5009]. That is, the minimum detectable flaw size is not the smallest flaw that a particular NDE technique is capable of resolving. Instead, the minimum detectable flaw size is a larger flaw that, if it exists, will be detected in almost every inspection. Minimum detectable flaw sizes vary locally depending on the component geometry and the applied NDE technique. Some NDE techniques are limited to surface features, while others are intended for volumetric inspections. Inspection challenges for AM components may affect standard minimum flaw size estimates (e.g., Tables 1 and 2 in NASA-STD-5009).

The ability for an AM component to be inspected varies based on the component material, geometry, and surface finish [Todorov et al., 2014]. A review of detection capability for different zones within an AM component can help bound the sizes of possible undetected flaws by truncating larger flaws sizes that might be reliably detected. In ideal cases, some areas of a component might be inspectable and can be shown to be damage tolerant through standard assessments. On the other extreme, identifying regions that are un-inspectable helps focus further assessments. For example, developing targeted NDE inspections or more focused AM process controls for un-inspectable regions of a component might help bound probable flaw sizes. Physics-based NDE simulation tools are commercially available; such tools might prove useful in assessing flaw detection capabilities for different inspection techniques for AM components with limited inspectability [Vienne et al., 2022].

For un-inspectable regions, there may be no minimum detectable flaw size, and the local NDE detection capability line in Figure 7.2.3-1 may not be applicable. In this scenario, any CIFS would be lower than the NDE detection capability.

7.2.4 Risk Scenarios

The relationships between the CIFS, the minimum detectable flaw size, and the inherent flaw distribution define the risk scenario for a component and thus the appropriate approach toward a fracture control rationale.

Once CIFS assessments are calculated for the appropriate control points, the results should be compared with the flaw state distributions. Ideally, the CIFS values will be larger than the flaw size associated with the majority of the inherent flaw distribution, and a damage tolerance rationale can be pursued using a probabilistic analysis to evaluate the remaining risk due to

process escape flaws or large inherent flaws. However, some CIFS assessments might show that the critical flow sizes are within the inherent flow size distribution. In such cases, risk reduction activities (e.g., process refinements, component redesign, etc.) would be necessary to support a flight rationale.

7.2.4.1 Risk Scenario 1: CIFS Within Inherent Flow Distribution

Risk Scenario 1 involves a situation where the CIFS falls within the inherent flow distribution, regardless of NDE detection capability. Figure 7.2.4.1-1 shows the outcomes of the process- and component-level assessments corresponding to Risk Scenario 1. In this scenario, the probability of a critical flaw in a critical location is high since inherent flaws have a relatively high frequency of occurrence. Thus, this scenario represents an unacceptable risk.

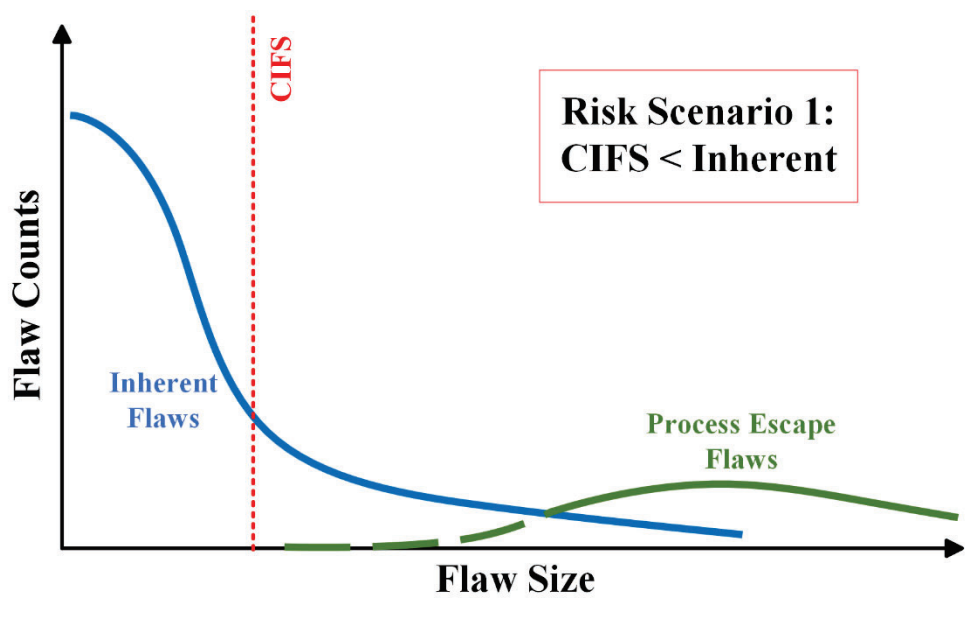


Figure 7.2.4.1-1. Illustration of Risk Scenario 1, where CIFS is within Inherent Flow Distribution

For components with a CIFS within the inherent flaw distribution, demonstration of damage tolerance through analysis is not possible, and even a risk-based approval of the component might be unlikely. To overcome these challenges, decreases in inherent flaw sizes resulting from refinements to the AM process would move the inherent flaw distribution away from the CIFS. Refinements in the AM process present an additional path to increasing the CIFS by improving the fracture properties of the material. The alternative is to increase the CIFS out of the range of inherent flaw sizes through component design changes. For example, reducing the applied stresses on the component or adjusting the geometry to reduce stress concentrations could result in a larger CIFS. In summary, for designs where the calculated CIFS is similar to the AM build inherent flaw size, a high flaw occurrence rate would drive part redesign and AM process alteration.

7.2.4.2 Risk Scenario 2: CIFS Smaller than Minimum Detectable Flaw Size

Risk Scenario 2 involves a situation where the CIFS is below the minimum detectable flaw size but is sufficiently outside the range of the inherent flaw distribution. This scenario applies to the un-inspectable AM component for any CIFS outside the range of the inherent flaw distribution, as there would be no minimum detectable flaw size. In this scenario (see Figure 7.2.4.2-1), the

risk associated with the inherent flaw is mitigated in that the CIFS is sufficiently above the inherent distribution, making the majority of inherent flaws non-relevant. The rationale must focus on controlling or detecting the process escapes through process monitoring or inspection and demonstrating adequate tolerance to large inherent flaws.

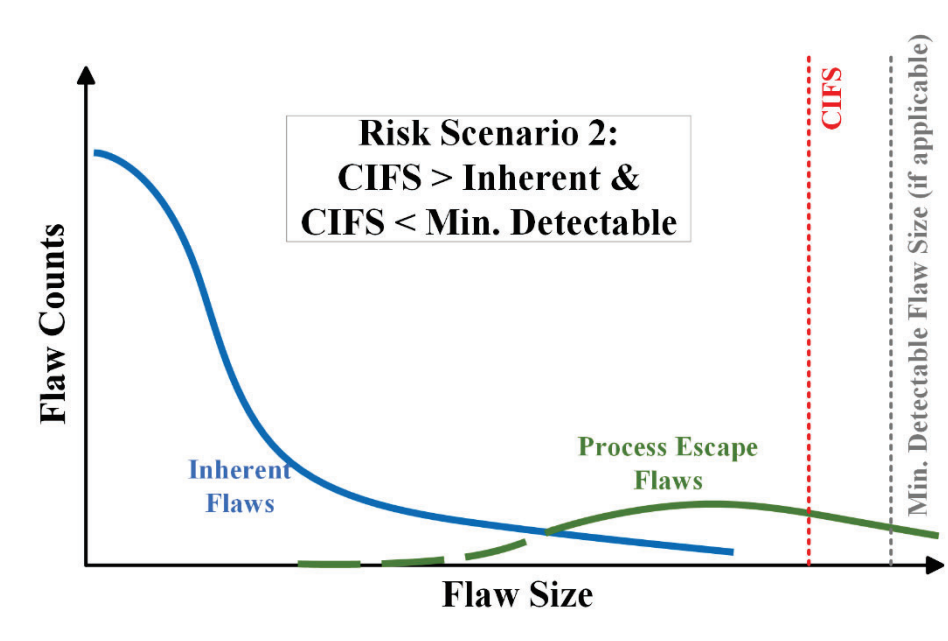


Figure 7.2.4.2-1. Illustration of Risk Scenario 2, where CIFS is below Detection Capability but above Inherent Flaw Distribution

Risk Scenario 2 relies on the CIFS being outside the inherent flaw distribution, but the degree to which the CIFS must be larger is an open question. There is some non-zero probability associated with large inherent flaws that might be reasonably expected to correspond to a CIFS. Alternatively, there may be physics-based rationale that can truncate the upper tail of the inherent flaw distribution (e.g., limits based on local part dimensions, such as thin wall structures). A PDTA supported by the inherent flaw distribution might be useful in defining the probability of failure associated with rare large inherent flaws and demonstrating the CIFS is sufficiently outside the inherent flaw distribution.

Adequate screening of the inherent flaws leaves the possibility of a part containing an undetected process escape flaw. In the absence of sufficient inspection, screening for process escape flaws would be based on preventing or detecting process escapes (rather than the process escape flaw). The PFMEA approach provides a methodology for rigorously evaluating an AM process to identify potential process escapes and assess the associated mitigations for each process escape. Such an assessment is necessarily risk-based, in that PFMEAs identify and assess only known or postulated failure modes. A component associated with Risk Scenario 2 would not be expected to comply with fracture control requirements as written but may be able to be shown to be associated with an acceptable risk.

7.2.4.3 Risk Scenario 3: CIFS Larger than Minimum Detectable Flaw Size

Risk Scenario 3 involves a situation where the CIFS is above the minimum detectable flaw size. Thus, the critical flaw can be detected reliably by NDE. This represents the nominal baseline risk condition and meets NASA-STD-5019 requirements. Figure 7.2.4.3-1 illustrates this scenario.

Note that Risk Scenario 3 requires that the CIFS be above the inherent flaw distribution, so that the likelihood of a critical flaw occurring is low.

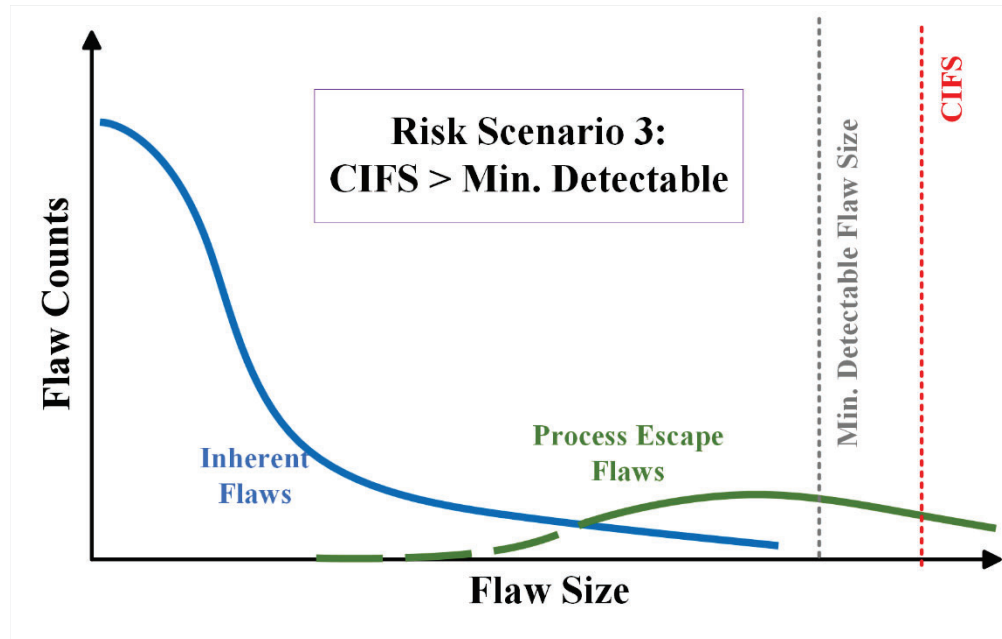


Figure 7.2.4.3-1. Illustration of Risk Scenario 3, with CIFS Larger Than Detection Limit

This scenario would not be possible globally for AM components with un-inspectable regions. However, local regions within an un-inspectable component may be compatible with Risk Scenario 3. In such cases, those regions would represent baseline risk and could be shown to be damage tolerant using standard approaches.

7.2.5 Zone-based Assessment

Standard damage tolerance assessments focus on a critical location in the subject component. Per NASA-STD-5019, damage tolerance assessments must account for a flaw in the worst-case location and orientation. However, additional variability in AM materials in terms of geometric complexity and material property gradients (including flaw state variation) may complicate the traditional bounding approach. A zone-based approach has been proposed [Gorelik, 2017] to appropriately account for additional variation in AM materials. The risk scenario paradigm lends itself to the zone-based approach.

Instead of defining bounding assumptions of inspection capability, structural demand, and material properties, the zone-based approach is intended to more accurately reflect the local conditions that affect the damage tolerance of the component. Figure 7.2.5-1 provides an example of the part-zoning approach. The component in this example contains a boss representative of a large volume of high-density material (shown in yellow) that limits NDE coverage using traditional techniques, resulting in an un-inspectable classification for this component. Part-zoning approaches can be used to assess the risks and develop a rationale for distinct regions within the component. In this example, the flanges of the part are low stress and readily inspectable using traditional NDE techniques (e.g., dye penetrant and radiography). Analysis might show that the CIFS is above the NDE capability and large relative to the inherent flaw distribution. Thus, the flanges would fall into Risk Scenario 3 and represent baseline risk. The thick, boss region of the example part is difficult for radiography to penetrate and has a

reduced inspection capability (i.e., a larger minimum detectable flaw or no detectable flaw size). However, stresses are low in this region, so the CIFS is large relative to the inherent flaw distribution. This region represents Risk Scenario 2. This region can be shown to be acceptable by developing a rationale demonstrating a sufficiently low risk of failure due to large inherent flaws and sufficient control of process escape flaws. Risk Scenario 1 is demonstrated by the tube walls that are subjected to high stresses. In this region, the CIFS is small enough to be within the inherent flaw distribution. Thus, these regions represent an unacceptable risk. The design should be modified to increase the CIFS (e.g., increasing the wall thickness), or the AM process should be refined to decrease the size and frequency associated with the inherent flaw distribution.

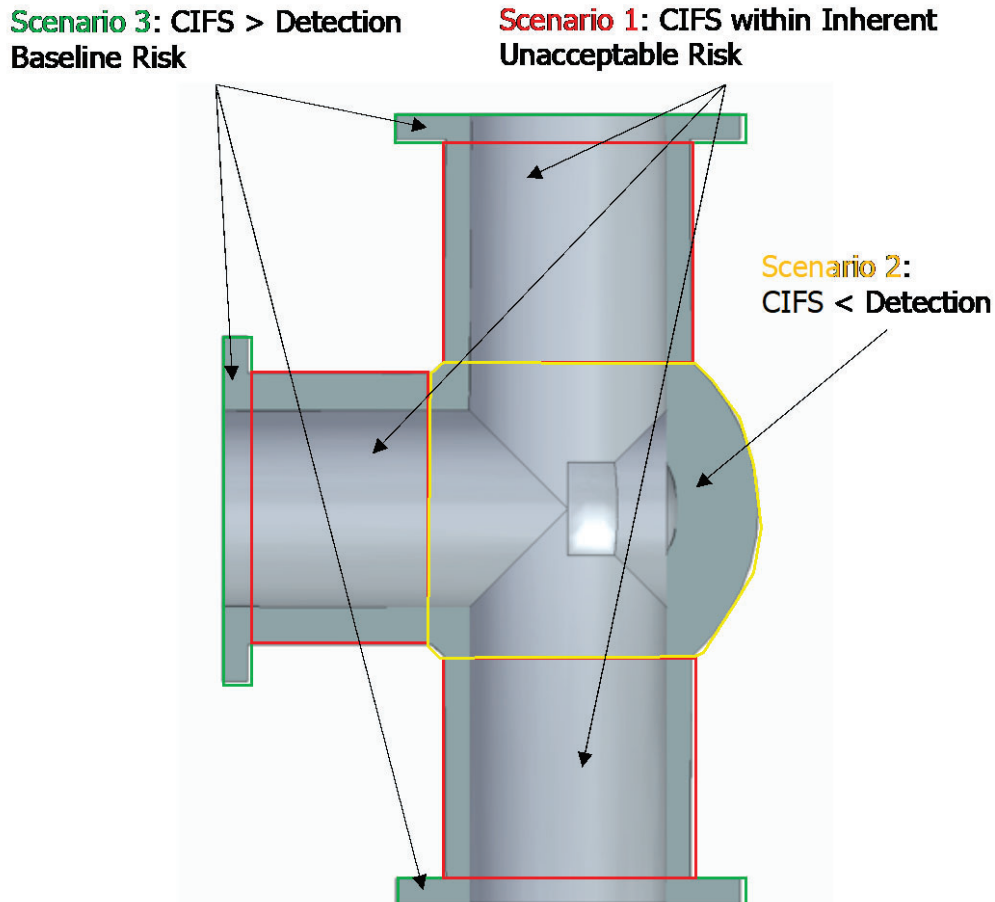


Figure 7.2.5-1. Example of Part-zoning Approach

The example illustrates how the part-zoning approach supports the overall risk assessment of the component. If the component is entirely associated with Risk Scenario 3 (green), then the part represents the baseline risk and is compliant with NASA-STD-5019. Note that baseline risk is not zero risk. If the component contains one region associated with Risk Scenario 1 (red), as for the example component, then the part contains a likely unacceptable risk, and steps should be taken to reduce that risk. More likely, a component will contain Risk Scenario 3 (green) zones and Risk Scenario 2 (yellow) zones. The risk in each zone contributes to the cumulative risk associated with the component [Millwater et. al., 2002].

F-4. Part-zoning approaches are a method for risk assessment of AM components with un-inspectable regions.

7.2.5.1 Assigning Part Zones

Part zoning relies on assigning zones to appropriate regions of the component. The choice of appropriate zones requires engineering judgment and should be primarily driven by similarity in local stress, geometry, material properties (including flaw state), and inspectability. Features that cause significant shifts in the expected NDE detection capability, significant changes in CIFS, or changes in material properties (including flaw state) should be treated as distinct zones.

AM influence factors (e.g., surface finish, fine geometries, location-specific properties, and anisotropy) can influence the identification of critical locations beyond the highest stress location. AM geometries might affect the applicability of characterized flaw distributions (i.e., near-surface material might have a different flaw distribution than bulk interior material). PDTA may be necessary to realize the potential of zone-based analysis, given the location-specific variability in material properties (including flaw state) observed in AM components and the stochastic nature of flaw occurrence and detectability [Gorelik, 2017].

Inspection information should be used to support the rationale for AM components, even if the inspection does not provide full coverage or meet the detection requirements of NASA-STD-5009. In such cases, the inspections can be used to provide some bounds on the possible flaw sizes within a component. In some cases, a zone of a component might be inspectable, in which case that zone could be assessed using standard fracture control rationales (Risk Scenario 3).

Once a component is zoned based on relevant AM influence factors, critical component locations are identified based on applied stresses and part geometry. Automated analysis techniques can support the identification of critical locations. Once identified, an appropriate damage tolerance analysis is conducted for the critical location. The results of the analysis for each zone are used to compile an overall component assessment. At a minimum, this assessment would be expected to identify the location in the component with the worst-case margin to the required service life. Statistically derived probabilities of failure based on the analytical service life in each zone may be desirable. Tools are available that can assist with probabilistic assessments (see Section 7.2.7). In essence, the zone-based approach divides a component into analytical subcomponents with similar properties, which allows for a higher fidelity assessment of critical locations in the part. The zoning process might be iterative to ensure that relevant part locations are appropriately assessed.

The characterized inherent flaw distribution supports the zone-based approach by providing information supporting zoning based on localized flaw distributions and criteria for critical initial flaws. In the simplest case, a bounding inherent flaw distribution is established for a particular AM process on a per-machine basis. If it is sufficiently bounding, then that flaw distribution would be broadly applicable across the zones. In cases where spatial variations in flaw state are characterized (e.g., for near-surface and bulk flaw states), the flaw state variation should be a factor in the part zoning approach, and the appropriate flaw state information should be applied to the applicable zones of the component. The degree to which flaw distribution information is accounted for in zone-based approaches is dependent on the needed fidelity to meet life requirements and the degree to which the inherent flaw population has been characterized.

7.2.6 Flaw Location Dependence

The distributions of AM flaws will vary with the component geometry. For example, interactions between parameter sets (e.g., those used for geometric contours versus those used for bulk material fill) may result in higher frequencies of AM flaws at the contour-to-bulk parameter interface. Near-surface porosity is commonly observed in L-PBF [Benedetti et al., 2018]. Flaw state may vary due to geometry that challenges the AM process (e.g., regions that have high interpass temperatures). In all cases, these factors should be evaluated for the potential impacts on the inherent flaw distribution and the potential for increased occurrence of process escape flaws. Robust design for AM can be used to mitigate these impacts. Ideally, the inherent flaw state is characterized in such a manner as to be bounding to typical flaw state variability due to AM influence factors.

7.2.7 Implementation of Probabilistic Damage Tolerance Analysis (PDTA)

Standard damage tolerance analysis is deterministic: measured or estimated values of material properties, loads, and crack sizes are input into the analysis, and the output is a prediction of the component service life. Probabilistic damage tolerance is an approach that allows the damage tolerance analysis inputs to take the form of random variables described by statistical distributions. Most directly, the statistical distributions are used to inform inputs to repeated evaluations of crack propagation models, resulting in an estimate of the probability of failure associated with the component described by the analysis. The most common statistical input variable in a PDTA is a flaw distribution, given in terms of the size and occurrence rate of a flaw. Example flaw distributions, represented as exceedance curves that combine flaw size distribution and average frequency of occurrence, are shown in Figure 7.2.7-1.

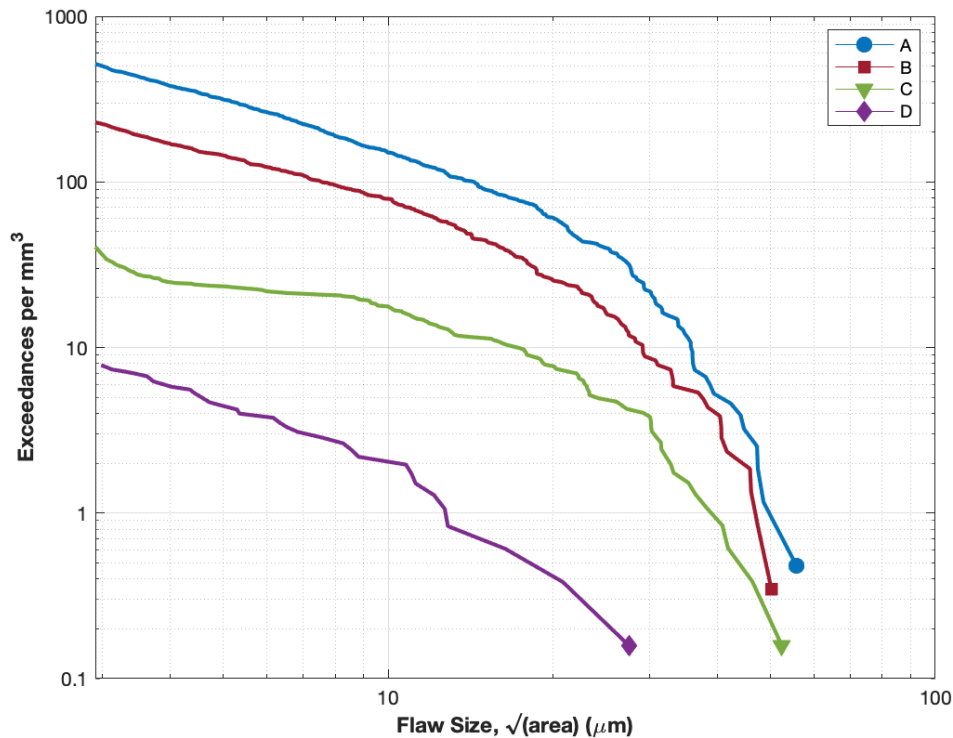


Figure 7.2.7-1. Example Flaw Distributions of AM GrCop42 Manufactured with Different Specimen Thicknesses [adapted from Demeneghi et al., 2021]

Probabilistic damage tolerance approaches have been successfully employed for aircraft certification. For example, PDTA is used in certification of titanium turbine engine rotors where rare material defects that can be below the NDE detection capability can arise during the alloy melting process [Rotor Integrity Sub-Committee, 1997]. The probabilistic approach lends itself to the un-inspectable AM component problem by providing a means to bound the probability of failure associated with an undetected AM flaw.

7.2.7.1 PDTA Advantages

Currently, NASA-STD-5019 requires that a deterministic fracture analysis be conducted assuming that the largest undetectable flaw size exists at the worst-case location in the component. The flaw must then be shown not to lead to component failure within the target service life, with an appropriate safety factor. Thus, the probability of failure associated with such an analysis is binary; the component has, analytically, 0% probability of failure prior to the analytically determined component life, and 100% probability of failure afterward. This approach is simplistic but is generally recognized to be conservative. This worst-case location approach leads to an analysis that is bounding for the component, as any flaw in any other location would be expected to have a higher service life.

The probabilistic approach to damage tolerance provides potential benefits over the standard deterministic damage tolerance approach. First, absent other factors, a flaw is generally less likely to be in the critical location than it is to be somewhere else in the component, by virtue of the critical location representing less overall volume. Second, there is some probability associated with a critical flaw even being present in the part in the first place. Probabilistic approaches can account quantitatively for both probabilities, reducing the conservatism of the traditional analysis approach and potentially extending the expected component service life. Additionally, a probabilistic approach provides an accounting of the component probability of failure, rather than the implied binary failure probability associated with standard, deterministic damage tolerance analysis. As a result, service life evaluations could be based on an appropriately determined acceptable probability of failure rather than on a factor of service lives. More advanced analyses can account for additional probabilistic inputs (e.g., material properties, applied loads, and NDE probability of detection) to refine the analysis. However, PDTAs remain specialized and are dependent on the quality of the input probabilistic data. Currently, NASA-STD-5019 requires the use of PDTA to be reviewed and approved by the responsible Fracture Control Board.

7.2.7.2 Application of PDTA to Un-inspectable AM Components

Probabilistic approaches provide a potential means for assessing the risk of component failure due to AM flaws that might be undetected. The key input into such an analysis for AM components is an appropriately bounded flaw distribution that describes the AM flaw size and frequency of occurrence. Such a distribution might be developed based on approaches such as those discussed in Section 7.6. Multiple flaw distributions might be required for an analysis. For example, relatively small inherent flaws are expected to be likely to occur in an L-PBF component. Process escape flaws are expected to be rare but potentially significantly larger. Different distributions are likely needed to describe each of these categories. Component geometry might affect the required distributions. For example, many L-PBF processes generate higher occurrence rates of flaws close to the surface relative to flaws observed in the bulk of the

material. A specific near-surface distribution might be required to appropriately evaluate components produced using such processes.

The probabilistic approach represents a significant departure from standard damage tolerance analysis for NASA applications in that results are provided in terms of probability of failure rather than expected service life. Additionally, the methods for PDTA, while well-developed, remain limited to specific applications (e.g., titanium turbine rotors). Development of the workflows, knowledge of the critical inputs, and assessment of the analysis influence factors are critical to understanding and implementing PDTA for AM applications.

7.2.7.3 Current Applications of PDTA to AM

One promising PDTA tool for AM applications is DARWIN, an analysis code developed by the Southwest Research Institute (SwRI) in collaboration with turbine engine manufacturers and funded primarily by the FAA. Developed originally in the late 1990s, DARWIN was designed to assess damage tolerance issues arising from rare metallurgical defects that occur in titanium rotor disk forgings. DARWIN has been accepted by the FAA as a means of compliance to certain federal regulations on analysis of safety-critical turbine engine components in civil aviation. Over the intervening years, DARWIN's capabilities have expanded to accommodate more general flaw populations, different crack geometries, and more advanced finite element (FE) models. These advancements place DARWIN in a position to be leveraged to solve damage tolerance problems for AM materials and components [McClung, 2022]. As inputs, DARWIN takes a FE model containing stresses, distributions of flaws (called *anomalies* in the DARWIN tool), and material properties. DARWIN processes the input FE model and divides the component into zones based on probability of failure (note that these zones are distinct from the part zones discussed in Section 7.2.5). Failure probabilities are calculated by superimposing a crack propagation model onto the FE model geometry and running a crack growth prediction analysis (using approaches similar to NASGRO). These deterministic analyses are conducted repeatedly within a Monte Carlo simulation framework using a randomly assigned (sampled) initial flaw size for each run based on the provided flaw (anomaly) distribution. From these repeated runs, a probability of failure is calculated for each part zone and for the overall component (see Figure 7.2.7.3-1).

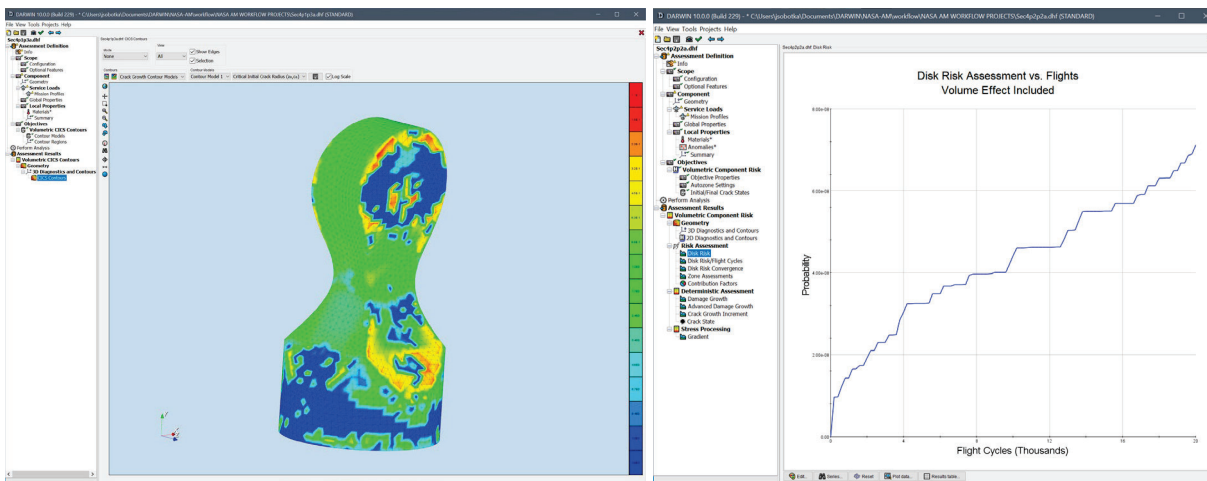


Figure 7.2.7.3-1. Example Results from DARWIN Tool [Sobotka et al., 2023]

Recently, under a NASA-funded project, researchers at SwRI have explored the application of PDTA to AM materials. Enright and McClung [2020] applied three example flaw distributions to a DARWIN analysis of a test case geometry. The flaw distributions represented distributions obtained from extensive flaw characterization data, a reduced set of flaw characterization data, and an inverse probability of detection curve corresponding to an NDE technique. The results showed that the probabilistic approach allowed for longer service lives relative to the deterministic analyses at the same risk level. Additionally, more extensive flaw characterization data generally resulted in predictions of lower probabilities of failure. In both cases, the improved service life and probabilities of failure are the result of the removal of conservatism relative to the standard NASA damage tolerance approach, particularly through accounting for the flaw occurrence probability rather than assuming a flaw is present. The removal of these conservatisms is appropriate since the more refined probabilistic analysis is able to account for more realistic analysis assumptions regarding flaw occurrence. Such approaches require confidence that the probabilities of flaw occurrence used in the analysis are representative of the actual flaw probabilities in the component or material. Ideally, such inputs would be demonstrably conservative. Additionally, the researchers demonstrated the ability to assess the CIFS at different regions of the component, which can help inform further assessment of critical component locations and refine zones for targeted NDE inspections [Enright and McClung, 2020].

These initial results demonstrate the potential usefulness of PDTA for AM applications, although major hurdles remain, particularly in the realm of developing appropriately representative flaw distributions.

F-5. With validation, PDTA has the potential to reduce conservatism relative to standard NASA damage tolerance approaches by adopting design-specific analysis assumptions (e.g., flaw occurrence rates).

R-3. The NASA Fracture Control Methodology Panel should review available PDTA tools, their capabilities and limitations, and the availability and relevancy for NASA applications. *(F-5)*

NASA-HDBK-5026, which contains guidance for meeting structural requirements for AM components, is still in draft form. As of this writing, NASA-HDBK-5026 is expected to contain a section with guidance on the application of PDTA to AM. Completion and release of this handbook would provide helpful guidance to users of PDTA on considerations specific to AM. General guidelines for the use of PDTA in NASA applications would be appropriate to add to NASA-HDBK-5010 “Fracture Control Implementation Handbook for Payloads, Experiments, and Similar Hardware.”

R-4. The OCE should update NASA-HDBK-5010 with PDTA use guidelines. *(F-5)*

7.2.7.4 Probability of Failure

The probability of failure values calculated by the DARWIN tool represent a new metric for damage tolerance within NASA. Traditionally, deterministic damage tolerance analysis tools like NASGRO provide a number of safe lives, which is compared with a minimum safe life metric (typically four safe lives per NASA-STD-5019). Probability of failure calculated through a PDTA will likely increase as cycles are applied to the component. Additionally, probability of

failure is potentially non-zero from the beginning of the component's life. As such, an acceptable probability of failure value will have to be assigned, similar to the safety factor of four that is applied to standard deterministic damage tolerance analyses. That acceptable probability limit will need to correspond to a number of cyclic loads or service lives (i.e., the probability of failure after one service life). As one example, the FAA defines a design target risk as a benchmark for the probability of failure of titanium alloy components in aircraft engines that are assessed using PDTA. The FAA has set the benchmark at one event in one billion flight cycles for individual components and five events in one billion flight cycles for the overall engine [FAA AC 33.14-1].

Threshold risk likelihoods for NASA applications vary based on the criticality of the mission or project and the risk management system imposed. One example is provided in GPR 7120.4D, where the likelihood of a safety event occurrence is less than 1 in 100,000 events, corresponding to a likelihood score of 1 on the NASA 5×5 risk matrix. However, GPR 7120.4D is applicable to suborbital programs and small payloads, not human-rated flight vehicles [GPR 7120.4D]. Another example comes from the Human System Risk Management Plan, which sets the probability of a “very low” likelihood event at 1 in 10,000, which is an order of magnitude higher than defined in the GPR document [JSC-66705]. Again, this document does not specifically cover human-rated flight vehicles for which threshold risks are set by the responsible program. Regardless, if PDTA approaches are adopted, then thresholds for acceptable risks at a component level need to be defined.

F-6. Quantitative bounds on acceptable probabilities of failure are not standardized in NASA documentation (e.g., NASA-HDBK-5010, JSC 66705, GPR 7120.4D, etc.) and vary by Program based on the Program's risk tolerance.

An acceptable probability of failure might vary based on the classification of the part (e.g., fracture critical or non-fracture critical) or the risk tolerance of the mission. While fracture critical components are associated with a catastrophic failure mode, some missions might be more or less risk tolerant. For example, a robotic mission might be more accommodating to higher probabilities of failure than a crewed mission.

7.2.8 Role of Specialized Inspection Techniques

The AM community is investigating specialized inspection techniques, including CT and *in-situ* monitoring, for use in AM applications. These techniques show promise for providing reliable detection capabilities for AM flaws, but challenges remain, and integration of these tools with improved understanding of AM material flaw states and probabilistic assessments would support fracture control rationale.

7.2.8.1 X-Ray CT

CT is a powerful technology for the inspection of the complex structures possible with AM, as it can capture information about internal features and voids, as well as surface features, through the construction of a 3D model of the part from X-ray data. However, this method has limitations in resolution based on the spot size of the X-ray beam on the part, which is dependent on the voltage and power of the beam, among other factors. Ensuring sufficient X-ray penetration through the sample requires increasing these parameters, which can impact resolution. Thus, particularly large parts or those with dense or thick regions can be inspected but with a lower resolution. See Section 7.5.1.2 for additional discussion of CT capabilities and limitations.

Currently, there are no widely accepted probability of detection standards for CT, although some have been proposed (e.g., Kim et al. [2019]). Developing methodologies for CT probability of detection demonstration would support the use of CT for part screening. Approaches based on demonstrated inspection capabilities using representative quality indicators can be used to demonstrate CT inspection capabilities for specific combinations of parts, materials, and AM processes, although such an approach does not necessarily meet the special NDE requirements in NASA-STD-5009. CT detection capabilities are affected by many variables (e.g., material, geometry, and X-ray parameters), and CT can be expensive and time consuming. For these reasons, scans of complex parts with sufficient resolution for flaw detection can be impractical. These limitations impede the common use of CT as standard, quantitative NDE per NASA-STD-5009.

With further development, CT may have a significant role in process qualification (e.g., inherent flaw state characterization). However, high cost and long lead time considerations limit the potential use of CT for full inspection of production hardware.

The ability to compute probability of failure for separate zones of the part can inform inspections and set the required resolution limits. Regions that have a low probability of failure or contribute little to the overall probability of failure in the part may be able to be investigated with lower resolution NDE methods while maintaining sufficient flaw detectability. Lower resolution methods could be CT with lower resolution parameters or other NDE techniques (e.g., ultrasonic evaluation). As the same geometric features that make CT easier (e.g., being small and thin) can serve as critical locations in parts, using probabilistic tools to identify regions that contribute most to probability of failure could lead to targeted high-resolution inspections compared with inspections intended for the whole component. For example, the added expense associated with super-high-resolution CT may be worthwhile for certain high-criticality components within the size capabilities of those techniques. Eventually, sufficient confidence in the probabilistic assessment might enable some reduction in NDE inspection in regions with sufficiently low probabilities of failure.

O-1. Integrating PDTA approaches with CT inspection could alleviate challenges with probability of detection by allowing inspection tailoring by component region.

7.2.8.2 *In-situ* Monitoring

In-situ monitoring describes several techniques that are used to monitor a part for indications of flaws while it is being built. These in-process inspections can locate flaws that would be more difficult to detect post-build. For example, flaws in internal channels or flaws that will otherwise be obscured by later material additions may be difficult to detect post-build. At the most basic level, *in-situ* process monitoring is widely used to avoid build errors that might damage the AM machine. For example, most L-PBF machines end the build if a part warps and starts to impact the re-coater blade. *In-situ* techniques have the potential for a wider range of applications, including the detection of flaws that do not result in a failed build but could compromise structural integrity. At the current state of development, *in-situ* monitoring approaches provide qualitative assessments of the material quality produced by an AM build. However, as *in-situ* monitoring evolves and improves, these techniques might develop the robustness necessary to replace traditional NDE techniques [Williams et al., 2023]. If this level of advancement is realized, then previously un-inspectable AM parts might be assessed using *in-situ* techniques, eliminating the need to develop specific, risk-based rationales for such components.

In-situ melt pool monitoring, thermal imaging, ultrasonic, eddy current, optical, and acoustic methods have been explored to detect AM flaws. *In-situ* monitoring techniques generally examine only the layer of material currently being deposited. However, some techniques (e.g., ultrasonic or X-ray) can penetrate to previously deposited layers. Such techniques are slow and focused, meaning they cannot be regularly applied over the whole surface but could be used for regions of concern. See Section 7.5.3 for additional discussion of *in-situ* monitoring techniques.

Current *in-situ* monitoring techniques are challenged by a low detection reliability. Many monitoring techniques have a high false positive rate, where indications detected by the monitoring system do not correlate to a physical flaw. Often, indications can represent a process deviation that will be corrected on subsequent layers as the material is remelted, which is a natural occurrence within many AM processes. A positive indication from an *in-situ* method may only correlate to a physical flaw some percentage of the time. This high false positive rate makes decision-making regarding flaw detection difficult in terms of stopping or continuing AM builds or assessing the fitness for service of a completed part.

F-7. *In-situ* monitoring is not a replacement for standard or special NDE.

Instead, at the current state of development, the primary role of *in-situ* monitoring for an un-inspectable part rationale lies in confirmation of process control, identification of material quality in critical areas, and detection of major process escapes. First, with appropriate metrics, *in-situ* monitoring could be used to confirm that an AM build is operating within the expected process window, thus confirming the material properties and flaw distributions established for that process are appropriate to apply to the analysis of a component fabricated using the process. Establishing a monitoring baseline for a component that can be used as a “fingerprint” for subsequent production of that component provides confidence that the AM process is operating as intended, there are no process escapes, and the inherent flaw state is consistent. Second, *in-situ* monitoring can help assess material quality in critical regions that might require additional inspection or characterization. For example, if *in-situ* monitoring were to signify a particularly hot or cold location during the build, then that location can be targeted for additional assessments (e.g., first article inspections, flaw state characterization, or design or process improvements). Finally, current monitoring systems may be capable of detecting large flaws with higher reliability and may be useful for bounding the maximum flaw sizes associated with some types of process escape flaws or screening for large inherent flaws. These approaches may provide rationale to limit the range of credible flaw sizes included in an inherent or process escape flaw distribution. If the *in-situ* monitoring technique can be shown to reliably detect a particular flaw size, then that flaw size can have the associated likelihood reduced from the flaw distribution or, if appropriate, removed from the flaw distribution.

Integration of *in-situ* monitoring tools with probabilistic tools (e.g., DARWIN) could focus the application of the *in-situ* monitoring techniques to component regions where flaws would have the highest probability of causing component failure. These types of tools might support decision making regarding which *in-situ* monitoring indications are worth acting upon. For example, less critical regions of the build may be more tolerant to flaws than other regions of a component, informing acceptability of components with detected process escapes.

One of the goals of *in-situ* monitoring is to make a system capable of correcting flaws as they occur. In-process control is standard practice in some DED techniques, where the power of the energy source is varied to create a consistent melt pool size. In these processes, the volume of

the material being deposited and a constantly changing thermal environment makes in-process control of the melt pool necessary to ensure material quality. In L-PBF, quality results can generally be achieved without actively modulating the parameters during build. However, in-process control of machine parameters would allow repair or recovery of a build when an unacceptable variation was indicated. This is challenging due to the difficulty in interpreting *in-situ* monitoring data and the potential for more significant flaws to arise from the attempt to correct the error. The difficulties in interpretation of the *in-situ* monitoring data are due to false indications or flaws healing during the build; these limitations will likely lessen over time as *in-situ* monitoring techniques are improved. The potential for flaws to be generated by the correction process are a concern, as using *in-situ* data for *in-situ* repair is non-viable if correcting the process creates greater issues than the initial flaw. A correction that would require pausing the build process for any significant amount of time could lead to atypical cooling, causing possible warping or weakened build layers. Probabilistic tools could be used to inform evaluations of the potential severity of a detected flaw and decisions regarding *in-situ* repairs. A high probability of failure for a flaw in a critical zone could make the risk of complications from attempting an *in-situ* repair worthwhile, while for zones with low probability of failure the flaw may be tolerable.

A future state might include closed-loop control of a L-PBF process, allowing for automated parameter changes to preempt flaw formation events. This goal will be challenging to obtain, as the techniques would need to detect the subtle signs that the process is moving in a direction that could cause flaws.

7.2.9 Design for Inspectability

AM techniques provide an unprecedented level of freedom for designers, which enables designs that may be more functional than those produced using traditional manufacturing techniques. However, this ability to generate an almost infinite array of structural designs means that some designs do not readily accommodate NDE inspections.

Adopting a “design for fracture control” or “design for inspectability” philosophy in AM component design can reduce the risk associated with un-inspectable AM components. By accounting for NDE detection capabilities in the design phase, the component can be designed to accommodate inspection in critical areas or limit the regions of the part that are otherwise un-inspectable. Evaluating CIFS during the design phase can help ensure that CIFS are large enough to be detectable by a chosen NDE method or unlikely to occur during normal AM process operation. Minimizing the use of challenging features outside high-margin locations can reduce the sensitivity of the design to inherent AM flaws. In areas of low margins, AM designs can be modified to lower stresses or improve inspectability. However, this approach can be overextended. For example, highly topologically optimized structures may concentrate loading into relatively small regions of the component. Such highly optimized structures may fail catastrophically in the event of a failure of the highly loaded features, whereas a more conventional design might allow for redistribution of loads and a more benign failure mode.

7.2.10 Detected Flaws

The previous discussion defines a means to account for the potential detrimental effects of inherent and process escape flaws in AM components, assuming those flaws go undetected. This assumption is in line with standard damage tolerance assumptions regarding the presence of an undetected flaw. If a flaw is detected, then AM components should be assessed through the non-

conformance process, as is typical for aerospace parts. Cost and schedule benefits provided by AM should weigh heavily when assessing nonconformances on AM components. AM generally allows for the production of complex hardware at significantly reduced costs per unit compared with more traditional manufacturing processes. Thus, the resources associated with scrapping parts are reduced.

The intent of the rationale outlined is not to support the use of components with detrimental defects or with sub-standard material quality. In particular, given the lack of experience with applying *in-situ* inspection and PDTAs to AM components, caution is warranted in using these approaches to assess the suitability of AM components with known defects. Using a conforming component is preferable to justifying the use of a nonconforming component in terms of safety and structural integrity. The effort required to evaluate and show nonconforming components as acceptable may, in many cases, outweigh the expense required to make a replacement.

7.2.11 Additional Considerations

7.2.11.1 Residual Risks

The described framework contains several residual risks that are not fully accounted for in the approach. These include the risks associated with process escape flaws from unidentified types of process escapes, extreme values in the inherent flaw distribution, and insufficient characterization of the inherent flaw state.

7.2.11.1.1 Flaws from Unidentified Types of Process Escapes

A PFMEA may be used to methodically assess the AM process to identify the types of potential process escapes and activities that could mitigate the risk associated with those process escapes. However, the PFMEA approach is only as good as the rigor and current level of understanding associated with its development. Types of process escapes that are not identified during the PFMEA represent a risk in that the potential for those process escapes to result in a flaw are not accounted for in the rationale. This risk may be reduced by pooling resources and experience to develop an appropriately comprehensive listing of potential AM process escapes. As the pool of AM users grows, the likelihood of a user encountering a rare or unusual process escape or process escape flaw increases. Sharing information between AM users regarding lessons learned and identified process escape flaws can reduce risk for the entire metallic AM community. Shared results from root cause failure analyses of failed AM parts would be particularly valuable. Currently, AM knowledge tends to be siloed; facilitating sharing of lessons learned and AM component process escapes in a way that protects proprietary and export-controlled information would reduce the chances of a failure due to an unknown or undetected process escape.

O-2. AM competitive factors (e.g., business, organizational, legal, cultural, etc.) minimize open knowledge transfer (e.g., best practices, lessons learned, etc.).

7.2.11.1.2 Extreme Values in Inherent Flaw Distribution

While the frequency of inherent flaws distribution is expected to support direct characterization, extreme values in the inherent flaw distribution may be sufficiently rare that they are not readily observed and may not be included in the baseline mechanical property definition. Probabilistic approaches may be useful for assessing the risk associated with large inherent flaws. Truncating the extreme values of the inherent flaw distribution might address this risk. There may be some

physics-based limit on the size of an inherent flaw, or a sufficient inspection technique might be capable of detecting the largest inherent flaws.

7.2.11.1.3 Insufficient Characterization of Inherent Flaw State

The inherent flaw state should be characterized and representative of the AM process. This includes accounting for relevant influence factors of the AM build (e.g., thermal history, part geometry, thin walls, spatial variation, and AM system differences) and other aspects of the AM process (e.g., heat treatment, feedstock quality, and surface finishing). Insufficient characterization of the inherent flaw state leaves a risk that process characterization data (e.g., design properties) do not sufficiently capture the effects of the inherent flaws.

However, the definition of a sufficient flaw state characterization has not been established. Additional work is needed to understand the potential sources of variability in a flaw state, the means of describing and using flaw state information in analyses, and the sensitivity of the material property response to variability in the flaw state. A critical aspect will be characterization of the inherent flaw state throughout the appropriate AM process window, including the potential need to assess material flaw state outside the bounds of nominal operation.

7.2.11.2 Role of Process Control

Without supporting inspection data, fracture control approaches for un-inspectable hardware must necessarily rely on damage tolerance tests or process control rationale to make up for the limitations of unbounded fracture analysis. Of these, process control rationales may be most broadly applicable, as complex geometry likely precludes robust damage tolerance testing for many AM components.

7.2.11.2.1 Process Development

Aerospace-quality parts are expected to be composed of aerospace-quality materials, which precludes the presence of significant material defects in the nominal material condition. Components produced via AM are no exception. AM materials are process sensitive, so robust process controls are necessary to ensure consistent production. Significant process-specific defects (e.g., hot tearing, contour peeling, high levels of porosity, etc.) are expected to be evaluated during process-development activities.

Inadequate process development presents a risk of high occurrence rates of process escape flaws. Rationale based on characterization of the inherent flaw distribution is not intended to account for material inadequacies due to insufficient process development. In scenarios where process escape flaws are common, inclusion of these process escape flaws in the inherent flaw distribution is not recommended, as assumptions that apply to the inherent flaw distribution (e.g., bounding limits on extreme values or the influence of the inherent flaws on material properties) may not apply.

7.2.11.2.2 Process Monitoring

An AM process must be appropriately developed and characterized, and it must be continuously monitored to ensure consistency. NASA-STD-6030 enforces this consistency through documentation and control of process parameters and the implementation of statistical process control. Witness coupons (e.g., tensile and fatigue test specimens and metallurgical examination specimens) are produced on each build and are intended to be tested or otherwise evaluated to

ensure the AM process remains within the established bounds of the developed process window. A key assumption of the inherent flaw distribution is that the process remains reasonably consistent such that assumptions of the nature of the inherent flaw distribution are broadly applicable to components built with the characterized process. In this sense, the inherent flaw state becomes a critical material parameter that should be assessed and controlled for high criticality AM components. In some cases, the addition of specialized witness coupons that evaluate flaw state may be beneficial for demonstrating sufficient process consistency.

7.2.11.2.3 Known Process Escapes

The previously described approach assumes that the AM process is operating within its qualified boundaries, ensuring that assumptions regarding consistency in material quality remain valid. In situations where known process escapes occur (e.g., an outside-the-limit process-monitoring parameter or a mechanical witness test result that falls below the acceptance criteria), the AM build material cannot be assumed to contain the representative inherent flaw distribution. As a result, established mechanical properties, particularly those influencing fatigue and fracture mechanisms, may not be applicable. In addition, the build must be evaluated for flaws generated by the detected process escape. Assessments of nonconforming AM components should address both risks. At the current state of technology, process escapes may not always be detected. As discussed in Section 7.2.10, the costs and risks associated with evaluating an AM component with a known process escape may outweigh the costs of producing a replacement component.

7.2.11.3 Flaw Occurrence Rates

Flaw occurrence rates for AM materials are often orders of magnitude more frequent than flaws associated with more traditional materials, particularly wrought materials. While many of these flaws would be expected to be benign, an AM process that generates significant quantities of small flaws or occasional large flaws may not be sufficient for all applications. Fracture control assumptions relying on limited flaw occurrence rates (e.g., one flaw per part) may need to be reevaluated. That is, the typical assumption of the worst-case flaw in the worst-case location may have less conservatism for AM materials due to the potential for interactions between multiple flaws or damage sites. Such interactions are more likely due to the higher flaw frequency of occurrence for this product type. Additionally, the mechanisms leading to flaw formation can generally occur anywhere within an AM component. In contrast, flaws in conventionally manufactured materials might be more likely to occur in certain areas (e.g., stress concentrations, machined locations, etc.).

7.2.12 Future Work

7.2.12.1 Flaw Characterization

Methodologies for appropriately characterizing the inherent flaw distributions are needed. Inspection approaches for inherent flaw characterization are discussed in Section 7.5, but few techniques can obtain the required resolutions to evaluate inherent flaws, and those that can are expensive and time consuming. Optimal means of assessing for inherent flaw state should balance the challenges of characterizing inherent flaws with the resolution needed on the inherent flaw state definition. Inherent flaw characterization should account for variability within the process box and other relevant influence factors. Section 7.6 discusses considerations for characterizing the inherent flaw state.

Once inherent flaw data are obtained, questions remain about the information required to appropriately describe the distribution. Flaw criticality is influenced by size and overall frequency of flaw occurrence, by flaw morphology (e.g., aspect ratio, sphericity, etc.), and by location within the component. Current probabilistic analysis techniques rely on flaw size as an analog for the more detailed flaw morphology metrics. AM may require more information regarding the characteristics of the flaws to account for the potential effects of these flaws.

7.2.12.2 PDTA Tool Assessment

In addition to the DARWIN tool discussed in Section 7.2.7.3, other probabilistic assessment tools have been developed for different applications. Examples include the Extremely Low Probability of Rupture (xLPR) Probabilistic Fracture Mechanics Code, the Probability of Fracture (PROF) code, and Probabilistic Fatigue Assessment of Components with Defects (ProFACE).

The xLPR Probabilistic Fracture Mechanics Code software is used by the United States (US) Nuclear Regulatory Commission for the probabilistic assessment of dissimilar metal welds in nuclear piping applications. The tool can model fatigue initiation and growth, propagation of existing surface cracks, and effects of environmentally assisted crack growth. However, the model geometries are limited to axial and circumferential cracks in pipes [Homiack et al., 2021].

The PROF tool was developed by the US Air Force for probabilistic risk assessment for fatigue damage in aircraft. PROF calculates the probability of exceeding the critical fracture toughness given distributions of possible initial crack sizes, flight loads, and material fracture toughness [Hovey et al., 1998].

The ProFACE analysis package was developed by Politecnico di Milano in Italy. This package is based on a fatigue approach that compares component flaw sizes with critical flaw sizes for the relevant stress state. As a result, the ProFACE approach accounts for crack initiation life from a possible flaw rather than modeling crack propagation life [Romano et al., 2019].

Existing PDTA tools have been developed for specific applications and for the industry needs and regulatory frameworks they were intended to support. These tools will need to be verified and validated to support the widespread acceptance of this technique for demonstrating compliance with NASA fracture control requirements. Due to the specialized nature of PDTA, tools will likely need to be developed or advanced to complement the NASA workflows and use cases. As an historical example, the deterministic damage tolerance analysis tool NASGRO has been continually developed for over 30 years with guidance and input from NASA and other government agencies and is an accepted tool for demonstrating damage tolerance by analysis in NASA-STD-5019. A similar path might be needed for a PDTA analysis tool. To facilitate this, an assessment of available PDTA tools should be performed with a focus on the capabilities and limitations and alignment with NASA approaches. For PDTA tools that show promise, sensitivity studies should be performed to help understand key inputs to the analysis and build expertise in the use of these tools and the interpretation of their results.

7.2.12.3 PDTA Integration into Structural Analysis Workflows

For PDTA approaches to be adopted, the use of these tools must be integrated into existing NASA structural analysis workflows. For example, in DARWIN, the FE model used for the PDTA is important to the analysis in terms of stress modeling accuracy and computational time. Anomaly characterization in terms of AM material evaluation and appropriate exceedance curve

generation must be understood and performed appropriately. Finally, material properties in terms of fracture data, flaw state, and inspection capability need to be applied to the model in the appropriate regions. Thus, the development of training and case studies will be important to teach analysts how to use the tool and the means to apply the results to AM-specific problems. Ideally, these cases would test the limits of the analysis tools by including extreme examples of design and loading aspects. For example, analysts should consider various features, including, but not limited to:

- Thin sections.
- Thick sections.
- Rapid thickness transitions.
- Overhangs.
- Stress concentrations.
- Mixed loading (e.g., pressure plus bending).

The following are functions of the previous aspects but should be covered by pilot case studies:

- High sensitivity to surface flaws.
- High sensitivity to sub-surface flaws.
- High sensitivity to nonlinear flaws.
- Effects of flaw state density (high and low).

With development of appropriate analysis inputs and verification and validation of analysis tools, PDTA has the potential to facilitate damage tolerance analysis for AM components.

7.2.12.4 Integration with Computational NDE

NDE simulation tools that can predict the probability of detection are in development [Vienne et al., 2022]. When based on modeling the physics of an NDE inspection technique (e.g., CT) interacting with a specific component geometry, the simulation tools have the potential to produce a computationally derived probability of detection. Such tools may be able to determine a spatially dependent minimum detectable flaw size that could be compared with CIFS locally within a component. If validated, computational NDE approaches could support PDTA by defining more explicitly the detection capabilities of a particular NDE technique and improving the fidelity associated with comparisons of detectable flaw sizes and critical initial crack sizes. For example, development of integrations between DARWIN and computational NDE approaches would support more robust rationales using probabilistic approaches.

7.2.12.5 Flaw Location Effects

Material generated by L-PBF tends to have a higher concentration of flaws near the component surface, where AM process parameters (e.g., laser on/off settings and laser turnaround time) can have a significant impact on the melt pool stability. Thus, probabilistic and deterministic damage tolerance analysis may have to account for different flaw distributions in different component regions based on distance to a free surface. In some scenarios, inspection capability may be higher for regions near a surface, so location-specific probability of detection estimates may be important. In an ideal case, critical flaws may be more detectable than might otherwise be the case because of the increased likelihood of that flaw occurring near the surface.

7.3 Flaw Types

As discussed in Section 7.1, the inherent flaw state is defined by the AM process. Inherent flaws are representative of the nominal operation of a qualified AM process. Thus, the specific nature of the inherent flaw state will vary based on the AM process category (e.g., L-PBF versus DED), the AM system, part post-processing, and other potential influence factors.

A baseline assumption is that a developed, understood, and characterized AM process is in place to support the definition of a flaw state. In an established AM process, assumptions regarding the consistency in flaw state and the effects of the inherent flaw state on material properties are reasonably supported by process qualification and characterization efforts. This baseline assumption of a mature AM process is appropriate in the context of fracture critical AM components, as only robust AM processes should be considered for fracture critical spaceflight hardware production.

While the inherent flaw state is dependent on the specifics of the AM process, some AM flaw types are more likely than others to be inherent. Recently, Mostafaei et. al. [2022] have published a comprehensive review of the current state of understanding of AM flaws in the PBF AM process category, and the reader is referred to that publication for an in-depth review. However, brief discussions of the categorization of common L-PBF flaws in the context of inherent and process escape flaw categorization are provided in the following sections.

7.3.1 Porosity

Porosity is commonly observed in metallic L-PBF materials and falls broadly into three classes: LoF, gas-entrapped porosity, and keyhole porosity. Each class of porosity arises through a different mechanism within the L-PBF process and can be distinguished based on the flaw size and morphology [Poudel et al., 2022]. The porosity shape in L-PBF is often indicative of the flaw formation mechanism. Irregular voids can indicate LoF pores where incomplete melting occurs, while large spherical and quasi-spherical voids can indicate keyhole porosity generated by the melting process. Small spherical voids often indicate gas-entrapped porosity, which is typically transferred from the powder feedstock.

7.3.1.1 Lack of Fusion (LoF)

LoF flaws are characterized by irregular voids that tend to occur between melt pool tracks. LoF flaws may or may not contain unmelted powder [Brennan et al., 2021]. A typical inherent LoF flaw is shown in Figure 7.3.1.1-1. For material subjected to hot isostatic pressing treatment, LoF flaws can collapse into crack-like features like the one shown in Figure 7.3.1.1-2.

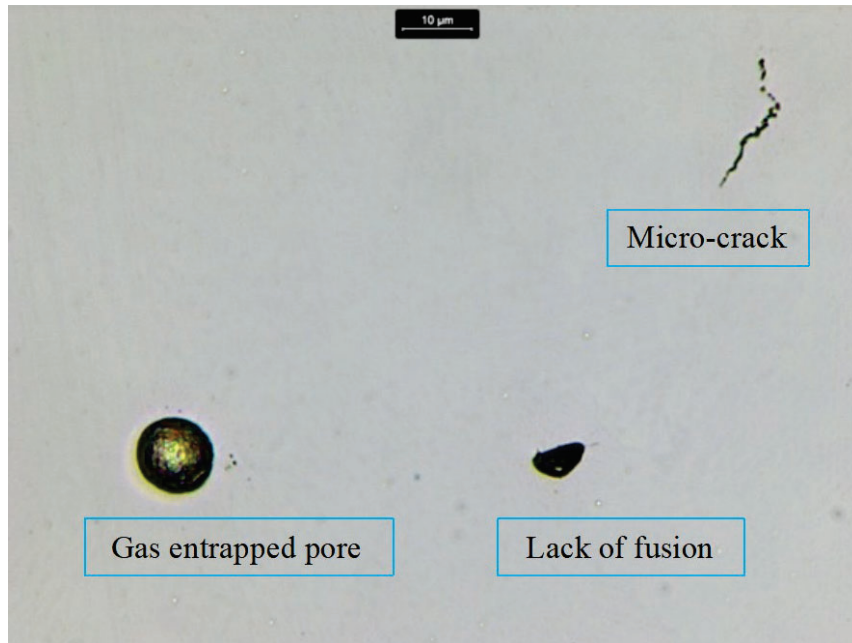


Figure 7.3.1.1-1. Examples of Flaws in L-PBF Materials

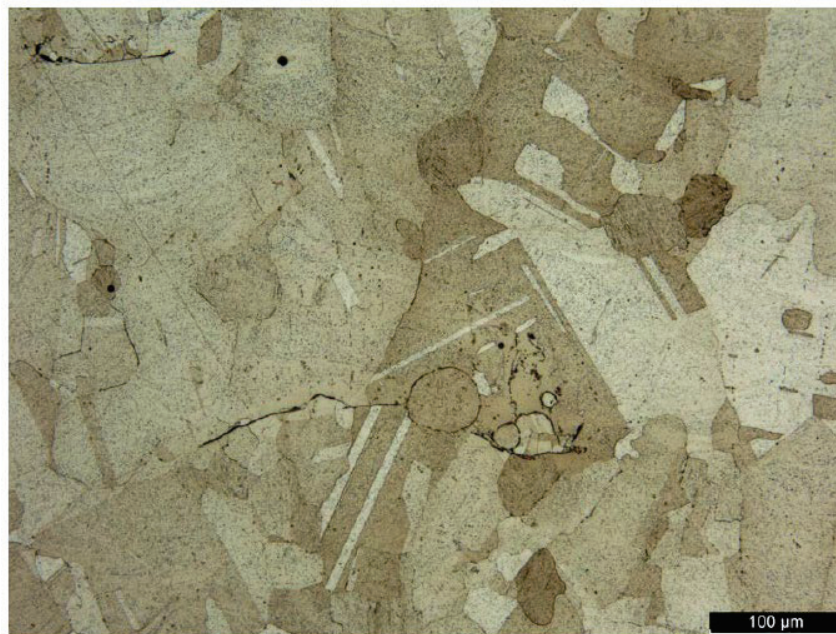


Figure 7.3.1.1-2. Collapsed LoF Flaw in L-PBF Alloy 718 Post Hot Isostatic Press [Wells, 2016]

Small LoF flaws like that shown in Figure 7.3.1.1-1 can be observed even in well-controlled L-PBF processes, albeit with occurrence rates low enough to have minimal effect on the mechanical properties. Such flaws would be classified as inherent and characterized based on the metallurgical quality assessments as part of the AM process development and qualification.

The occurrence of LoF flaws is associated with the melt pool geometry, which is affected by the energy source scanning parameters (i.e., power and scan speed) and build geometric parameters (i.e., hatch spacing and layer thickness). Additionally, specific material properties (e.g., density,

melting temperature, and thermal conductivity) affect the melt pool size through influences on the melt pool dynamics or interactions with the energy source. Since melt pools are roughly semicircular when viewed in cross-section perpendicular to the energy source scan direction, sufficient overlap between neighboring melt pools on the same layer and previously melted layers is required to avoid LoF flaws. Theoretically, a set of process parameters can be selected that would eliminate LoF flaws by ensuring sufficient melt pool overlap [Mukherjee and DebRoy, 2018]. In practice, melt pool size does not remain in a steady state, instead varying due to interactions with inhomogeneities in the powder bed or attenuation of the energy source due to interactions with the build environment. Other mechanisms leading to the occurrence of LoF flaws include flaws caused by unfavorable feedstock particles that prevent full melting due to packing density or chemistry changes [Mostafaei et al., 2022].

In some cases, periodic or large LoF flaws may be indicative of a process escape or a lack of robust process development. Periodic LoF flaws are typically associated with improper hatch-spacing parameters or powder bed irregularities, where the melt-pool size is not sufficient to lead to complete penetration of the melt pool into prior layers. Large LoF flaws might be associated with a process escape (e.g., toolpathing errors or transient parameter deviations, leading to incomplete wetting in W-DED processes).

7.3.1.2 Keyholes

Keyhole porosity is associated with vaporization mechanics caused by high heating rates within the melt pool. Under certain processing conditions, the energy input to the feedstock is sufficient to cause vaporization, leading to a gas bubble within the melt pool. This gas bubble, containing a mixture of vaporized metallic material and environmental process gas, becomes entrapped upon solidification [Mostafaei et al., 2022].

Keyhole porosity is associated with an excess of energy imparted to the feedstock material. The amount of keyhole porosity tends to increase for processing parameters with high input energy density that causes over-melting of material. Keyholing can be reduced by proper selection of the build parameters but must be balanced with obtaining sufficient energy input to produce minimal amounts of LoF porosity.

Keyholes tend to form more favorably at regions of non-steady-state energy source operations (e.g., energy source turnarounds or track starts and ends). In these regions, the non-steady-state operation of the energy source increases the likelihood of over-melting, leading to keyhole flaws [Mostafaei et al., 2022].

7.3.1.3 Gas Entrapment

Porosity can be caused by the entrapment of environmental gases within the material. In L-PBF processes, gas entrapped porosity arises primarily from the powder feedstock. Powder feedstocks for AM processes are commonly produced using a gas atomization procedure where molten material interacts with a high-speed stream of process gas. The solidification mechanics of the powder droplets can lead to capture of the process gas within the powder particle, forming a metallic bubble. This entrapped gas porosity is retained within the final AM material if there is not sufficient time between melting and solidification for the gas bubble to escape the melt pool [Gratl et al., 2022a]. Entrapped gas porosity can also arise from interactions with moisture in the feedstock or due to gas solubility variations during cooling [Mostafaei et al., 2022].

Figure 7.3.1.3-1 shows representative gas entrapped pores in a cross-section of heat-treated L-PBF Alloy 718.

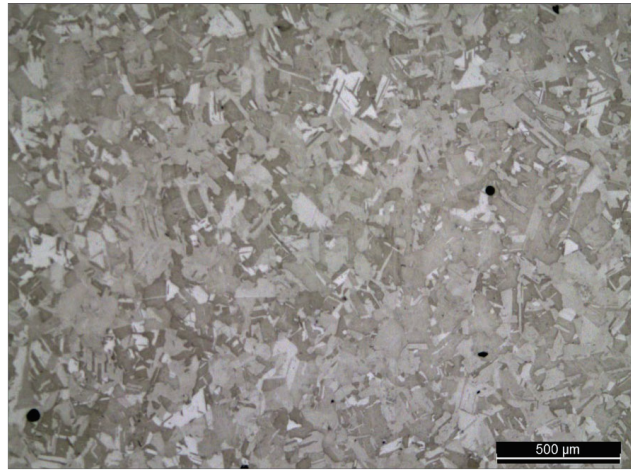


Figure 7.3.1.3-1. L-PBF Alloy 718 showing Small Entrapped Gas Porosity

7.3.2 Other Flaw Types

7.3.2.1 Spatter

Spatter results from particles ejected from the melt pool that redeposit back onto the powder bed. The spatter particles can be molten material that ejects from the melt pool due to vaporization pressures, partially melted material that is not subsumed into the melt pool, or un-melted material from the powder bed that is ejected due to environmental gas heating.

Spatter flaws manifest in several ways. Spatter particles can affect the packing density of the powder bed, leading to LoF flaws due to insufficient feedstock density. Figure 7.3.2.1-1 shows an embedded spatter particle and an associated LoF flaw. Large spatter particles can interact with the powder recoat system, leading to powder bed inhomogeneities and associated LoF flaws. Spatter can lead to chemical inclusions that form undesirable phases within the material. For spatter particles that do not redeposit into melted areas of the powder bed, the particles may remain within the powder handling system, affecting the feedstock particle size distribution and chemistry. This can lead to LoF flaws, due to insufficient melting or packing density around larger spatter particles, or out-of-tolerance chemistry that affects subsequent metallurgical performance.

Spatter occurs as part the AM process, although the specifics of the process parameters influence the degree to which spatter is generated. Specifically, energy source parameters that lead to high temperatures within the melt pool are more likely to generate the vaporization mechanisms necessary to cause particle ejection [Mostafaei et al., 2022]. Some degree of spatter-induced flaws would be expected to be inherent to an L-PBF process. However, spatter-generated flaws likely have a highly stochastic nature in that there is some probability associated with the spatter redepositing on the powder bed in a manner that affects the component.

Spatter occurrence can be exacerbated by process escapes (e.g., incorrect scanning parameters or insufficient process gas flow). Such process escapes would be associated with a higher probability of generating a spatter particle and a higher probability of that particle landing on an impactful area of the powder bed.

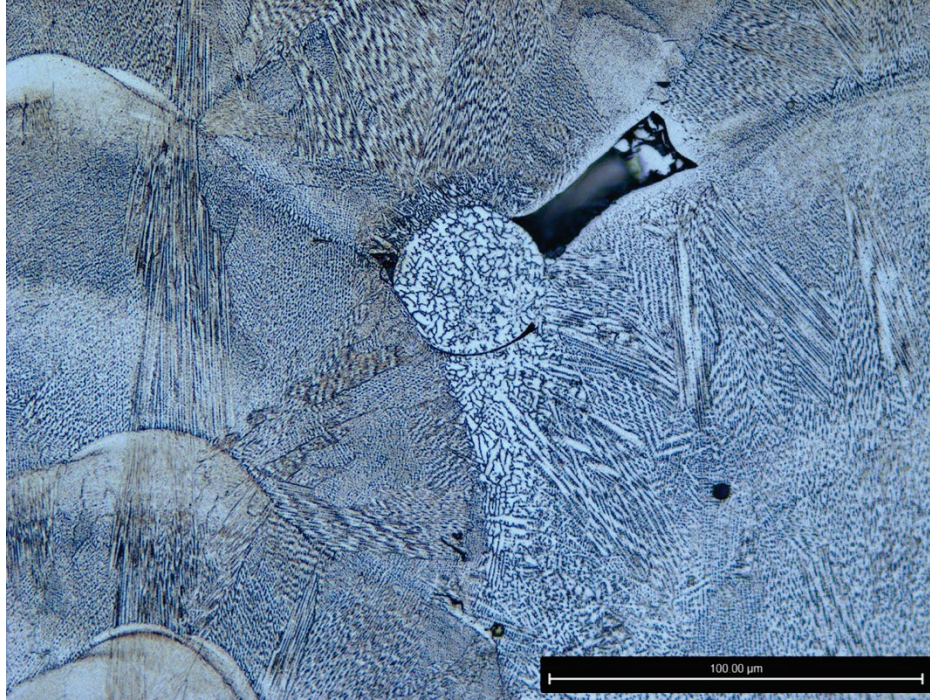


Figure 7.3.2.1-1. Embedded Spatter Particle with Associated LoF Flaw

7.3.2.2 Chemical Inclusions

Chemical inclusions consist of a range of compounds that form due to the reaction of the metal alloy with environmental gases or from impurities entrapped in the feedstock. Chemical inclusions take the form of oxides or nitrides and are frequently observed in alloys containing aluminum or titanium. Figure 7.3.2.2-1 shows an example of a titanium nitride inclusion found in L-PBF Alloy 718.

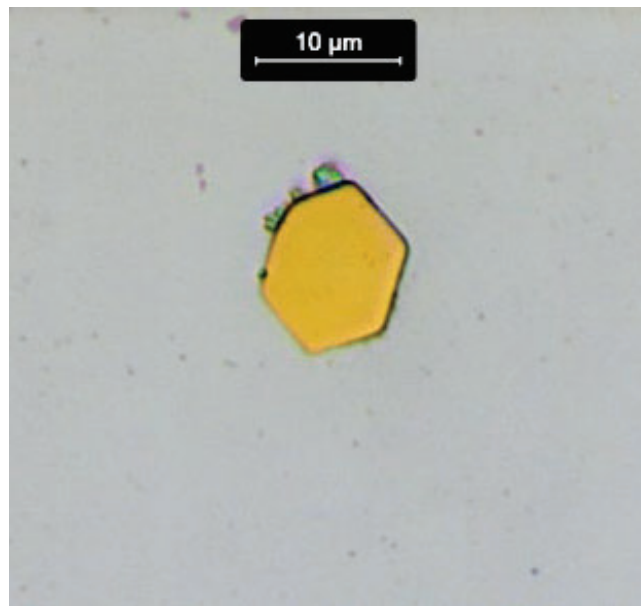


Figure 7.3.2.2-1. Titanium Nitride Inclusion in L-PBF Alloy 718 produced at MSFC

Advances in alloy development have resulted in alloys with chemistries tailored for the AM process. Several aluminum alloys have been modified to improve material properties and buildability through the addition of dispersed ceramic particles that tend to refine grain sizes and reduce the propensity for solidification cracking [Rometsch et al., 2022]. While intentionally added, these ceramic particles represent potential inherent flaws in the sense that, like porosity-type flaws, inclusions that reach a size or density threshold may begin to have detrimental impacts on the material performance. For such alloys, inclusions should be characterized, and processing controlled to ensure a consistent baseline with the desired material properties. Inconsistency in the dispersion of the inclusions (e.g., through coalescence or agglomeration) could detrimentally affect properties.

7.3.3 Process Escape Flaws

While the distinction between inherent and process escape flaws is not based on flaw type, some flaws are expected to be primarily caused by AM process escapes. Flaws arising from residual stress cracking (e.g., the cracks formed in the L-PBF Alloy 625 component shown in Figure 7.3.3-1) are expected to be primarily process escape flaws. In this case, the process escape might have been a lack of sufficient design for AM to mitigate residual stress cracking or a deviation in the AM processing parameters leading to greater residual stress development. Another example is the “skipped layer” flaw shown in Figure 7.3.3-2 that occurred in an L-PBF Alloy 718 build due to an intentional build artifact that caused the machine to skip melting of this region of the component during several layers.

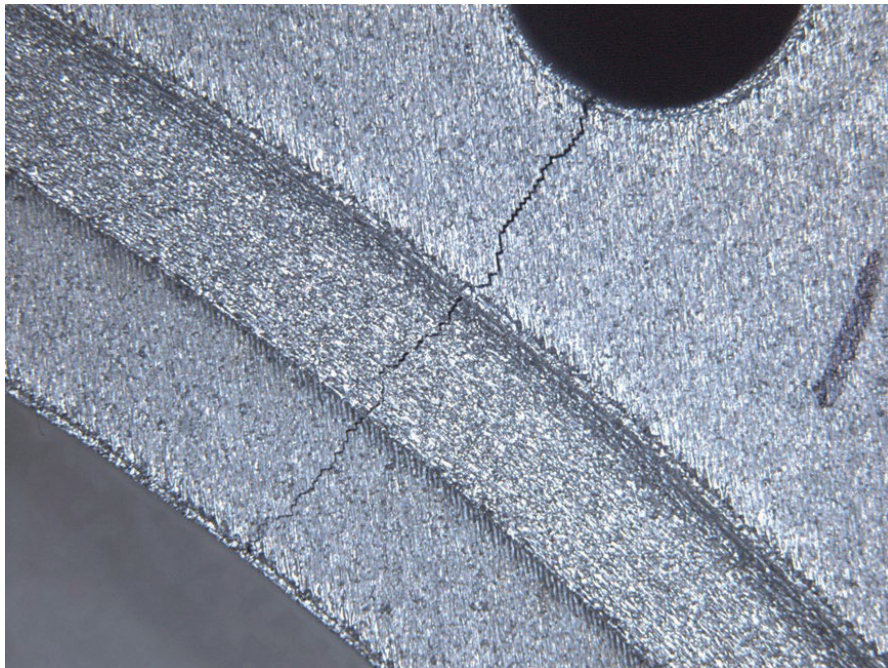


Figure 7.3.3-1. Residual Stress Crack in L-PBF Alloy 625 Component

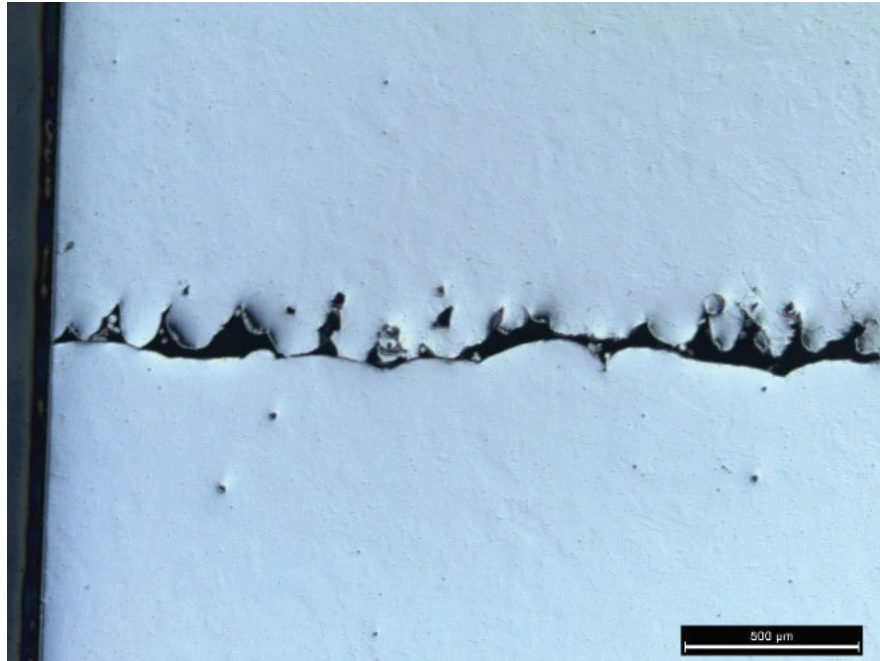


Figure 7.3.3-2. Skipped Layer Flaw

These examples illustrate the need for robust AM process controls to ensure the types of process escape flaws that arise from inadequate process or part qualification do not manifest in critical applications. First article inspections and periodic article or sub-article inspections provide a means to monitor the AM process for residual stress-induced flaws.

7.4 Effect of AM Flaws

7.4.1 Material Properties

As with all materials, the physical and mechanical properties used for component design should be representative of the material used for the component. For traditional materials, variability in material properties is controlled using specifications that define acceptable limits on chemistry, heat treatments, and other influence factors. For AM materials, flaw state represents an additional influence factor that will likely vary within some range based on the specifics of the AM process. Design properties should reflect the impact of the material flaw state.

7.4.2 Tensile

The inherent flaw state of a qualified AM process is expected to have relatively low quantities of small AM flaws. Such flaw states are not expected to have a significant impact on static material properties for AM materials. Wilson-Heid et al. [2019] found that tensile strengths for L-PBF 316L stainless steel were not significantly affected by individual embedded flaws up to ~2.5 mm (0.1 inch) in diameter, although tensile elongation began to decrease for a 1.8 mm (0.07 inch) diameter flaw. However, low ductility materials may show greater sensitivity to individual flaws of smaller sizes. For example, Boyce et al. [2017] observed ductility loss in L-PBF 17-4 stainless steel for sub-sized tensile specimens with individual flaws on the order of 1 mm (0.04 inch).

Elambasseril et al. [2019] found varying flaw states through the build height of an EB-PBF Ti-6Al-4V process. The varying flaw state densities had an impact on the tensile properties, with samples with higher flaw quantities exhibiting decreased ductility. However, the strength values

were comparable, and the material with the least porosity exhibited the lowest strength, likely due to differences in the α -lath size [Elambasseril et al., 2019]. These trends would be expected to be similar for a L-PBF process.

Figure 7.4.2-1 shows tensile stress-strain curves for two builds of L-PBF Alloy 718. These builds were post-processed with the same heat treatments, and all test specimens were machined. A ventilation error occurred during the processing of the second build, leading to an increase in LoF flaws. The effect of the flaws manifested as significantly reduced elongation at fracture, as apparent from comparing the truncation of the stress-strain curves representing material containing significant LoF defects. However, the yield stress was similar between the two builds. Additionally, the ultimate strength was lower for the build with flaws, reflecting the lack of full strain hardening due to premature failure due to defects [Wells, 2016]. These trends are common in AM materials, with strength properties for AM materials similar to those of wrought products and relatively unaffected by flaw state. However, ductility is more sensitive to flaws [Snow et al., 2020]. Extremely high occurrence rates of inherent flaws could have significant effects on static strength and material ductility, but such issues would be expected to be resolved during AM process development, such that a severely detrimental flaw state would not be representative of a qualified AM process.

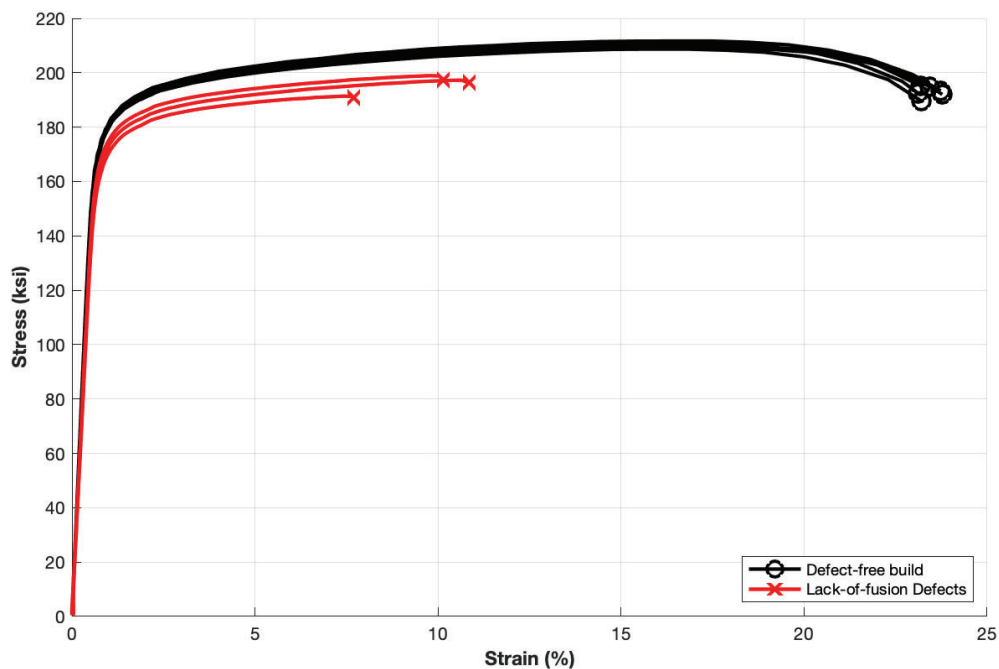


Figure 7.4.2-1. Stress-strain Curves from L-PBF Alloy 718 [adapted from Wells, 2016]

7.4.3 Fracture Toughness

Fracture toughness properties are affected by flaw state in a similar manner to tensile properties, in that high flaw quantities reduce the ductility of the material and concentrate stresses.

Figure 7.4.3-1 shows ASTM E1820 fracture toughness test results for two L-PBF Alloy 718 specimens. The specimens were produced on the same build, post-processed in the same manner, and tested at $-196\text{ }^{\circ}\text{C}$ ($-320\text{ }^{\circ}\text{F}$). An approximately one-third reduction in initiation toughness was observed, as evidenced by the lower resistance curve measured from the specimen with observed flaws (diamond markers). This specimen contained a high quantity of LoF flaws at the fracture plane. Figure 7.4.3-2 shows the fracture surface. The gold-colored LoF flaws show in

sharp contrast to the fully consolidated material, which is shown in blue due to a heat-tinting treatment that was applied post-test to indicate the extent of crack propagation during the test.

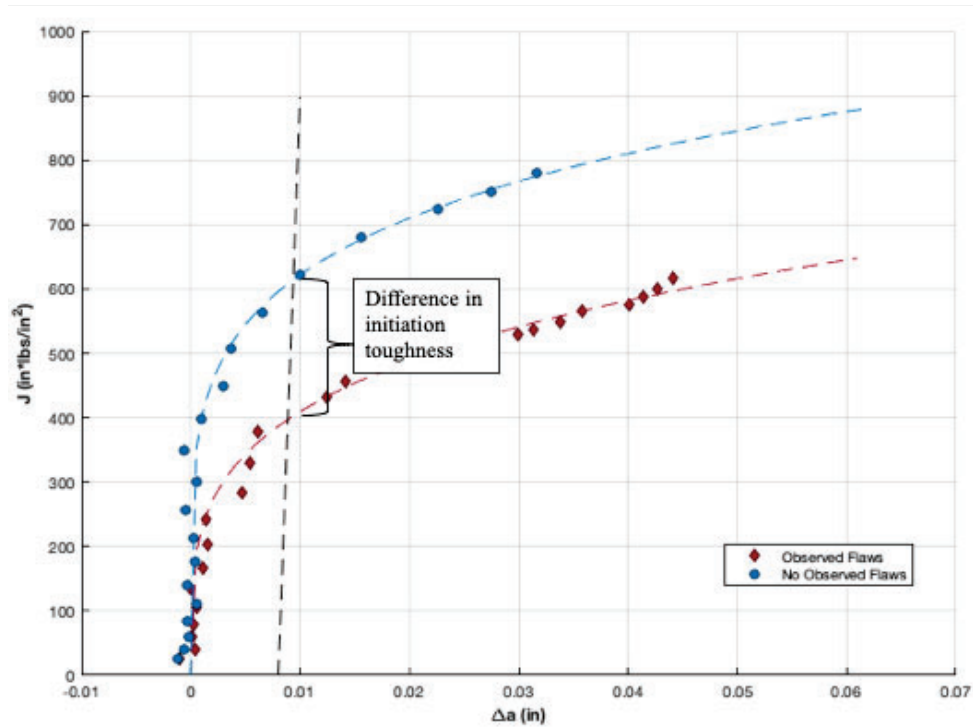


Figure 7.4.3-1. Fracture Toughness Tests from L-PBF Alloy 718 with Different Flaw States

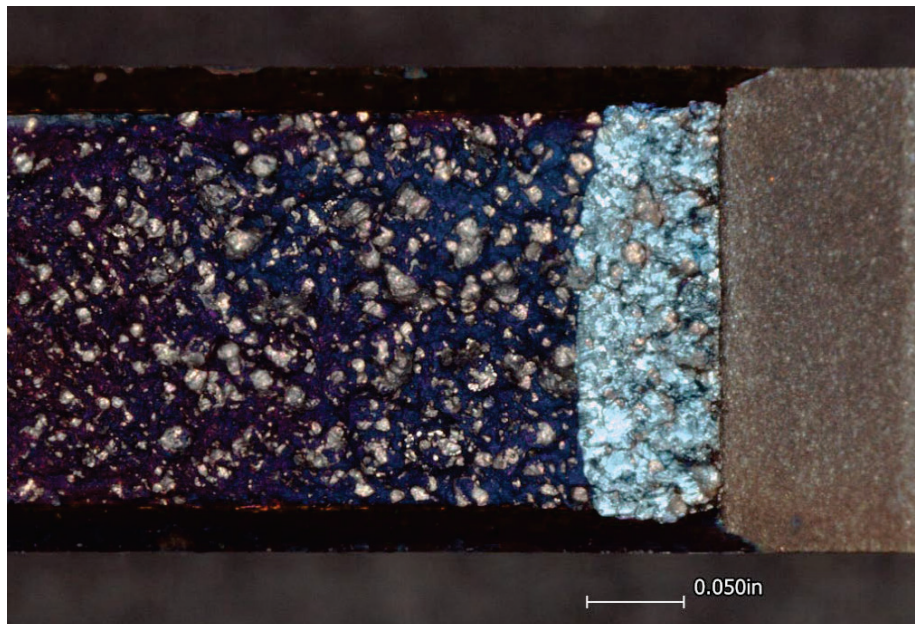


Figure 7.4.3-2. Fracture Surface of L-PBF Alloy 718 Specimen showing Significant Population of LoF Flaws

The severely detrimental flaw state for the material in these two examples is not representative of an inherent flaw state in a controlled L-PBF process. In these examples, process gas flow errors lead to an increased occurrence of LoF flaws. This is a process escape; thus, these are process escape flaws. Individual inherent flaws are unlikely to significantly impact the material properties in a controlled AM process. However, variability in the population of the inherent flaws may become significant enough to begin to affect static properties, and characterization of process capabilities should account for the acceptable limits of the flaw state generated by the AM process.

7.4.4 Creep

Several references on creep properties of AM materials point to the interaction of microstructural phases as the main influences on creep behavior [Spigarelli et al., 2022; Kuo et al., 2018]. For example, Son et al. [2020] performed creep tests on L-PBF Alloy 625 at durations to 6 months. They found no significant reduction in creep strength relative to wrought products but did observe a decrease in the creep elongation. Several mechanisms were proposed, but the root cause of the elongation loss was not conclusively determined. The authors speculate that chemical interactions in the microstructure led to the creep elongation reduction but acknowledge that an increase in porosity for the L-PBF material relative to the wrought material may have impacted the results [Son et al., 2020].

7.4.5 Fatigue

AM flaws typically have a more significant impact on material properties under cyclic loading, where the localized effects of the flaws can lead to earlier crack initiation and propagation compared with flaw-free material. AM flaws often, but not always, act as initiation sites for fatigue cracks. Reviews of fatigue and crack growth rate properties of AM metals are available from Becker et al. [2021] and Sanaei and Fatemi [2021].

Fatigue performance is affected by material flaws or inclusions. Murakami [2002] described equations relating the size of a flaw or inclusion (using the square root of the projected area of the flaw) and the microstructure to the material fatigue limit. Larger flaws led to decreases in the fatigue limit [Murakami, 2002]. This approach has been extended to understanding the effects of flaw size on fatigue in AM materials [Radhakrishnan et al., 2022; Benedetti et al., 2018; Yamashita et al., 2017].

Sanaei and Fatemi [2020] showed that fatigue life for L-PBF and E-PBF Ti-6Al-4V correlated with the size of the initiating flaw apparent on the fracture surface of the fatigue coupon. However, the magnitude of this effect was microstructure dependent. Ti-6Al-4V materials with lamellar microstructures typically exhibited longer fatigue lives with similar flaw sizes relative to martensitic microstructures. A reasonably good agreement between the apparent initiating flaw on the fracture surface and an initiating flaw size predicted from metallurgical cross-sections and an extreme value statistical approach was demonstrated [Sanaei and Fatemi, 2020].

Benedetti et al. [2018] conducted CT scans of L-PBF Ti-6Al-4V fatigue test specimens. They found that the size of the initial flaw leading to fatigue failure represented greater than the 98th percentile flaw size based on extreme value distribution methodologies, indicating that the maximum flaw size drives the fatigue failure. Hot isostatic press treatments reduced the flaw sizes in the material, leading to a smaller initiating flaw and an associated improvement in fatigue life [Benedetti et al., 2018].

However, the effect of AM flaws may be material dependent. For example, Radhakrishnan et al. [2022] performed fatigue tests on L-PBF Alloy 718 with as-built microstructures and observed that fatigue failures initiated from relatively large LoF flaws, typically on the order of 250 microns (μm) (0.01 inch) [Radhakrishnan et al., 2022]. Muhammad et al. [2021] found that, for heat-treated L-PBF Alloy 718 with low densities of small porosity, crystallographic facets sometimes served as the initiating feature, suggesting that fatigue properties for AM Alloy 718 may not be as sensitive to flaw state as other AM alloys [Muhammad et al., 2021]. These results were confirmed by Dodaran et al. [2022], who ran crystal plasticity simulations and demonstrated that grain size was more influential than flaw size on fatigue life until the flaw size was a significant percentage of the overall grain size [Dodaran et al., 2022].

7.4.6 Fatigue Crack Growth Rate

Fatigue crack growth rates for L-PBF materials tend to be comparable with growth rates for wrought products. Studies have shown that AM Ti-6Al-4V and AM Alloy 625 are relatively insensitive to flaw state for Region II crack growth rates. However, microstructural features are important, as fine grain structures result in lower threshold stress intensity factors relative to more coarse microstructures due to the reduced degree of crack closure. Grain structures in the AM material resulting from the AM build can influence crack growth propagation, resulting in anisotropic crack growth properties [Becker et al., 2021].

Poulin et al. [2019] conducted studies on the effect of porosity on L-PBF Alloy 625 by varying build parameter sets to induce varying concentrations of LoF flaws. They observed that threshold stress intensity and Paris region crack growth rates were similar for porosity levels up to $\sim 1\%$, while specimens with $\sim 3\%$ porosity exhibited growth rates that were slower than the denser material. The authors attribute this effect to microstructural differences between the materials and crack branching that is facilitated by the high flaw density. At high applied stress intensity, the growth rates began to trend with porosity, with higher porosity resulting in lower critical toughness values [Poulin et al., 2019].

7.4.7 Factors affecting Flaw Severity

Sanaei et al. [2019] investigated the spatial variability of flaws in L-PBF Ti-6Al-4V and 17-4 PH stainless steel. They found that the spatial variability of AM flaws was dependent on the processing parameters, post-build heat treatment, and surface finishing. For Ti-6Al-4V built with optimized processing parameters, they found no significant variability in spatial distributions for the examined build height and circumferential location around the specimen axis. However, they did observe high concentrations of AM flaws near the surfaces of their specimens. This near-surface trending was reduced when the as-built surfaces were removed. The spatial variability of the AM flaws decreased following a hot isostatic press treatment. In general, more spherical flaws, indicative of entrapped gas porosity, were more evenly distributed, while more irregular LoF flaws showed more significant spatial variability. As entrapped gas porosity is expected to be caused by gas entrapment in the powder feedstock, this porosity would be expected to be more randomly distributed than LoF flaws that are generated by interactions with the energy source that are influenced by the build geometry [Sanaei et al., 2019].

Flaw location may have a significant effect on the criticality of an AM flaw. For example, Benedetti et al. [2018] found a higher density of flaws within a region 0.4 mm (0.016 inch) in depth around a fatigue coupon made from L-PBF Ti-6Al-4V. This near-surface porosity served as the initiating flaws for fatigue tests with both as-built and electropolished surface finishes.

Benedetti et al. [2018] observed that the electropolishing treatment did not remove sufficient material to eliminate the near-surface porosity, instead exposing that porosity to the surface. Similarly, initiating defects for hot isostatic pressed or shot-peened coupons were located some depth into the coupon as the result of residual stresses that retarded crack growth at the surface and for a small distance into the coupon [Benedetti et al., 2018].

In FE simulations of idealized AM flaw shapes, Shao et al. [2023] found distance from the surface to be a significant influence factor on the criticality of a flaw relative to that flaw's size. They found that a near-surface flaw would rapidly propagate to become a surface-connected flaw under fatigue loading. Additionally, spherical flaws may be more detrimental to fatigue performance than elongated LoF flaws of the same size. This effect was attributed to the stress gradient developed by the flaw geometry, where the elongated LoF flaw generated a higher stress at the flaw surface that decayed quickly, leading to crack arrest. In contrast, the spherical flaws exhibited a more gradual stress gradient, which allowed for sufficient crack driving forces to maintain crack propagation [Shao et al., 2023].

These findings indicate that AM flaw criticality is dependent on its shape, size, and location within the component. Improved understanding of the effects of flaw location within a component may support rationales that account for the location-dependent properties of AM components.

7.5 Characterization Methods for AM Flaws

Characterization of flaws common to the AM process is an essential aspect of potential certification methods. NDE and *in-situ* monitoring are of particular interest as they can be applied to production hardware. Grounding the accuracy of these methods with higher fidelity (often destructive) approaches is necessary to establish levels of confidence in NDE and calibrate *in-situ* monitoring. Establishing flaw distributions for probabilistic approaches may require a combination of comprehensive destructive analysis and NDE.

7.5.1 Nondestructive Evaluation (NDE)

NDE encompasses a variety of techniques used to inspect for or observe flaws. Because the part is not intentionally damaged or fundamentally altered during inspection, NDE can be applied to production hardware and is often scalable for a large quantity of parts. For certain materials, geometries, and flaws, a given NDE technique may have limited or no applicability.

Comprehensive comparisons of various NDE techniques are discussed in Waller et al. [2014], Lopez et al. [2018], and Duarte et al. [2021]. NDE techniques will have varying applicability to AM flaw detection. Common inspection techniques and considerations for their use in AM flaw detection are discussed.

7.5.1.1 Radiography

A common NDE technique is X-ray imaging, or radiography. A part is placed between an X-ray source and an X-ray detector, measuring the number of X-rays that pass through the part, which is affected by attenuation. The extent of attenuation is a function of the thickness of the section and the atomic density of the material. Flaws (e.g., cracks, pores, and delamination) can be observed in the radiograph because the X-ray attenuation is decreased due to the discontinuity in the thickness being probed by the X-ray beam. However, the detectability of high-aspect-ratio flaws (e.g., cracks or delamination) is dependent on the orientation of the flaws relative to the X-ray beam. To be detectable, the flaw must be oriented such that the X-ray beam encounters a

localized reduction in material density. Radiography is best used for materials with consistent thickness. For complex geometries, radiography is of limited applicability due to the difficulty of interpreting superimposed features.

The geometric complexity common to many L-PBF parts challenges radiography, limiting the potential use case for that AM process category. However, radiography has seen use for inspection of larger DED structures with thin sections [Lopez et al., 2018; Chabot et al., 2020]. Figure 7.5.1.1-1 shows example radiographs of L-PBF test specimens, with test blocks with complex geometries (left) illustrating challenges in radiograph interpretation and mechanical test specimens (right) with a detected flaw.

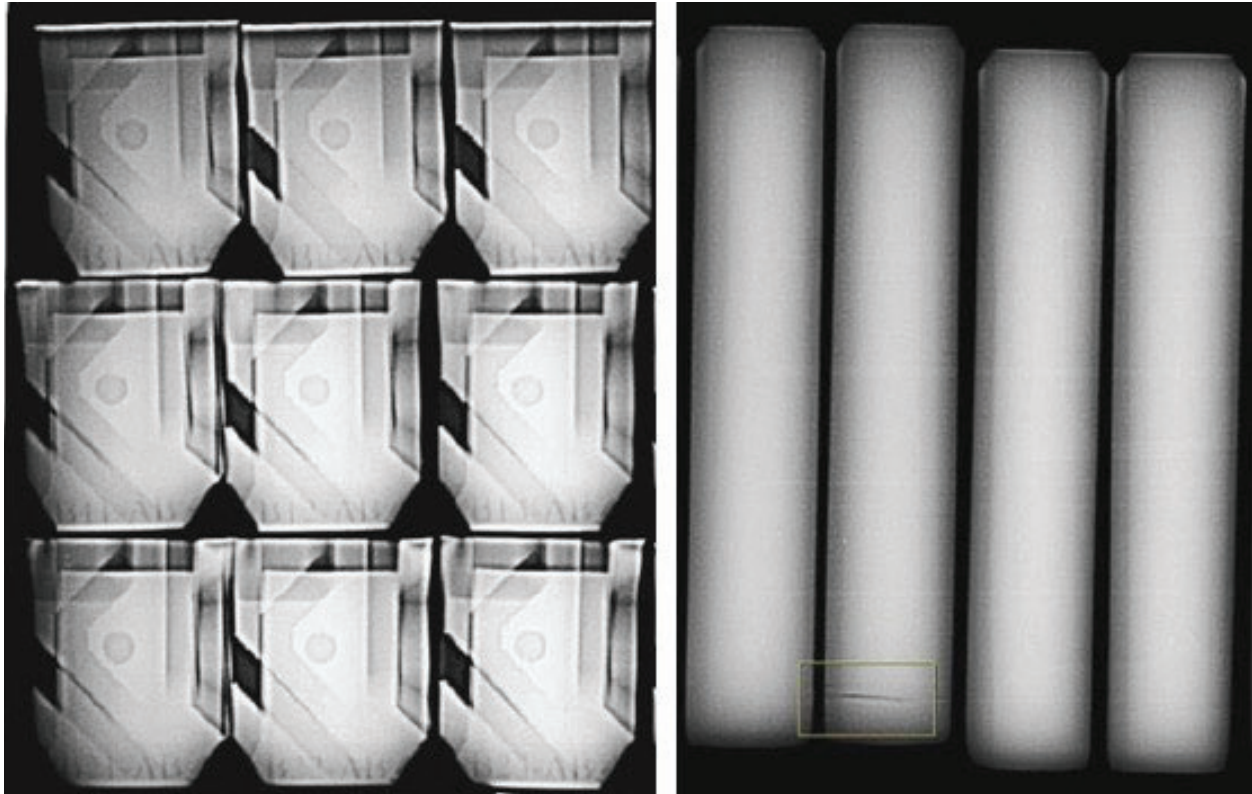


Figure 7.5.1.1-1. Radiographs of L-PBF Test Specimens

Radiography has limited applicability for inherent flaw characterization. Radiography results in a two-dimensional (2D) representation of flaws, which makes accurate determination of inherent flaw characteristics difficult. Additionally, geometric complexity causes difficulty in interpreting radiographic data, and resolutions for radiography are not as high as for CT.

7.5.1.2 CT

CT is frequently used to investigate L-PBF AM parts. A part is placed on a rotating stage and exposed by an X-ray source taking several images as the sample rotates. In other configurations, the X-ray source and detector rotate around the part. Unlike simple radiographs, a reconstruction process is used to combine the radiographs to create a 3D representation of the part.

Figure 7.5.1.2-1 shows a schematic of a CT source/detector arrangement [Howell, 2020].

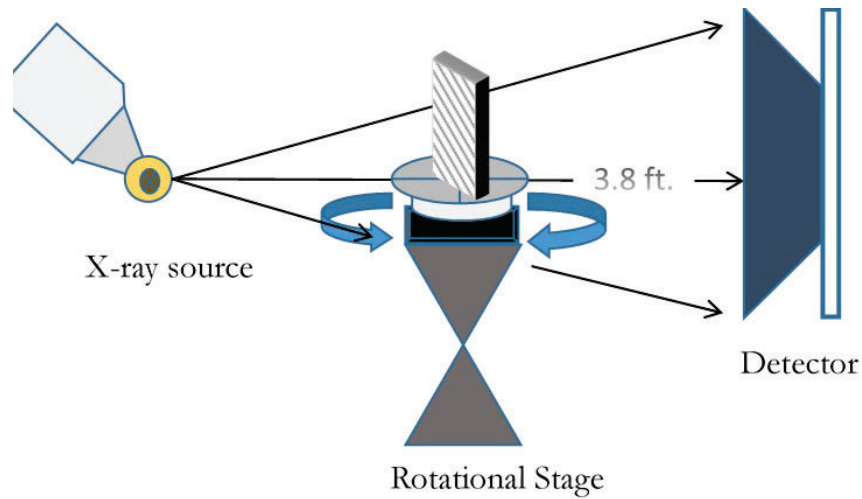


Figure 7.5.1.2-1. Example Source/Detector Arrangement for X-ray CT [Howell, 2020]

The addition of the third dimension in the X-ray data allows for a more informative description of flaw location and shape. This alleviates some challenges with radiography; however, it is necessary that some X-rays penetrate the component's thickest section. Steels and nickel-based alloys, for which X-ray attenuation effects are more significant, are particularly challenging to radiography (compared with aluminum and titanium alloys). For these alloys, the maximum thickness that can be penetrated is decreased. Different X-ray CT setups can accommodate larger or smaller parts at varying resolutions. Figure 7.5.1.2-2 shows an example of a test block and the CT results of different sized features therein [Burke, 2021].

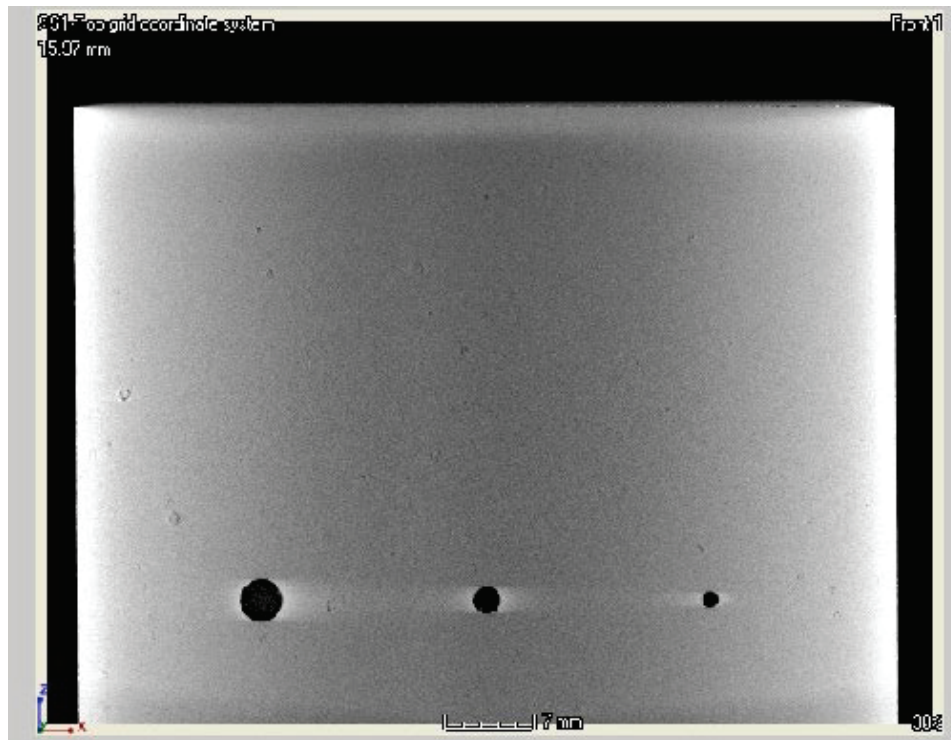


Figure 7.5.1.2-2. Cross-section Image taken from X-ray CT Scan of Part with Varying Flaw Sizes [Burke, 2021]

Additional approaches for CT scanning include micro- and nano-CT systems, which enable higher resolution scans of smaller features at the expense of sample size limitations and increased scan time. Some specialized laboratory setups exist for these techniques and for synchrotron sources. While production-scale CT systems can obtain micron-level resolutions, nano-CT can resolve sub-micron features, although flaw sizes associated with high detection reliability are likely larger. Nano-CT requires limited sample sizes, and small (~1-mm) sections need to be extracted from areas of interest, limiting the applicability to production hardware. Analysis of powder and its porosity is a common application of synchrotron CT. Figure 7.5.1.2-3 shows a CT scan of a powder sample used in AM and a section taken from a part built with the same powder [Gordon et al., 2020]. While these high-resolution techniques have limited applicability to production hardware scanning due to the limits of sample size and scan times, these systems have the capability to characterize the flaw sizes expected to be part of the inherent flaw state. As such, CT presents the current best approach for nondestructively characterizing inherent flaw states. However, like radiography, CT is limited by component geometry, and high-resolution scans require small material volumes.

F-8. CT represents the best nondestructive technique for characterizing inherent AM flaws.

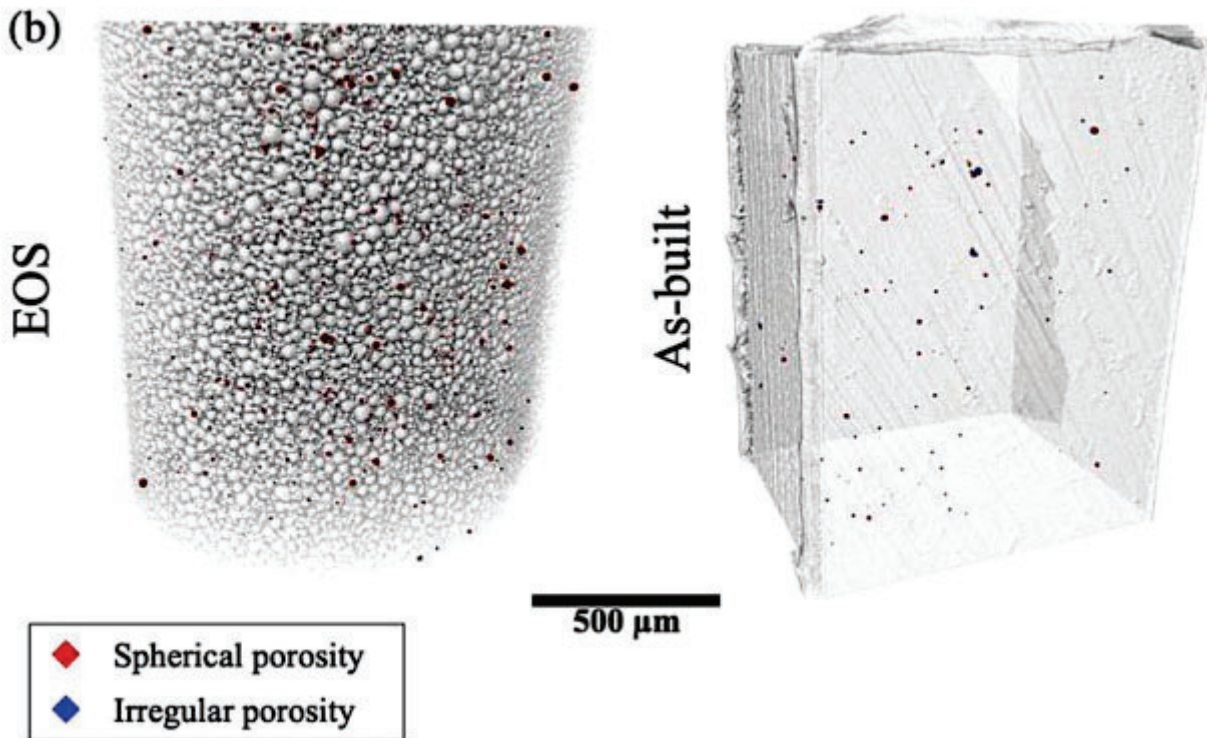


Figure 7.5.1.2-3. CT Renderings of Powder Particles (left) and Section from Part (right) [Gordon et al., 2020]

7.5.1.3 Dye Penetrant

Liquid dye penetrant techniques allow for the physical observation of flaws that interact with a free surface. A liquid dye is applied onto the part surface, which penetrates and fills surface-exposed flaws. The part is rinsed to remove excess penetrant, and the dye remaining in the defects is revealed by a developer chemical. Typically, fluorescent penetrant is used, which is

viewed under an ultraviolet light. Figure 7.5.1.3-1 shows an example dye penetrant inspection, revealing cracks/delamination in a BP-DED part.

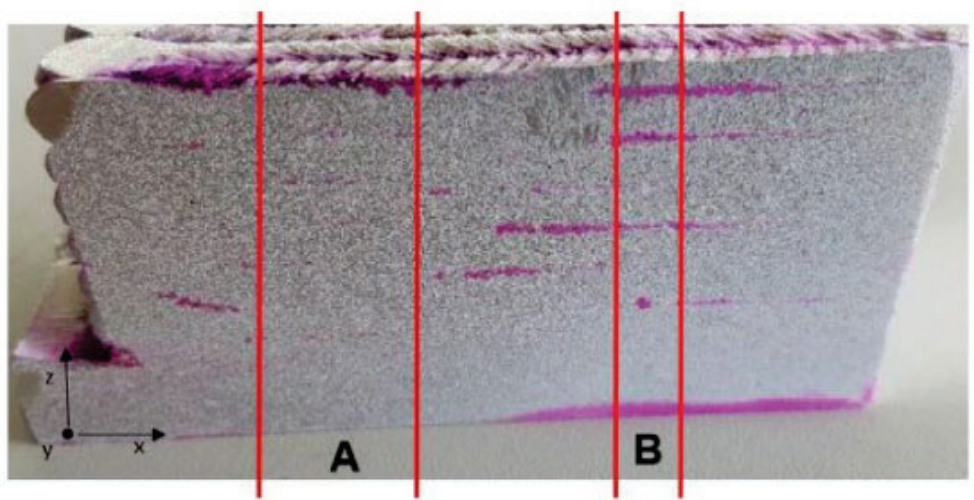


Figure 7.5.1.3-1. Dye Penetrant Inspection on a BP-DED Part showing Several Flaws [Lopez et al., 2018]

For AM components manufactured using L-PBF, surface roughness poses challenges to penetrant inspections. Duarte et al. [2021] show that surface roughness obfuscates the identifiable flaws when using a Level 4 sensitivity dye, but a Level 2 sensitivity dye can reliably reveal surface-exposed cracks. Removing the excess penetrant from the surface is the primary concern to reduce background noise that complicates detection of surface features. Method D penetrant inspection uses an additional emulsifier to rinse the surface and may help remove excess penetrant, reducing background noise. Post-build surface finishing processes (e.g., machining or chemical etching) can remove sufficient material that dye penetrant inspection becomes possible. However, flaw detection is limited to surface-connected features, making the technique of limited applicability for inherent flaw state characterization.

Liquid dye penetrant has been shown to reveal cracks on sectioned planes of material produced via DED [Seow et al., 2020]. Penetrant inspection is not as sensitive to material characteristics as ultrasound or X-ray inspection, so it is useful for high-density materials.

7.5.1.4 Ultrasound

Ultrasound techniques use transducers to create and measure mechanical (sound) waves traveling through a part. When mechanical waves interact with various flaws, reflections in the sound waves are generated and can be detected by the transducers. Ultrasonic techniques have some applicability for inspection of AM components but do not have the capability to identify individual flaws to the degree necessary for inherent flaw characterization.

Two basic ultrasound configurations are used. *Pulse-echo*, where the sending and receiving transducers are located on the same side of the part, detects echoes from internal features or the back wall of the part. *Through-transmission*, where the sending and receiving transducers are located on opposite sides of the part, detects variations in the time of flight of sound waves through the part. The inspections are performed using either single transducers or a “phased-array,” which uses a configuration of multiple transducers to improve inspection capability. Figure 7.5.1.4-1 shows a readout of pulse-echo time-of-flight measurements [Lopez et al., 2018].

The inspection zones correspond to the A and B zones identified in Figure 7.5.1.3-1. Notice that in zone B the time is much shorter, indicating a feature that reflected the sound waves. The time of flight between transmitting and measuring reflected sound waves is a function of the speed of sound in the material which, for isotropic microstructures, is related to the Young's modulus and density. For complex anisotropic microstructures, accurate speeds of sound data are often unknown.

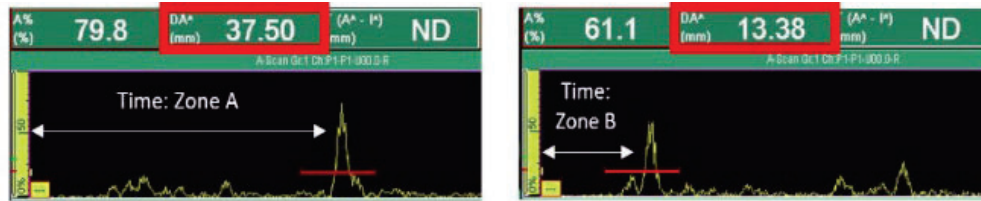


Figure 7.5.1.4-1. Ultrasonic Inspection Results for Two Locations (Zone A and Zone B) in a Part [Lopez et al., 2018]

Surface roughness common to AM parts can impair the interfacing of the part and transducers. This can be circumvented by ultrasonic techniques where the part is immersed in a fluid [Duarte et al., 2021]. Nonhomogeneous microstructures can influence the ultrasound signal, so parts without homogenizing heat treatments may be less inspectable with ultrasound. Applications of ultrasonic inspection to AM parts are focused mostly on larger structures with simpler geometries (e.g., DED) and for alloys with low elastic modulus and speed of sound (e.g., aluminum). Specific flaw geometries or distributions are difficult to extract with ultrasonic inspection due to the difficulty of signal interpretation, so the primary use case is the identification of significant flaws (e.g., delamination).

Resonant ultrasonic spectroscopy approaches, where the part is excited by ultrasonic waves and the resultant resonant frequencies are measured, have been shown to be useful for detecting differences in AM materials. For example, Rossin et. al. [2020] demonstrated the capability of resonant ultrasonic spectroscopy to detect microstructural recrystallization in AM Inconel 625. The resonant behavior is affected by the microstructure and the flaw state [Rossin et al., 2020]. Such techniques are not capable of resolving individual flaws, which limits their usefulness for characterizing flaw distributions. However, such techniques might be a means to check for consistency in the material behavior as part of a process control check.

7.5.1.5 Eddy Current

Eddy current inspection techniques detect flaws by imposing local electrical fields on a part and measuring discontinuities in the induced eddy currents. As an example, Figure 7.5.1.5-1 illustrates the use of eddy current probes to inspect holes in an AM component. Like ultrasonic testing and radiography, this technique works best on continuous surfaces, and, like penetrant, the results can be affected by surface finishes [Waller, 2014]. Although the electric fields only penetrate a few millimeters, relatively small flaws can be detected [Lopez et al., 2018].

Figure 7.5.1.5-2 shows a schematic of the electric fields induced in a part with and without a flaw [General Dynamics, 1967]. Du et al. [2018] performed eddy current measurements for different intentionally seeded flaws in an AM material and showed the capability to detect flaws as small as 200 μm (0.008 inch). Other works have assessed eddy current inspection for AM materials and note a detectable flaw size on the order of 500 μm (0.020 inch), depending on defect depth [Geatko et al., 2022; Kobayashi et al., 2019]. However, the flaw size associated with high detection reliability (high probability of detection) is likely larger. Eddy current may

have some limited applicability for inherent flaw detection but would be limited to relatively large inherent flaws and flaws that are within the eddy current penetration depth.



Figure 7.5.1.5-1. Examples of Eddy Current Inspection of Holes on AM Component [Waller, 2014]

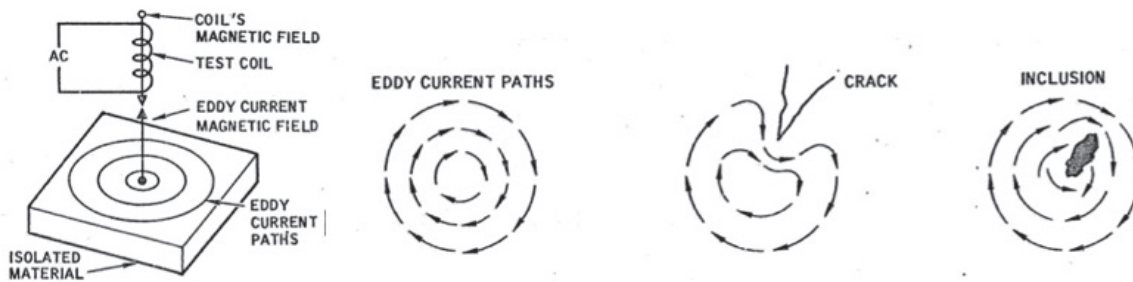


Figure 7.5.1.5-2. Schematic of Induced Electric Fields in Part With and without Flaw [General Dynamics, 1967]

7.5.1.6 Thermographic Imaging

Thermographic imaging uses a thermal camera to image components that have been heated using a variety of approaches (e.g., pulsed and stepped heating). Geometric discontinuities (e.g., voids, delamination, cracking, separations) conduct heat differently than dense material, and the differences can be observed using a thermal camera. Figure 7.5.1.6-1 shows examples of features identified in a 316L stainless steel panel manufactured with intentional flaws. Stepped thermography (right) shows improved spatial resolution over pulsed thermography (left) [D'Accardi et al., 2019]. Feature detectability is limited based on the flaw aspect ratio (i.e., the ratio of the area to the depth). Only shallow features are detectable unless the feature is large. The flaw size resolution is limited based on the infrared camera capabilities and aspect ratio considerations. Thermography is best suited to detecting large features (e.g., delamination) that are near the surface.

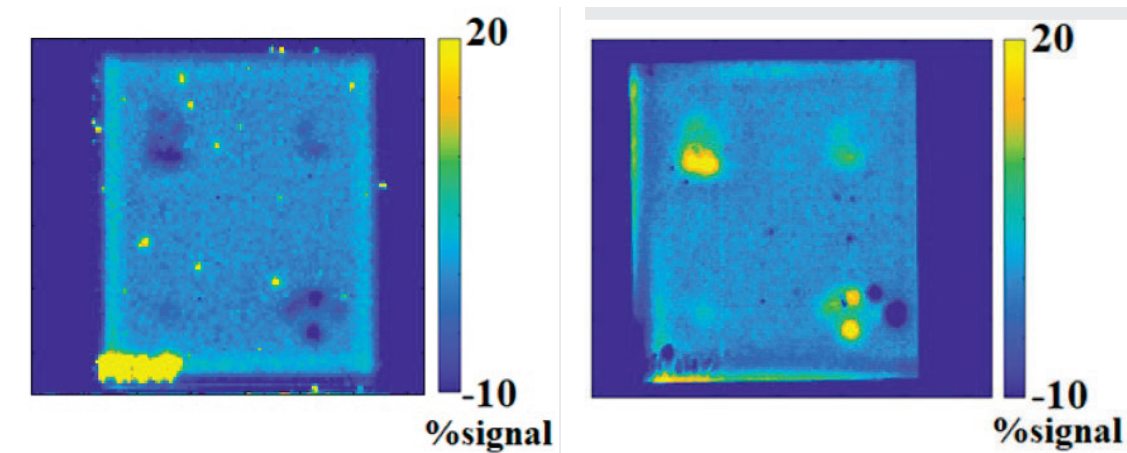


Figure 7.5.1.6-1. Processed Thermography Images of AM Component with Intentional Defects, imaged using Pulsed Thermography (left) and Stepped Thermography (right) (component is 35 mm high) [D’Accardi et al., 2019]

7.5.2 Destructive Methods

Destructive characterization methods are common in AM, especially during development of process parameters. Direct observation of flaws allows for quantitative descriptions of the defect geometries and distributions.

7.5.2.1 Metallographic Inspection

The most common method to identify flaws in AM materials is to section them for metallographic inspection. In the qualification of AM processes, analyzing sectioned coupons plays a central role and is often used to establish the “ground truth” description of the material microstructure and flaw state.

Optical microscopes can characterize many flaws in a single image, with resolution on the 2- to 5- μm (0.08- to 0.2-micron) scale. This resolution is sufficient for resolving the small flaws expected to make up much of the inherent flaw distribution. Optical microscopy allows for location-specific flaw observation. However, complex geometries can only be observed in a single (or a few) cross-section(s), and tracking flaws along 3D structures is difficult (see Section 7.5.2.2). Furthermore, sectioning of small or complex features can be difficult, requiring careful machining for accurate sections to be extracted. Metallographic imaging is destructive, which means this technique cannot be used directly on parts that are intended for service.

Another limitation of sectioning parts for metallography is the limited size of sampled areas relative to the component size. In addition, there is a tradeoff between field of view and resolution in optical imaging. This can be somewhat circumvented by making mosaic montages with a robotic stage. Figure 7.5.2.1-1 shows a montage from an L-PBF Alloy 718 coupon with significant powder reuse. Figure 7.5.2.1-2 shows a zoomed-in location with oxide defects.

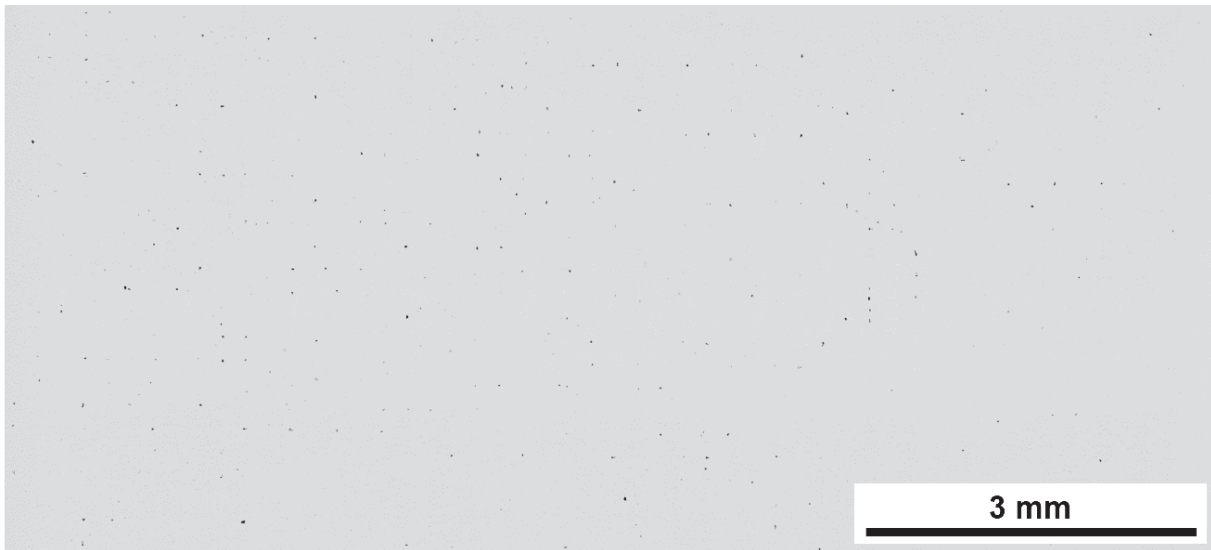


Figure 7.5.2.1-1. Optical Montage from Alloy 718 Sample Made with Reused Powder

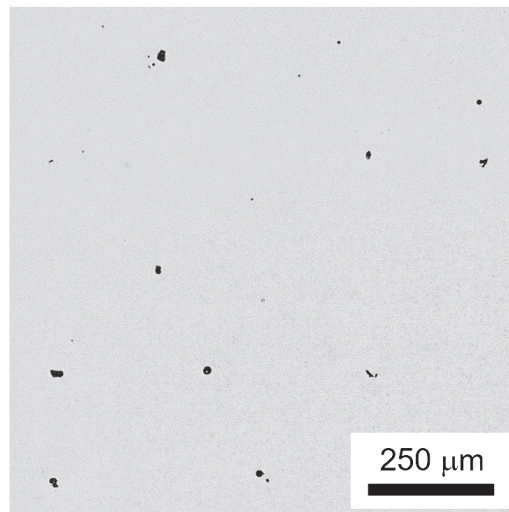


Figure 7.5.2.1-2. Optical Image of Alloy 718 Sample Made with Reused Powder

Some studies have worked to understand how to appropriately represent the 3D nature of the AM flaw state with the high-resolution 2D information obtained through metallographic sectioning. Sanaei et al. [2019] compared the results of 3D flaw characterization data obtained via CT with 2D flaw characterization data obtained via metallographic examinations. The metallographic examination used to obtain 2D data was higher resolution than the 3D CT data, so a smaller flaw size was able to be detected and characterized. The authors found that a sufficient number of 2D cross-sections would reasonably represent the flaw population characterized by the 3D CT methodology when the flaw population was primarily small, spherical porosities. The 2D cross-section approach was less effective at characterizing larger flaws with complex morphologies (i.e., interconnected flaws). For example, the authors observed clusters of relatively small porosities in 2D cross-sections that appeared as larger, interconnected flaws in the lower resolution 3D method. In application, such flaws might coalesce rapidly into a larger flaw more closely represented by the 3D methodology. Thus, accuracy of the flaw characterization using 2D metallographic examinations is dependent on the flaw type and size, with 2D approximations

of spherical porosity being more effective than approximations of flaws with complex shapes and high aspect ratios [Sanaei et al., 2019]. In summary, metallographic sectioning provides the highest potential resolution for resolving inherent AM flaws but is limited by small inspection volumes, 2D representations of 3D flaw structures, and the necessity of destructive examination.

7.5.2.2 Serial Sectioning

Serial sectioning is a modification of the optical metallographic imaging technique that uses a robotic polishing machine to remove a controlled amount of material in steps, creating a series of adjacent location images. This approach allows significantly more flaws to be detected compared with manual metallographic inspection (due to the larger sampling volume) and can be used to extract multiple images of a single flaw to reveal a 3D shape description. Figure 7.5.2.2-1 shows a reconstruction of serial-sectioning data to visualize pores.

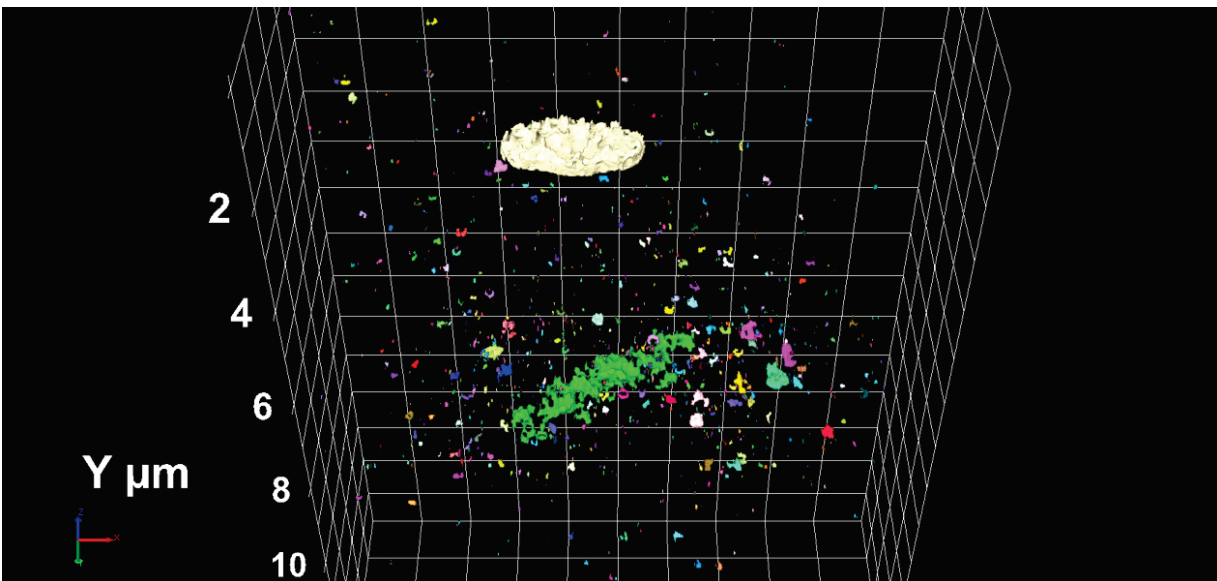


Figure 7.5.2.2-1. 3D Visualization of Pores Collected using 3D Serial Sectioning

Serial sectioning allows for the highest-resolution depiction of the 3D flaw state currently attainable. However, the resources required for sectioning, polishing, and imaging limit the sampling size. Serial sectioning is likely the best technique for characterizing the flaw state, at least at a highly local level. Multiple sectioning regions are likely appropriate to fully understand the flaw state in a sample or component.

Serial sectioning imaging plays a major role in computational modeling approaches for predicting microstructure and properties in L-PBF. For example, the AFRL AM Modelling Series [Chapman et al., 2021] uses serial sectioning to characterize the microstructure in 3D for deformation simulations in AM microstructures.

7.5.3 *In-situ* Monitoring

The layer-by-layer nature of AM enables *in-situ* monitoring using a variety of sensors. Process escape flaws resulting from common root causes (e.g., incomplete spreading, recoater blade interaction, local overheating, excessive spatter, warping) may be observable on a layer basis but are not necessarily observable in the completed part, motivating layer-wise *in-situ* monitoring.

One of the main considerations for *in-situ* monitoring is the data requirements. Individual AM builds can lead to hundreds of gigabytes of monitoring data, often requiring computer vision or machine learning approaches to automate data analysis.

A current limitation of *in-situ* monitoring is establishing the correlation between an indication detected by the *in-situ* monitoring approach and a physical flaw. This is particularly true in L-PBF processes, where subsequent layers can “heal” flaws generated during previous build layers by remelting. Thus, at the current state of development, *in-situ* monitoring approaches are best thought of as being able to detect process deviations in an automated manner, rather than detecting individual flaws. The detected process deviations may be conservatively assumed to result in a material flaw, but the capability of *in-situ* systems to detect and characterize inherent flaws is limited [Williams et al., 2023].

7.5.3.1 Powder Bed Imaging

Powder bed imaging is one of the most common forms of *in-situ* monitoring. Issues during powder spreading (e.g., recoater blade impact, inadequate spreading, and superelevation) can be observed with optical images. Figure 7.5.3.1-1 shows a machine learning application for powder bed imaging, where different spreading defects have been segmented [Scime et al., 2020].

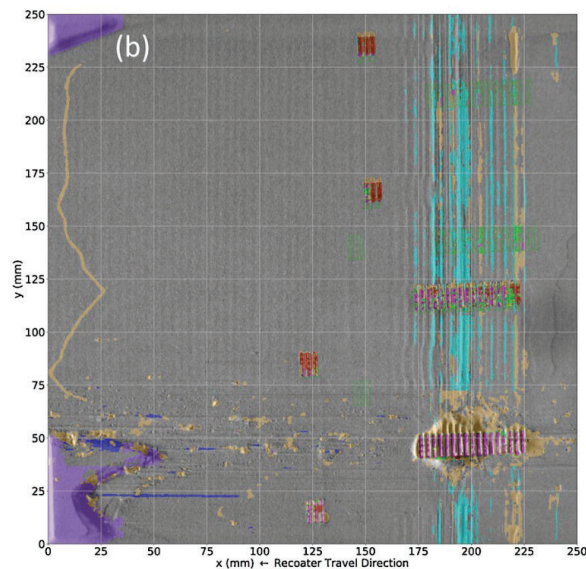


Figure 7.5.3.1-1. Image of Powder Spreading Defects Segmented using Machine Learning Application [Scime et al., 2020]

7.5.3.2 Thermography

Thermal imaging has emerged as another primary form of *in-situ* monitoring. Similar to the thermographic imaging described in Section 7.5.1.6, local thermal anomalies can be observed with a thermal camera, which can indicate flaw formation (e.g., keyhole pores or geometric flaws).

Zalameda et al. [2013] demonstrated the use of thermography for process control of a wire-feed DED system, where energy source power was controlled to maintain a consistent melt pool size. Zalameda et al. [2013] also investigated the use of flaw detection using thermal cooldown rate. Work by Snow et al. [2023] shows how layer-wise thermal images can detect large spatter

particles that can result in LoF porosity, as confirmed by CT scans. Figure 7.5.3.2-1 depicts an 850- μm (0.033-inch) pore originating from a spatter particle observed over seven layers.

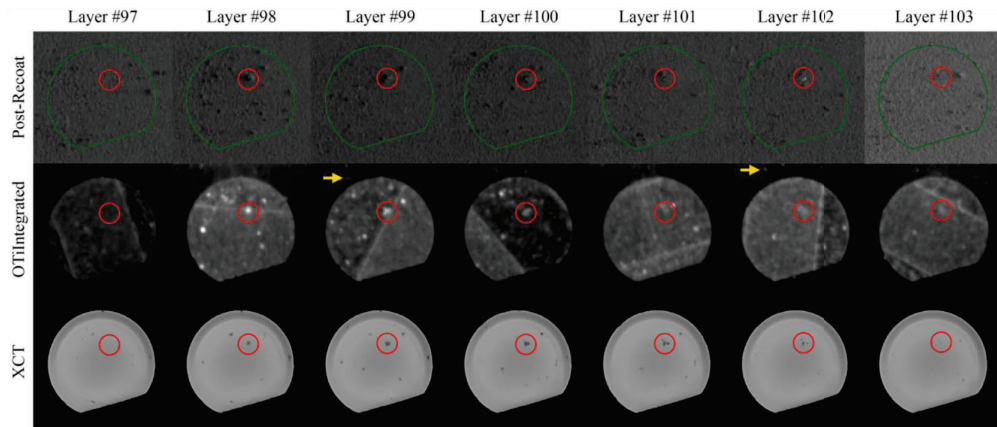


Figure 7.5.3.2-1. Images of Single Part where Layer is increasing in the Columns
Top row shows optical images, middle row shows optical thermography images, and bottom row shows CT slices from printed parts [Snow, 2023].

Melt-pool scale thermal imaging is an emerging *in-situ* technique that can identify anomalous melt pool behavior (with varying levels of quantification) [Forien et al., 2023]. Forien et al. showed that melt-pool imaging can identify defective struts in lattice structures. Scime and Beuth [2019] applied computer vision to melt-pool images to identify melting conditions consistent with keyhole void formation.

7.5.4 Flaw Descriptors and Distributions

Characterizing flaw distributions is of particular interest for AM process qualification and certification, and there are many flaw descriptors from which distributions can be generated. Typically, flaw sizes are necessary for CIFS calculations, where fracture mechanics analysis predicts the flaw size that would lead to a service failure. As shown, characterization techniques measure varying levels of flaw size and shape detail.

Flaws must be identified from inspection data. Individual features or observations are extracted from inspection data through a segmentation process so that the feature can be measured. This can be done by hand using simple, intensity-based thresholding (i.e., brightness cutoff) or by machine learning segmentation techniques for complex segmentation.

7.5.4.1 Particle Description

The following is a list of common particle descriptors that can be measured in 2D or 3D from any of the discussed techniques where an image of the particle is measured. The labels are listed as 2D descriptors for simplicity.

- Area.
- Perimeter.
- Equivalent circular diameter: calculation of diameter based on area.
- Aspect ratio: description of feature “flatness,” using the width to height ratio.
- Circularity: measurement of the roundness of a flaw, using perimeter and diameter.
- Feret diameter: measurement of the flaw length along a certain direction.

- Elliptical axes: measurement of the major and minor axes of an ellipse bounding the flaw shape.

A more comprehensive list of such descriptors can be found in ISO9276-6, “Representation of Results of Particle Size Analysis” [Hentschel and Page, 2003].

7.5.4.2 Proximity to Part Features

An ideal “steady state” L-PBF process relies on a consistent melt pool shape, with sufficient melt pool overlap. There are numerous sources of variation that can cause the process to drift from “stability” such that flaws are formed. Table 7.5.4.2-1 lists part features that can lead to flaw formation.

Table 7.5.4.2-1. Notable Features that can lead to Porosity Formation in LPBF

Feature	Source	Effect
Corners and sharp features	Build design	Thermal buildup due to small laser tracks.
Contours (near surface)	Process	Thermal buildup due to powder bed.
Down skin and low angle	Build design	Thermal buildup due to powder bed.
Top skin	Process	Top layer is never remelted.
Laser track starts and stops	Process	Inconsistent laser power due to ramping on/off.
Stripe/island boundaries	Process	Introduces more starts and stops.
Inconsistent powder spreading	Feedstock	Thick powder layers can be poorly consolidated, and thin layers can lead to heat buildup.

These features often warrant additional consideration to identify flaws. Building coupons that incorporate some of these features allow for more robust parameter development.

7.6 Procedures for Representative Inherent Flaw State Characterization

An appropriate characterization of the inherent flaw state generated by an AM process is a key aspect of the proposed approach to fracture control for un-inspectable components. However, characterization of the inherent flaw state must account for the numerous AM process variabilities and limitations of inherent flaw characterization methods.

AM material flaw state is expected to vary based on the AM process input parameters. For L-PBF, this would correspond to parameters that influence the shape of the melt pool (e.g., laser speed, laser power, and layer thickness). Other influence factors may have significant impacts, including thermal history, part geometries (thin walls), and interactions between different parameter sets. An appropriate flaw state definition would account for these variability sources by conservatively bounding the potential flaw state developed by the worst-case combination of these influence factors or characterizing the effects of the influence factors directly.

Many common inspection techniques, as discussed in Section 7.5, may not be practical for flaw state characterization. For example, most conventional NDE approaches are incapable of resolving the flaws that are expected to be representative of most inherent flaw distributions. Of the NDE techniques with sufficient resolution (e.g., CT), considerations of sampling size and geometry limit the volume of material that can be characterized. High-resolution data can be obtained through sectioning techniques, but these approaches are destructive and have sampling volume limitations. Appropriate approaches are needed for evaluating the characteristic inherent flaw state generated by an AM process.

Broadly applicable flaw state characterization might be accomplished by adjusting machine parameters to generate material reflective of the variability within the AM process. However, care must be taken to ensure that artificial machine parameter adjustments remain appropriately representative of the nominal process operation. A more appropriate approach might be to produce bespoke “flaw state characterization” coupons or builds that are designed to represent challenging build geometries, relying on build-geometry-induced thermal history to bound the flaw state variability. For critical applications, characterizing flaw state on the component geometry might be the most effective means of confirming that the inherent flaw state characterization is sufficiently representative.

Flaw state should be characterized with the material in the final post-processing state for the application, including all relevant post-processing steps (e.g., hot isostatic press, heat treatment, surface finishing, etc.). If the material is used at high temperatures, then some evaluation of the potential for flaw state evolution during high-temperature service should be performed. For example, evidence suggests [Pegues et al., 2020] that pores containing inert environmental gases might grow during high-temperature application following hot isostatic press treatment to close trapped porosity.

NASA-STD-6030 requires assessments of the material quality for the establishment of a QMP, including assessments of AM influence factors (e.g., surface texture, build geometry, or build restarts) [NASA-STD-6030]. The inherent flaw state evaluation expands on this existing requirement by providing a statistical definition of the inherent flaw state that can be used for further assessment. As an additional advantage, the flaw state characterization provides another baseline for establishing process equivalency, in addition to metallurgical and material property baselines.

Procedures for producing material for flaw state characterization have not yet been developed. Considerations for appropriate inherent flaw state characterization include the role of influence factors (e.g., thermal history and part geometry), the volume and location of sampled material, and the variability in flaw state generated by the process.

7.6.1 Evolution of Flaw Population Data

Flaw population information is expected to evolve as AM processes are implemented, produced material is evaluated, and component performance information is gathered. Continuous evaluation of flaw state has two major benefits. First, flaw state monitoring provides confirmation of process consistency over time. Second, additional data help refine the inherent flaw distribution, particularly in the “upper tail” of the distribution where larger flaw sizes may not be common enough to be directly characterized without multiple AM builds. Additional refinement of the upper bounds of the inherent flaw distribution is important, as fatigue and fracture mechanisms are often “weakest link” phenomena (i.e., the most critical flaw that is present will tend to be the source of subsequent crack initiation and growth).

7.6.2 Process Equivalence

The NASA AM process qualification schema relies on a material equivalence argument, where an initial material state and process is developed, characterized, and qualified, and subsequent material processes are shown to be sufficiently equivalent to the initial material state such that the initial characterization data are applicable to the subsequent material [NASA-STD-6030]. For critical applications, flaw state should be one of the metrics by which process equivalency

is judged. A well-defined baseline AM process should establish acceptance criteria based on microstructural features. For critical components, such acceptance criteria should include criteria related to flaw state.

NASA-STD-6030 requires establishing an AM process and defining the resulting material quality baseline in the form of a QMP. In addition to the relevant processing parameters, the QMP definition includes metrics related to the microstructure and mechanical properties of the material produced by the QMP-defined process. NASA-STD-6030 defines a “registration” approach, whereby a material process is compared with an existing QMP and assessed for equivalency. Processes that produce material with sufficient equivalency can be “registered,” and material characterization data can be applied to both processes. This requires confidence in the equivalency of the processes. Flaw state provides an additional metric through which the equivalency comparisons can be established.

7.6.3 Flaw Distributions

Flaw distributions describe the population of AM flaws and can be used as inputs into probabilistic assessments. Flaw size versus occurrence rate is the most useful information for PDTA (see Section 7.2.7). Other attributes (e.g., location or shape) may be useful in some cases for predicting damage tolerance or fatigue life. Example AM flaw distributions described by exceedance curves are shown in Figure 7.2.7-1.

7.6.3.1 Build Parameter Influences

The AM process influence factors can affect the flaw distribution. For example, Nezhadfar et al. [2021] found variability in flaw state based on build preheat temperature for L-PBF 316L stainless steel. Builds that were not preheated showed differences in flaw size relative to those that were preheated. Similar results were found by Romano et al. [2018] on L-PBF AlSi10Mg material produced using three different AM processes. Demeneghi et al. [2021] used CT to examine flaw populations in L-PBF GRCop-42 and found that flaw state varied with as-built specimen thickness. The flaw populations were reduced following hot isostatic press treatment. Figure 7.6.3.1-1 shows CT scan results for the specimens in the work by Demeneghi et al. [2021]. The example flaw distributions shown in Figure 7.2.7-1 represent the flaw states for the specimens in the study by Demeneghi et al. that underwent a hot isostatic press cycle, demonstrating process sensitivity on resulting material flaw state.

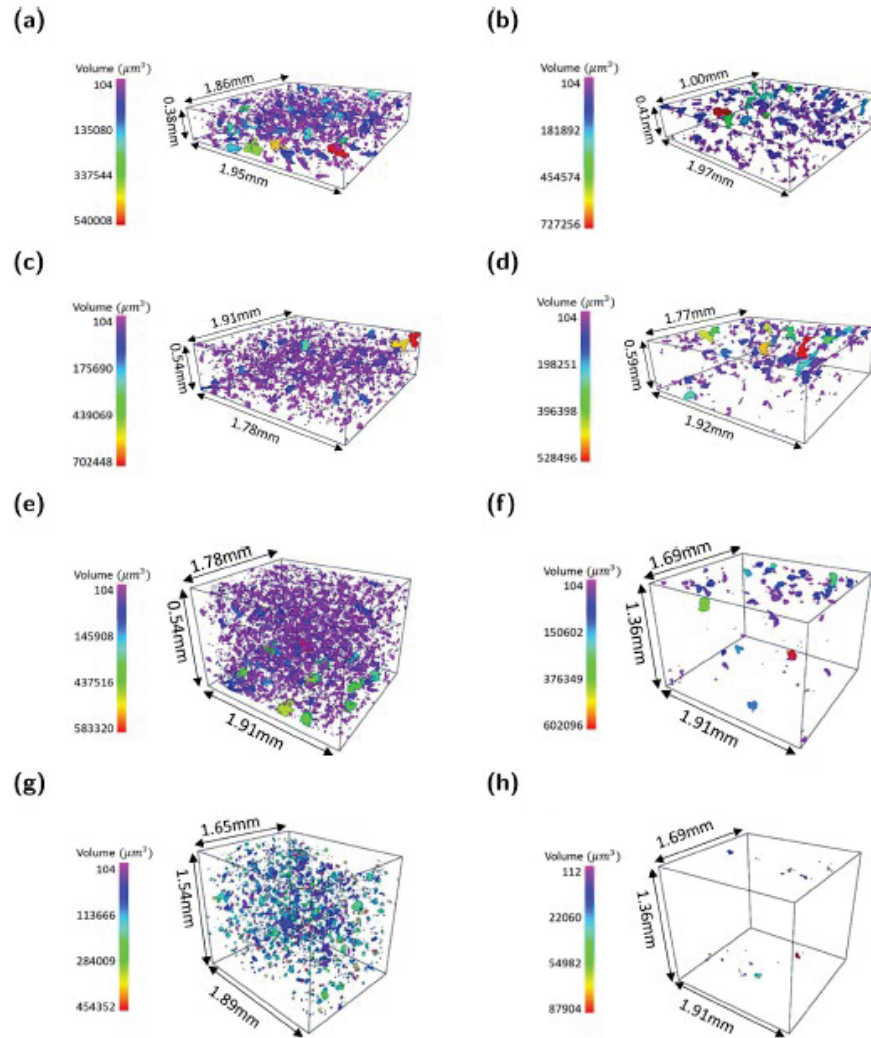


Figure 7.6.3.1-1. Variation in Flaw State for AM GRCo-42 Manufactured with Different Specimen Thicknesses [Demeneghi et al., 2021]

These factors of build location, component cross-section size, and flaw type variability must be accounted for in any probabilistic assessment of AM flaws. A conservative bounding distribution may be appropriate until sufficient expertise can be developed to understand the variability associated with AM flaw distributions.

7.6.4 Influence of AM Build Thermal History on Flaw State

Currently, many AM systems operate using a fixed set of process parameters that define the feedstock deposition and energy-source operation. For example, some key parameters in L-PBF include, but are not limited to, laser speed, laser power, and feedstock layer thickness. During process development, the set of process parameters is defined for the machine and feedstock material that results in successful builds and acceptable material quality. The parameters are then locked and used for subsequent production.

Despite the locked build processes, variability in material quality can arise due to changes in the build temperature. Builds can run “hot,” corresponding to a condition where the temperature of the previously deposited layer is relatively high due to reduced time between layers or low

thermal mass to conduct heat. Builds can also run “cold,” where the time between layers is sufficient for the previously built layers to dissipate accumulated heat. Thermal history is affected by challenging part geometries (e.g., overhangs, thin walls, and tapered cross-sections) that influence the heat transfer from the top build layer. The temperature associated with previously solidified material changes the mechanics of the melt pool in terms of size and cooling rate, which affects flaw state and microstructure [Mostafaei et al., 2022]. Robust parameter development ensures that an acceptable material quality is obtained in these hot and cold scenarios and that acceptable limits on thermal history effects are defined and controlled. This defines the “process box.” Conceptually, the process box defines the AM process limits for acceptable material quality. Rigorous AM process development includes understanding the process box edges to ensure builds do not cross the limits of acceptable material quality.

The thermal history of the build is dependent on the geometry of the build. In a part-agnostic approach to AM process development, the edges of the process box might be probed by adjusting laser power and speed to vary the energy density applied to the feedstock, which simulates variations in melt pool characteristics imposed by thermal history. This approach to process box definition has disadvantages, as adjustments to build parameters may not be representative of thermal-history-driven material-quality variation, and many AM system manufacturers do not allow for laser parameter adjustments.

Instead, an alternative approach might be to use the AM build geometry to affect changes in the thermal history and examine the material quality at any thermal extremes. This would require an understanding of the factors influencing thermal history, so that specimens can be produced for examination. Ideally, a modeling approach could be used to predict and bound the thermal history extremes for characterization specimens and to ensure that AM components do not exceed the characterized process box.

7.6.5 Thermal History Studies

As part of this assessment, a study was commissioned to investigate the influence of part geometry on build thermal history, develop approaches to modeling the thermal history, and identify potential geometric influences on flaw state. The work was led by Dr. Albert To at the University of Pittsburgh, an expert in thermal modeling for AM (see Appendix A). To study the influence of part geometry, five challenge geometries were identified for L-PBF builds using Alloy 718 and standard process parameters. The challenge geometries were built on an EOS M290 L-PBF machine. A FLIR A700 camera collected *in-situ* thermal imaging data, and part-scale thermal analysis was completed for each geometry. The study was to establish a link between the thermal history and the flaw population. The thermal analysis provides a path forward for identifying and tailoring process parameters for specific part geometries.

The five challenge geometries are identified in Figure 7.6.5-1 and included a brick, stepped brick, thin wall, cone, and arch. The brick was included as a reference for comparison with the other builds. Overhang, thin wall, and changing cross-section geometric features are included in the set of five challenge geometries. Two builds of each challenge geometry were produced, for a total of 10 parts.

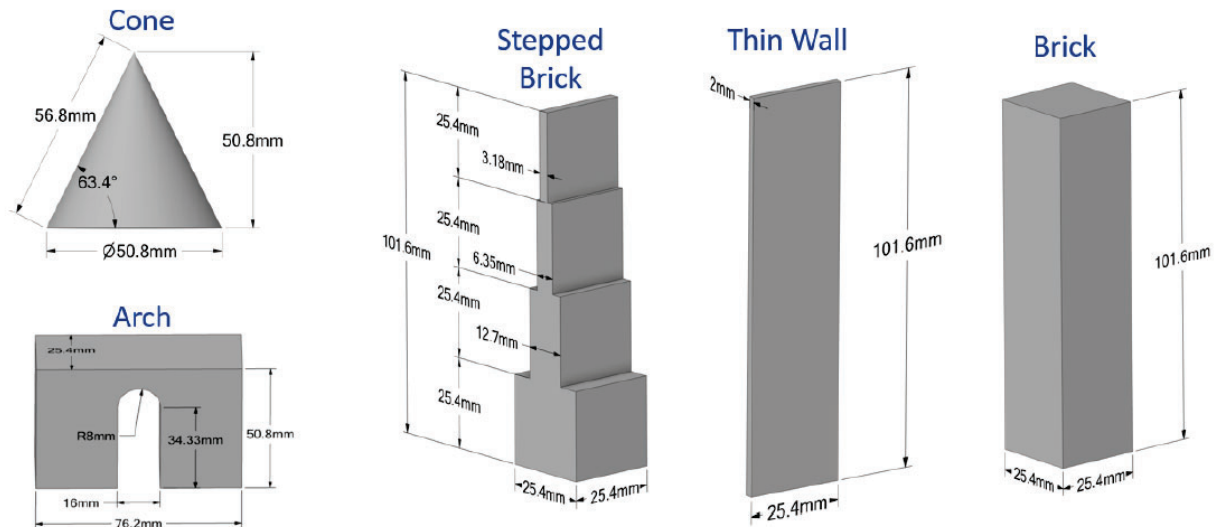


Figure 7.6.5-1. Identification and Dimensions for Five Challenge Geometries (see Appendix A)

In-situ thermal imaging data were collected for each build. The image data were post-processed to identify the interpass temperature and heat map. The interpass temperature is the average temperature between successive layers with temperature and pixel intensity calibrated for 0 to 650 °C (32 to 1202 °F). The heat map identified the pixel intensity (temperature) at locations within each layer. The thermal imaging indicated that the highest interpass temperatures did not occur at the last build layer. The heat map identified that the highest pixel intensities occurred near the part boundaries (see Figure 7.6.5-2).

Part-scale process simulations were completed for each of the five challenge geometries. The Pittsburgh Additive Manufacturing Simulator was used, which combines matrix-free FE modeling and graphic processing unit computing to perform layer-wise part-scale thermal process simulations. The analysis model was calibrated using the brick, thin wall, and stepped brick, while using the cone and arch for validation. The calibration approach using three data sets provides accurate results for multiple geometries as compared with using thermal imaging data for one build. The simulation results captured the trends in the interpass temperature and showed a maximum error of less than 30 °C for all five geometries. A comparison of the interpass temperature and the process simulation result (with a one and two standard deviation confidence interval) for the cone is shown in Figure 7.6.5-3.

The builds, *in-situ* thermal imaging, and thermal process simulations have been completed with a final report (provided in Appendix A). The next step in identifying the relationship between thermal history and flaw population influenced by the part geometry is to perform flaw state characterization on the builds. Images of regions of interest identified by thermal imaging will identify porosity and other microstructure features. The microstructure features can be compared between regions with low and high interpass temperatures and heat map values to establish potential relationships.

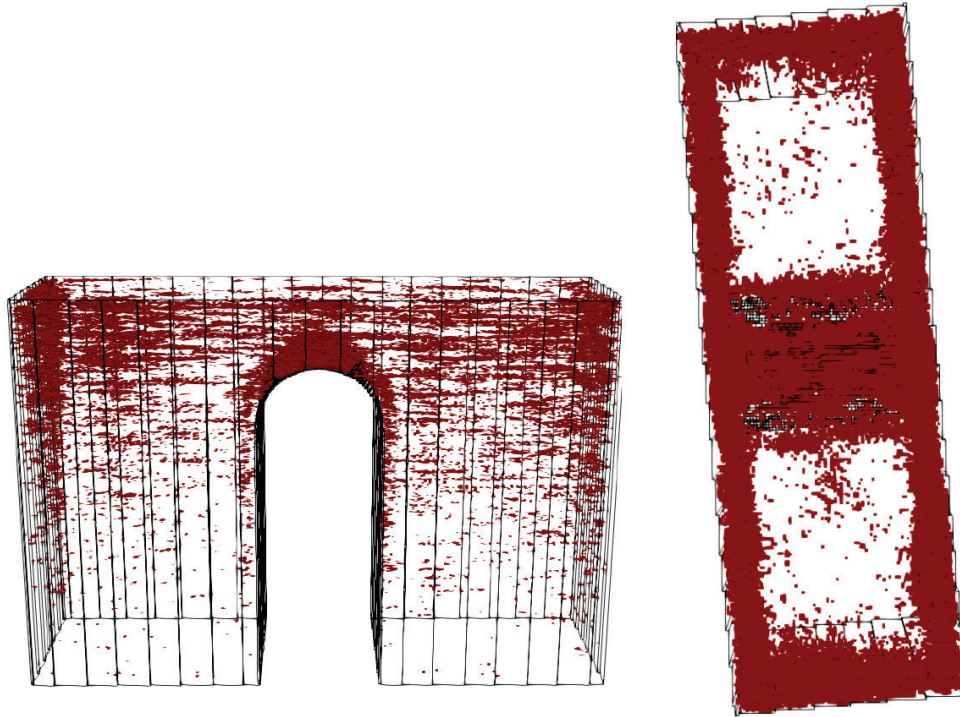


Figure 7.6.5-2. Example Geometry showing Locations of High Pixel Intensity Registered to Build Geometry (see Appendix A)

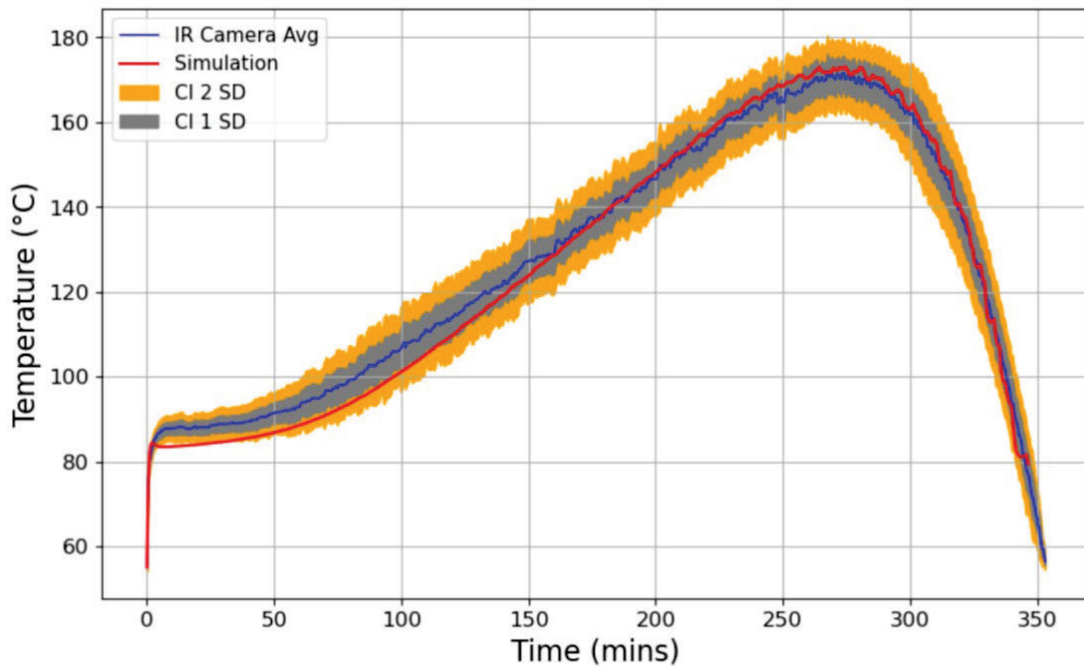


Figure 7.6.5-3. Comparison of Interpass Temperature for Cone from Thermal Imaging Camera and Process Simulation (see Appendix A)

7.7 Conclusions

AM is increasingly used for components for critical spaceflight applications, where failure would cause catastrophic consequences. For NASA missions, such components may be expected to meet the requirements in NASA-STD-5019, which include requirements for reliable inspection of flight components to screen for defects. However, some of these fracture critical AM components will be designed such that reliable inspections are not possible, at least for some regions within the component. Such un-inspectable fracture critical AM components represent a potentially significant mission risk. A philosophy is needed to provide a consistent and systematic approach for risk assessment and fracture control certification of un-inspectable AM components.

The proposed framework is based on understanding the relationships between the CIFS, the minimum detectable flaw size (when available), and the inherent flaw size distribution. AM flaws are categorized based on their occurrence both within and outside nominal AM process operation. An inherent flaw is representative of the characterized nominal AM process operation, and a process escape flaw is a flaw that is not representative of the characterized nominal AM process operation.

The risk to the component posed by inherent flaws can be assessed by characterizing the type, size, and distribution of inherent flaws generated by the AM process. This flaw state characterization, in terms of flaw size and rate of occurrence, should appropriately account for influence factors, including the range of possible operating parameters for the AM machine. Once characterized, the inherent flaw state is compared with the CIFS for critical locations in a component. For robust designs, the CIFS should be sufficiently above the sizes associated with the inherent flaw state. Scenarios where the CIFS is within the inherent flaw distribution represent an unacceptable risk, and designs should be modified to increase the CIFS, or the AM process should be refined to reduce the inherent flaw size. NDE inspections should supplement these assessments to the greatest degree practical. While flaw sizes determined from standard NDE (e.g., per NASA-STD-5009) may not be applicable; NDE might be used to appropriately bound the upper ends of potential inherent or process escape flaw sizes. Variability within material properties, inspection capability, or structural demand can be assessed using zone-based approaches, where the damage tolerance of the component is assessed based on local conditions that affect the damage tolerance rather than through a component-bounding approach.

The risks associated with inherent and process escape flaws can be assessed using PDTA, where the risk of failure is calculated based on the probability of a critical flaw arising in a critical location. PDTA approaches generally result in a less conservative but more representative assessment of the fracture risk relative to standard deterministic damage tolerance analysis. PDTA is used for certification of specific engineering applications, notably as part of FAA certification of titanium turbine wheels in the aviation industry. Policies on acceptable probabilities of failure and guidelines for the appropriate use of PDTA need to be developed to fully realize the potential of PDTA within the NASA damage tolerance approach.

Once demonstrated to be tolerant to the inherent flaw size, the focus shifts to assessing the risk associated with process escape flaws. Risk assessments for process escape flaws must necessarily rely on AM process control arguments and may be supported by tools (e.g., PFMEA) to identify potential process escapes and their potential to produce process escape flaws. Specialized inspection techniques are under investigation to support AM component flaw

screening. CT is used for AM components, but methodologies for characterizing probability of detection for this method are needed to realize its potential for fracture control applications. Other efforts are focused on developing technologies for *in-situ* monitoring. While current *in-situ* monitoring methods are limited by low reliability for flaw detection, they are potentially useful for demonstrating process control during critical builds and detecting process escapes. Future development may lead to *in-situ* monitoring that can meet the flaw detection reliability needed for quantitative NDE or to closed-loop control systems that repair flaws as they are detected.

Characterization of inherent flaw distributions needs to be a fundamental aspect of fracture control rationale for un-inspectable components. However, inherent flaw characterization is challenged by the lack of techniques that can resolve small AM flaws. The most promising current techniques are CT and serial sectioning, each of which has practical limitations for use in flaw state characterization. In addition, procedures for performing builds that generate the appropriate material for flaw state characterization are needed. Such builds should generate representative material operating at the acceptable limits of the process, which may require adjusting build parameters or designing bespoke flaw state characterization coupons. Additional work is needed to develop approaches for characterizing inherent flaws, establish metrics for sufficient definition of the inherent flaw state, and establish approaches for generating representative material. These questions should be resolved to support the proposed framework for un-inspectable AM components.

A framework has been presented that relies on characterization of inherent flaws and prevention of process escape flaws to reduce risks related to un-inspectable AM flaws. While this represents an initial philosophy, the use of AM components in critical applications remains in its infancy, and the approach is expected to evolve and refine as additional experience is gained and lessons learned are accumulated and utilized.

8.0 Findings, Observations, and NESC Recommendations

8.1 Findings

- F-1.** Terminology related to AM material imperfections (e.g., *flaw*, *defect*, *anomaly*, etc.) is not consistent within the AM community, and NASA materials standards (e.g., NASA-STD-6016, NASA-STD-6030, etc.) do not distinguish between *flaws* and *defects*.
- F-2.** Distinguishing between AM flaws that arise during nominal AM build operation (i.e., inherent flaws) and those that occur due to a process escape (i.e., process escape flaws) allows for targeted approaches toward damage tolerance rationale for each flaw category.
- F-3.** Prevention or detection of process escapes is the primary means to screen for process escape flaws in un-inspectable AM components.
- F-4.** Part-zoning approaches are a method for risk assessment of AM components with un-inspectable regions.
- F-5.** With validation, PDTA has the potential to reduce conservatism relative to standard NASA damage tolerance approaches by adopting design-specific analysis assumptions (e.g., flaw occurrence rates).

- F-6.** Quantitative bounds on acceptable probabilities of failure are not standardized in NASA documentation (e.g., NASA-HDBK-5010, JSC 66705, GPR 7120.4D, etc.) and vary by Program based on the Program's risk tolerance.
- F-7.** *In-situ* monitoring is not a replacement for standard or special NDE.
- F-8.** CT represents the best nondestructive technique for characterizing inherent AM flaws.

8.2 Observations

- O-1.** Integrating PDTA approaches with CT inspection could alleviate challenges with probability of detection by allowing inspection tailoring by component region.
- O-2.** AM competitive factors (e.g., business, organizational, legal, cultural, etc.) minimize open knowledge transfer (e.g., best practices, lessons learned, etc.).

8.3 NESC Recommendations

The following NESC recommendations are directed as indicated:

- R-1.** The OCE should update NASA-STD-6030 to adopt consistent terminologies for AM material imperfections. *(F-1)*
- R-2.** The OCE should update NASA-STD-5019, NASA-STD-5009, and NASA-STD-6016 to standardize terminology related to flaws, defects, and material imperfections. *(F-1)*
- R-3.** The NASA Fracture Control Methodology Panel should review available PDTA tools, their capabilities and limitations, and the availability and relevancy for NASA applications. *(F-5)*
- R-4.** The OCE should update NASA-HDBK-5010 with PDTA use guidelines. *(F-5)*

9.0 Alternate Technical Opinion(s)

No alternate technical opinions were identified during the course of this assessment by the NESC assessment team or the NESC Review Board (NRB).

10.0 Other Deliverables

No unique hardware, software, or data packages, other than those contained in this report, were disseminated to other parties outside this assessment.

11.0 Recommendations for the NASA Lessons Learned Database

No recommendations for NASA lessons learned were identified as a result of this assessment.

12.0 Recommendations for NASA Standards, Specifications, Handbooks, and Procedures

The following updates to NASA standards, specifications, or procedures were identified as a result of this assessment.

- NASA-STD-6030 should be updated to use consistent terminology for AM material imperfections (*flaws, defects, anomalies*).
- NASA-STD-5019, NASA-STD-5009, and NASA-STD-6016 should standardize terminology related to flaws, defects, and material imperfections.
- NASA-HDBK-5010 should be updated with guidelines for the use of PDTAs.

13.0 Definition of Terms

Anomaly	A flaw.
AM Build	A single operation of the AM machine for the production of parts.
AM Machine	The hardware and software necessary to conduct an AM build.
AM Process	Collection of activities that contributes to the production of an AM part and leads to the final material state for part service, including feedstock handling, AM build, and post-build processing (heat treatment, machining, etc.).
AM System	The AM machine and other auxiliary equipment used for the production of an AM part.
Build Parameters	The collection of controllable settings that directs the operation of the AM machine during a build.
Damage Tolerance	A design concept under which an undetected flaw or damage is assumed to exist and is shown by fracture mechanics analysis or test not to grow to failure during the period equal to the service life factor times the service life [NASA-STD-5019].
Defect	One or more flaws whose aggregate size, shape orientation, location, or properties do not meet specified acceptance criteria and are rejectable [ASTM E1316].
Finding	A relevant factual conclusion and/or issue that is within the assessment scope and that the team has rigorously based on data from their independent analyses, tests, inspections, and/or reviews of technical documentation.
Flaw	An imperfection or discontinuity that may be detectable by nondestructive testing and is not necessarily rejectable [ASTM E1316].
Flaw State	A general term for the number, size, and distribution of flaws present in an AM material.

Fracture Critical	Classification that identifies a part whose individual failure is a catastrophic hazard and that requires damage tolerant analysis or other fracture control assessment to be shown acceptable for flight.
Imperfection	A departure of a quality characteristic from its intended condition [ASTM E1316].
Indication	The response or evidence from a nondestructive examination [ASTM E1316].
Inherent Flaw	A flaw that is representative of the characterized nominal operation of a qualified AM process.
Interpass Temperature	In a L-PBF process, the temperature of the top layer of the build after completion of the laser scanning and before deposition of the next powder layer.
Lesson Learned	Knowledge, understanding, or conclusive insight gained by experience that may benefit other current or future NASA programs and projects. The experience may be positive, such as a successful test or mission, or negative, as in a mishap or failure.
Material Property Suite	A maintained collection of AM material property information specific to a material and condition that includes material test data, material allowables and associated design values, and criteria needed to implement and maintain statistical process control for the AM process [NASA-STD-6030].
Observation	A noteworthy fact, issue, and/or risk that is not directly within the assessment scope but could generate a separate issue or concern if not addressed. Alternatively, an observation can be a positive acknowledgement of a Center/program/project/organization's operational structure, tools, and/or support.
Process Escape	An off-nominal event occurring during the execution of some process (e.g., a process failure during an AM build).
Process Escape Flaw	A flaw that is not representative of the characterized nominal operation of a qualified AM process.
Recommendation	A proposed measurable stakeholder action directly supported by specific finding(s) and/or observation(s) that will correct or mitigate an identified issue or risk.
Supporting Narrative	A paragraph, or section, in an NESC final report that provides a detailed explanation of a succinctly worded finding or observation. For example, the logical deduction that led to a finding or observation, and descriptions of assumptions, exceptions, clarifications, and boundary conditions.

14.0 Acronyms and Nomenclature List

µm	micron
2D	Two-dimensional
3D	Three-dimensional
AACT	Agency AM Certification Support Team
AM	Additive Manufacturing
BP-DED	Blown Powder Directed Energy Deposition
CIFS	Critical Initial Flaw Size
CT	Computed Tomography
DED	Directed Energy Deposition
FAA	Federal Aviation Administration
FE	Finite Element
GRC	Glenn Research Center
JPL	Jet Propulsion Laboratory
JSC	Johnson Space Center
KSC	Kennedy Space Center
LaRC	Langley Research Center
LoF	Lack of Fusion
L-PBF	Laser Powder Bed Fusion
M&P	Materials and Processes
MPS	Material Property Suite
MSFC	Marshall Space Flight Center
NDE	Nondestructive Evaluation
NESC	NASA Engineering and Safety Center
OCE	Office of the Chief Engineer
OSMA	Office of Safety and Mission Assurance
PDTA	Probabilistic Damage Tolerance Analysis
PFMEA	Process Failure Modes and Effects Analysis
PH	Precipitate Hardening
PROF	Probability of Fracture (code)
ProFACE	Probabilistic Fatigue Assessment of Components with Defects (code)
QMP	Qualified Material Process
STD	Standard
SwRI	Southwest Research Institute
W-DED	Wire Directed Energy Deposition
US	United States
xLPR	Extremely Low Probability of Rupture (probabilistic fracture mechanics code)

15.0 References

- ASTM E1316 (2023). “Standard Terminology for Nondestructive Examinations,” ASTM E1316-22a, April 26, 2023.
- ASTM E1817 (2022). “Standard Practice for Controlling Quality of Radiological Examination by Using Representative Quality Indicators (RQIs),” December 15, 2022.
- Becker, T. H., Kumar, P., and Ramamurty, U. (2021). “Fracture and Fatigue in Additively Manufactured Metals,” *Acta Mater.*, Vol. 219, 117240, October 2021. URL: <https://doi.org/10.1016/j.actamat.2021.117240>.
- Benedetti, M., Fontanari, V., Bandini, M., et al. (2018). “Low- and High-Cycle Fatigue Resistance of Ti-6Al-4V ELI Additively Manufactured via Selective Laser Melting: Mean Stress and Defect Sensitivity,” *Int. J. Fatigue*, Vol. 107, 2018, pp. 96-109. URL: <https://doi.org/10.1016/j.ijfatigue.2017.10.021>.
- Boyce, B. L., Salzbrenner, B. C., Rodelas, J. M., et al. (2017). “Extreme-Value Statistics Reveal Rare Failure-Critical Defects in Additive Manufacturing,” SAND2017-0719J, 2017.
- Brennan, M. C., Keist, J. S., and Palmer, T. A. (2021). “Defects in Metal Additive Manufacturing Processes,” *J. of Mater. Eng. and Perform.*, Vol. 30, 2021, pp. 4808–4818. URL: <https://doi.org/10.1007/s11665-021-05919-6>
- Burke, E. (2021). “NASA’s Agency Wide Efforts to improve Nondestructive Evaluation Methods for Additive Manufacturing,” International Conference on Additive Manufacturing, 2021.
- Chabot, A., Laroche, N., Carcreff, E., et. al. (2020). “Towards Defect Monitoring for Metallic Additive Manufacturing Components using Phased Array Ultrasonic Testing,” *J. Intell. Manuf.*, Vol. 31, 2020, pp. 1191–1201. URL: <https://doi.org/10.1007/s10845-019-01505-9>
- Chapman, M. G., Shah, M. N., Donegan, S. P., et al. (2021). “AFRL Additive Manufacturing Modeling Series: Challenge 4, 3D Reconstruction of an IN625 High-Energy Diffraction Microscopy Sample using Multi-modal Serial Sectioning,” *Integr. Mater. Manuf. Innov.*, Vol. 10, 2021, pp. 129–141. URL: <https://doi.org/10.1007/s40192-021-00212-9>
- D’Accardi, E., Altenburg, S., Maierhofer, C., et. al. (2019). “Detection of Typical Metal Additive Manufacturing Defects by the Application of Thermographic Techniques,” *Proceedings of the 15th International Workshop on Advanced Infrared Technology and Applications*, Vol. 27, No. 1, 2019, pp. 24. URL: <https://doi.org/10.3390/proceedings2019027024>
- Demeneghi, G., Barnes, B., Gradl, P., et. al. (2021). “Size Effects on Microstructure and Mechanical Properties of Additively Manufactured Copper-Chromium-Niobium Alloy,” *Mater. Sci. Eng. A*, Vol. 820, July 13, 2021. URL: <https://doi.org/10.1016/j.msea.2021.141511>
- Dodaran, M. S., Muhammad, M., Shamsaei, N., and Shao, S. (2022). “Synergistic Effect of Microstructure and Defects on the Initiation of Fatigue Cracks in Additively Manufactured Inconel 718,” *Int. J. Fatigue*, Vol. 162, September 2022. URL: <https://doi.org/10.1016/j.ijfatigue.2022.107002>.
- Du, W., Bai, Q., Wang, Y., and Zhang, B. (2018). “Eddy Current Detection of Subsurface Defects for Additive/Subtractive Hybrid Manufacturing,” *Int. J. Adv. Manuf. Technol.*, Vol. 95, 2018, pp. 3185–3195. URL: <https://doi.org/10.1007/s00170-017-1354-2>.

Duarte, V. R., Rodrigues, T. A., Machado, M. A., et al. (2021). “Benchmarking of Nondestructive Testing for Additive Manufacturing,” *3D Print. Addit. Manuf.*, Vol. 8, 2021, pp. 263-270. URL: <https://doi.org/10.1089/3dp.2020.0204>

Elambasseril, J., Lu, S.L., Ning, Y.P., et al. (2019). “3D Characterization of Defects in Deep-Powder-Bed Manufactured Ti–6Al–4V and Their Influence on Tensile Properties,” *Mater. Sci. Eng. A*, Vol. 761, 2019. URL: <https://doi.org/10.1016/j.msea.2019.138031>

Enright, M. and McClung, R. C. (2020). “Approximate Characterizations of Anomaly Populations in Additively Manufactured Materials for Fracture Risk Assessment through a DARWIN[®] Framework,” Project 18.24818, Southwest Research Institute, 2020.

Federal Aviation Administration AC 33.14-1. “Advisory Circular – Damage Tolerance for High Energy Turbine Engine Rotors,” AC 33.14-1 Change 1, 2017.

Forien, J. B., Guss, G. M., Khairallah, S. A., et al. (2023). “Detecting Missing Struts in Metallic Micro-Lattices using High Speed Melt Pool Thermal Monitoring,” *Addit. Manuf. Let.*, Vol. 4, 2023). URL: <https://doi.org/10.1016/j.addlet.2022.100112>.

Geatko, M., Hatala, M., Botko, F., et. al. (2022). “Eddy Current Testing of Artificial Defects in 316L Stainless Steel Samples Made by Additive Manufacturing Technology,” *Mater.*, Vol. 15, 2022. URL: <https://doi.org/10.3390/ma15196783>

General Dynamics (1967). “Eddy Current Volume I – Basic Principles,” NASA CR 61207, 1967.

GPR 7120.4D, (2012). “Risk Management,” Goddard Procedural Requirements 7120.4D, Goddard Space Flight Center, 2012.

Gordon, J. V., Narra, S. P., Cunningham, R. W., et. al. (2020). “Defect Structure Process Maps for Laser Powder Bed Fusion Additive Manufacturing,” *Add. Manuf.*, Vol. 36, 2020). URL: <https://doi.org/10.1016/j.addma.2020.101552>

Gorelik, M. (2017). “Additive Manufacturing in the Context of Structural Integrity,” *Int. J. Fatigue*, Vol. 94, 2017, pp. 168-177. URL: <https://doi.org/10.1016/j.ijfatigue.2016.07.005>

Gradl, P. R., Mireles, O. R., Protz, C. S., and Garcia, C. P. (2022a). *Metal Additive Manufacturing for Propulsion Applications*, AIAA, July 11, 2022. URL: <https://doi.org/10.2514/4.106279>

Gradl, P., Williams, B., Katsarelis, C., et. al. (2022b). “Having a Come-Apart: Lessons Learned from Additively Manufactured Hardware Failures,” NASA, November 3, 2022. URL: <https://ntrs.nasa.gov/citations/20220016137>

Hentschel, M. L. and Page, N. W. (2003). “Selection of Descriptors for Particle Shape Characterization,” *Particle Sys. Char.*, Vol. 20, 2003, pp. 25–38. URL: <https://doi.org/10.1002/ppsc.200390002>

Homiack, M., Facco, G., Benson, M., et. al. (2021). “NUREG-224 Extremely Low Probability of Rupture Version 2 Probabilistic Fracture Mechanics Code”, U.S. Nuclear Regulatory Commission, 2021.

Howell, P. A. (2020). “Nondestructive Evaluation (NDE) Methods and Capabilities Handbook,” NASA/TM-2020-220568/Volume I, 2020.

Hovey, P. W., Berens, A. P., and Loomis, J. S. (1998). "Update of the Probability of Fracture (PROF) Computer Program for Aging Aircraft Risk Analysis," AFRL-VA-WP-TR-1999-3030, Air Force Research Laboratory, Wright-Patterson Air Force Base, OH, November 1998.

ISO/ASTM 52900. "Additive Manufacturing—General Principles—Fundamentals and Vocabulary," International Standard, second edition, November 2021.

Jewett, R. P. and Halchak, J. A. (1991), "The Use of Alloy 718 in the Space Shuttle Main Engine," *Superalloys 718, 625, and Various Derivatives*, TMS, 1991.

JSC 66705 (2020). "Human System Risk Management Plan, Revision A," JSC 66705, Johnson Space Center, October 2020.

Kim, F. H., Pintar, A. L., Fox, J., et. al. (2019). "QNDE2019-1234 Probability of Detection of X-ray Computed Tomography of Additive Manufacturing Defects", *46th Annual Review of Progress in Quantitative nondestructive Evaluation*, 2019.

Kobayashi, N., Yamamoto, S., Sugawara, A., et. al. (2019). "Fundamental Experiments of Eddy Current Testing for Additive Manufacturing Metallic Material Toward In-Process Inspection," *AIP Conference Proceedings 2*, Vol. 2102, Issue 1, May 8, 2019. URL: <https://doi.org/10.1063/1.5099803>

Kuo, Y. L., Kamigaichi, A., and Kakehi, K. (2018). "Characterization of Ni-Based Superalloy Built by Selective Laser Melting and Electron Beam Melting," *Metall Mater Trans A*, Vol. 49, 2018, pp. 3831–3837. URL: <https://doi.org/10.1007/s11661-018-4769-y>

Lopez, A., Bacelar, R., Pires, I., et. al. (2018). "Nondestructive Testing Application of Radiography and Ultrasound for Wire and Arc Additive Manufacturing," *Add. Manuf.*, Vol. 21, 2018, pp. 298–306. URL: <https://doi.org/10.1016/j.addma.2018.03.020>

McClung, C. (2022). "DARWIN and Additive Manufacturing: Probabilistic Damage Tolerance for AM Parts," NASA Presentation, 2022.

Millwater, H. R., Enright, M. P., and Fitch, S. H. K. (2002). "A Convergent Probabilistic Technique for Risk Assessment of Gas Turbine Disks Subject to Metallurgical Defects," AIAA-2002-1382, 43rd AIAA/ASME/ASCE/AHS/ACS Structures, Structural Dynamics, and Materials Conference and Exhibit, 2002.

Mostafaei, A., Zhao, C., He, Y., et al. (2022). "Defects and Anomalies in Powder Bed Fusion Metal Additive Manufacturing," *Curr. Opin. Solid State Mater. Sci.*, Vol. 26, No. 2, 2022. URL: <https://doi.org/10.1016/j.cossms.2021.100974>

Muhammad, M., Frye, P., Simsiriwong, J., et al. (2021). "An Investigation into the Effects of Cyclic Strain Rate on the High Cycle and Very High Cycle Fatigue Behaviors of Wrought and Additively Manufactured Inconel 718," *Int. J. Fatigue*, Vol. 144, 2021. URL: <https://doi.org/10.1016/j.ijfatigue.2020.106038>

Mukherjee, T. and DebRoy, T. (2018). "Mitigation of Lack of Fusion Defects in Powder Bed Fusion Additive Manufacturing," *J. Man. Proc.*, Vol. 36, 2018, pp. 442-449. URL: <https://doi.org/10.1016/j.jmapro.2018.10.028>

Murakami, Y. (2002). *Metal Fatigue: Effects of Small Defects and Nonmetallic Inclusions*, Elsevier, 2002.

NASA-STD-5009 (2019). “Nondestructive Evaluation Requirements for Fracture Critical Metallic Components,” NASA-STD-5009, Version B, May 8, 2019.

NASA-STD-5019 (2020). “Fracture Control Requirements for Spaceflight Hardware,” NASA-STD-5019, Version A, Change 3, August 14, 2020.

NASA-STD-6030 (2021). “Additive Manufacturing Requirements for Spaceflight Systems,” NASA-STD-6030, Baseline, April 21, 2021.

Nezhadfar, P. D., Shamsaei, N., and Phan, N. (2021). "Enhancing Ductility and Fatigue Strength of Additively Manufactured Metallic Materials by Preheating the Build Platform," *Fatigue Fract Eng Mater Struct*, Vol. 44, 2021, pp. 257-270. URL: <https://doi.org/10.1111/ffe.13372>

Paulonis, D. F. and Schirra, J. J. (2001). “Alloy 718 at Pratt & Whitney – Historical Perspective and Future Challenges,” *Superalloys 718, 625, 706, and Various Derivatives*, TMS, 2001.

Pegues, J. W., Shao, S., Shamsaei, N., et al. (2020). “Fatigue of Additive Manufactured Ti-6Al-4V, Part I: The Effects of Powder Feedstock, Manufacturing, and Post-Process Conditions on the Resulting Microstructure and Defects,” *Int. J. Fatigue*, Vol. 132, 2020, URL: <https://doi.org/10.1016/j.ijfatigue.2019.105358>

Poudel, A., Yasin, M.S., Ye, J., et al. (2022). “Feature-based volumetric Defect Classification in Metal Additive Manufacturing,” *Nature Communications*. Vol. 13, Article 6369, October 26, 2022. URL: <https://doi.org/10.1038/s41467-022-34122-x>

Poulin, J. R., Kreitchberg, A., Terriault, P., and Brailovski, V. (2019). “Long Fatigue Crack Propagation Behavior of Laser Powder Bed-fused Inconel 625 with Intentionally-seeded Porosity,” *Int. J. Fatigue*, Vol. 127, 2019, pp. 144-156. URL: <https://doi.org/10.1016/j.ijfatigue.2019.06.008>

Radhakrishnan, J., Kumar, P., Li, S., et al. (2022). “Unnotched Fatigue of Inconel 718 Produced by Laser Beam-Powder Bed Fusion at 25 and 600 °C,” *Acta Mater.*, Vol. 225, 2022. URL: <https://doi.org/10.1016/j.actamat.2021.117565>

Romano, S., Bruckner-Foit, A., Brandao, A., et. al. (2018). “Fatigue Properties of AlSi10Mg Obtained by Additive Manufacturing: Defect-based Modelling and Prediction of Fatigue Strength,” *Eng. Fracture Mech.*, Vol. 187, 2018, pp. 165-189. URL: <https://doi.org/10.1016/j.engfracmech.2017.11.002>

Romano, S., Miccoli, S., and Beretta, S., (2019). “A New FE Post-Processor for Probabilistic Fatigue Assessment in the Presence of Defects and its Application to AM Parts,” *Int. J. Fatigue*, Vol. 125, 2019, pp. 324-341. URL: <https://doi.org/10.1016/j.ijfatigue.2019.04.008>

Rometsch, P. A., Zhu, Y., Wu, X., and Huang, A. (2022). “Review of High-Strength Aluminum Alloys for Additive Manufacturing by Laser Powder Bed Fusion,” *Mater. Design*, Vol. 219, 2022. URL: <https://doi.org/10.1016/j.matdes.2022.110779>

Rossin, J., Goodlet, B., and Torbet, C. (2020). “Assessment of Grain Structure Evolution with Resonant Ultrasound Spectroscopy in Additively Manufactured Nickel Alloys,” *Mater. Char.*, Vol. 167, 2020. URL: <https://doi.org/10.1016/j.matchar.2020.110501>

Rotor Integrity Sub-Committee (RISC) (1997). “The Development of Anomaly Distributions for Aircraft Engine Titanium Disk Alloys,” AIAA, 1997. URL: http://www.darwin.swri.org/html_files/pdf_docs/pubs/1997/aia1997.pdf

- Sanaei, N. and Fatemi, A. (2020). “Analysis of the Effect of Internal Defects on Fatigue Performance of Additive Manufactured Metals,” *Mater. Sci. Eng. A*, Vol. 785, 2020. URL: <https://doi.org/10.1016/j.msea.2020.139385>
- Sanaei, N. and Fatemi, A. (2021). “Defects in Additive Manufactured Metals and their Effect on Fatigue Performance: A state-of-the-Art Review,” *Pro. Mater. Sci.*, Vol. 117, 2021. URL: <https://doi.org/10.1016/j.pmatsci.2020.100724>
- Sanaei, N., Fatemi, A., and Phan, N. (2019). “Defect Characteristics and Analysis of their Variability in Metal L-PBF Additive Manufacturing,” *Mater. Design*, Vol. 182, 2019. URL: <https://doi.org/10.1016/j.matdes.2019.108091>
- Scime, L. and Beuth, J. (2019). “Using Machine Learning to Identify in situ Melt Pool Signatures Indicative of Flaw Formation in a Laser Powder Bed Fusion Additive Manufacturing Process,” *Addit. Manuf.*, Vol. 25, 2019, pp. 151–165. URL: <https://doi.org/10.1016/j.addma.2018.11.010>
- Scime, L., Siddel, D., Baird, S., and Paquit, V. (2020). “Layer-Wise Anomaly Detection and Classification for Powder Bed Additive Manufacturing Processes: A Machine-Agnostic Algorithm for Real-time Pixel-wise Semantic Segmentation,” *Addit. Manuf.*, Vol. 36, 2020. URL: <https://doi.org/10.1016/j.addma.2020.101453>
- Seow, C. E., Zhang, J., Coules, H. E., et al. (2020). “Effect of Crack-like Defects on the Fracture Behaviour of Wire + Arc Additively Manufactured Nickel-based Alloy 718,” *Addit. Manuf.*, Vol. 36, 2020. URL: <https://doi.org/10.1016/j.addma.2020.101578>
- Shao, S., Poudel, A., and Shamsaei, N. (2023). “A Linear Elastic Finite Element Approach to Fatigue Life Estimation for Defect-laden Materials,” *Eng. Fracture Mech.*, Vol. 285, 2023. URL: <https://doi.org/10.1016/j.engfracmech.2023.109298>
- Snow, Z., Nassar, A. R., and Reutzel, E. W. (2020). “Invited Review Article: Review of the Formation and Impact of Flaws in Powder Bed Fusion Additive Manufacturing,” *Addit. Manuf.*, Vol. 36, 2020. URL: <https://doi.org/10.1016/j.addma.2020.101457>
- Snow, Z., Scime, L., Ziabari, A., et al. (2023). “Observation of Spatter-induced Stochastic Lack-of-Fusion in Laser Powder Bed Fusion using in situ Process Monitoring,” *Addit. Manuf.*, Vol. 61, 2023. URL: <https://doi.org/10.1016/j.addma.2022.103298>
- Sobotka, J. C., Enright, M. P., McClung, R. C., Moody, J., (2023) “Maturation of a DARWIN® Framework to Support Fracture Control of Additively Manufactured Parts,” Southwest Research Institute, July 2023.
- Son, K. T., Kassner, M. E., and Lee, K. A. (2020). “The Creep Behavior of Additively Manufactured Inconel 625,” *Adv. Eng. Mater.*, Vol. 22, 2020. URL: <https://doi.org/10.1002/adem.201900543>
- Spigarelli, S., Paoletti, C., Cabibbo, M., et. al. (2022). “On the Creep Performance of the Ti-6Al-4V Alloy Processed by Additive Manufacturing,” *Addit. Manuf.*, Vol. 49, 2022. URL: <https://doi.org/10.1016/j.addma.2021.102520>

Todorov, E., Spencer, R., Gleeson, S. Jamshidinia, M., and Kelly, S. M. (2014). "America Makes: National Additive Manufacturing Innovation Institute (NAMII) Project 1: Nondestructive Evaluation (NDE) of Complex Metallic Additive Manufactured (AM) Structures: Interim Report," AFRL-RX-WP-TR-2014-0162, Air Force Research Laboratory, Wright-Patterson Air Force Base, OH, June 2014.

Vienne, C., Escoda, J., Touron, A., and Costin, M. (2022). "Assessing the Influence of CT Acquisition Parameters on Flaw Detectability Through Simulation," 11th Conference on Industrial Computed Tomography, *e-Journal of Nondestructive Testing*, Vol. 27, 2022.

Waller, J. M., Parker, B. H., Hodges, K. L., et. al. (2014). "Nondestructive Evaluation of Additive Manufacturing State-of-the-Discipline Report," NASA/TM-2014-218560, November 2014.

Wells, D. (2016). "Overview of Fatigue and Damage Tolerance Performance of Powder Bed Fusion Alloy N07718," ASTM/NIST Workshop on Mechanical Behavior in Additive Manufactured Parts, 2016.

Williams, J., Snodderly, K., Kottman, M., et al. (2023). "Strategic Guide: Additive Manufacturing In-Situ Monitoring Technology Readiness," ASTM International Additive Manufacturing Center of Excellence, 2023. URL: <https://amcoe.org/in-situtechnologyreadiness/>

Wilson-Heid, A. E., Novak, T. C., and Beese, A. M. (2019). "Characterization of the Effects of Internal Pores on Tensile Properties of Additively Manufactured Austenitic Stainless Steel 316L," *Exp. Mech.*, Vol. 59, No. 6, 2019, pp. 793-804. URL: <https://doi.org/10.1007/s11340-018-00465-0>

Yamashita, Y., Murakami, T., Mihara, R., et al. (2017). "Defect Analysis and Fatigue Design Basis for Ni-based Superalloy 718 manufactured by Additive Manufacturing," *Procedia Struct. Integrity*, Vol. 7, 2017, pp. 11-18. URL: <https://doi.org/10.1016/j.prostr.2019.12.014>

Zalameda, J. N., Burke, E. R., Hafley, R. A., et al. (2013). "Thermal Imaging for Assessment of Electron-Beam Free Form Fabrication (EBF3) Additive Manufacturing Welds," SPIE Defense, Security, and Sensing Conference, 2013.

Appendix A. NASA 5 Challenge Geometries Final Report

NASA 5 Challenge Geometries Final Report
Shawn Hinnebusch & Dr. Albert To
University of Pittsburgh
February 10, 2023

Introduction

This project aims to understand AM process-sensitive defects, characterize them, and establish viable inspection methods to lower bound them. Five challenge geometries are selected: the cone, arch, stepped brick, thin wall, and brick, shown in Figure 1, to provide parts of changing cross-sections, overhangs, and constant cross-sections to provide information on defect formation. Each part is printed separately (total of 10 builds) on the EOS M290 DMLS machine with a FLIR A700 camera to collect in-situ information for defect detection and collect layerwise temperature data. After the parts are printed, layerwise simulations are calibrated and then validated with all 5 geometries.

Laser Powder Bed Fusion

The parts are all built by the EOS M290 DMLS system using the default process parameters (Table 1) with stripes, contours, and many other controls. The only exception is that the strong connection setting is deactivated, which double scans the first layer. This simplifies the IR data capture and simulation processing. The final parts of this work are shown in Figure 2.

Table 1: Default LPBF process parameters for IN718 in EOS M290

	IN718
Layer thickness	40 μm
Hatch spacing	110 μm
Stripe width	10 mm
Stripe overlap	0.08 mm
Laser rotation angle	66.7°
Infill	960 mm/s 285 W
Contour 1	300 mm/s 138 W
Contour 2	800 mm/s 80 W
UpSkin	600 mm/s 153 W
DownSkin	2400 mm/s 145 W
Platform Temperature	80 °C

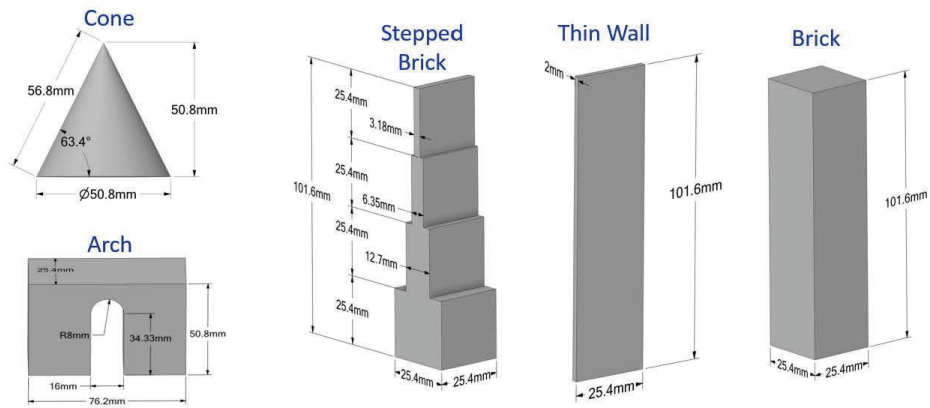


Figure 1: 5 Challenge geometries



Figure 2: Final parts manufactured and cut off the build plates

In-situ Monitoring

A FLIR A700 640x480 pixel detector with a 24° lens and records up to 30 FPS was used for all the builds. The camera has 3 temperature ranges 1: -20 °C to 120 °C, 2: 0 °C to 650 °C, and 3: 300 °C to 2000 °C with 0 °C to 650 °C being the range used in the experiments. Frames are recorded continuously, 30 FPS, for each of the builds requiring post-processing to each image to extract the layer information, part location, and various features. First, the maximum

temperature value is found in each frame, recording the time and peak value. The Otsu multi-threshold technique is applied to the peaks to separate the recoating and laser time. The CAD geometry is meshed using a voxelizer corresponding to the IR camera's 360-micron resolution. This creates a one-to-one location correspondence to each pixel. Knowing the center location on the build platform, the geometry is placed in the printing location and then overlaid with the exact pixels to check if the geometry exists. The temperature is recorded to the voxel mesh if the geometry is true. Instead of gaining temperature knowledge in a small sample of pixels, the entire part temperature field is known. The IR image in Figure 3 shows a higher temperature near the bottom (farthest away from gas flow) of the part compared to the top, which is not captured using a coarse sampling. The average temperature and standard deviation are calculated for each image. The part reconstruction creates a usable interface to set thresholds for interpass temperature and heatmap, finding specific locations of interest for defect formation. It is also essential for future work finding the spatter landing location. Each of the 5 challenge geometries has the IR data projected on the voxel mesh, then filtered by the heat map and interpass temperature to predict potential problematic areas where defects are expected in Figure 4 - Figure 11. Interpass temperature generally increases with layer height; however, the temperature can decrease if the laser scanning time is small. It is believed that increasing the interpass temperature will increase the spatter count creating more porosity. The heat map signatures are related to the laser's total intensity. The heat map intensity is generally highest around the edges of the part most likely due to short scan tracks in the stripes. A greater heat map signature results in a hotter melt pool, which is hypothesized to correlate to more melt pool instabilities, resulting in more porosity. All the above hypotheses will require ex-situ characterization experiments to prove.

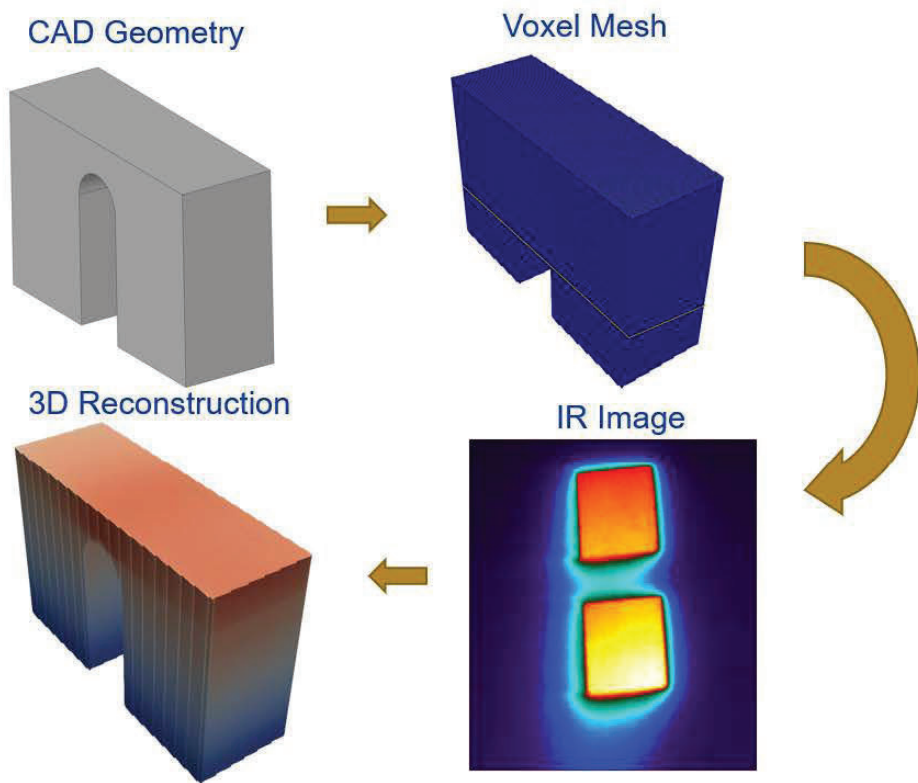


Figure 3: IR camera mesh projection workflow

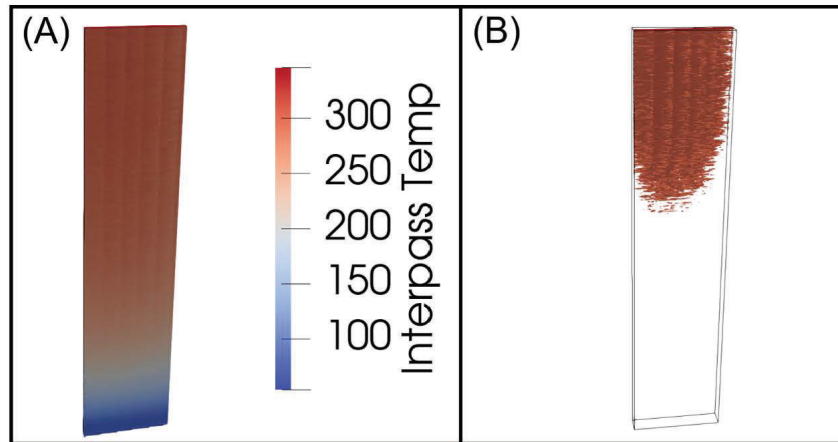


Figure 4: Interpass temperature of a thin wall structure in (A) and a threshold temperature of 300 °C shows particular locations of heat accumulation on the part.

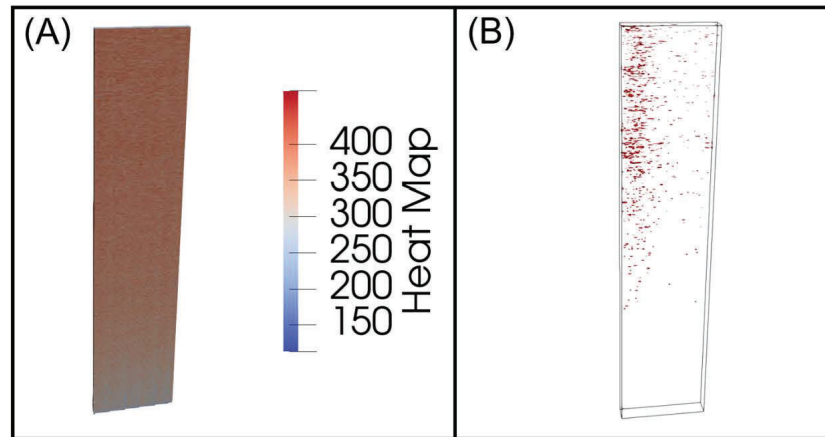


Figure 5: Heat map on the left (A) is the full thin wall structure. (B) has a threshold of 425 to show the areas of the highest laser intensity to focus on for defects.

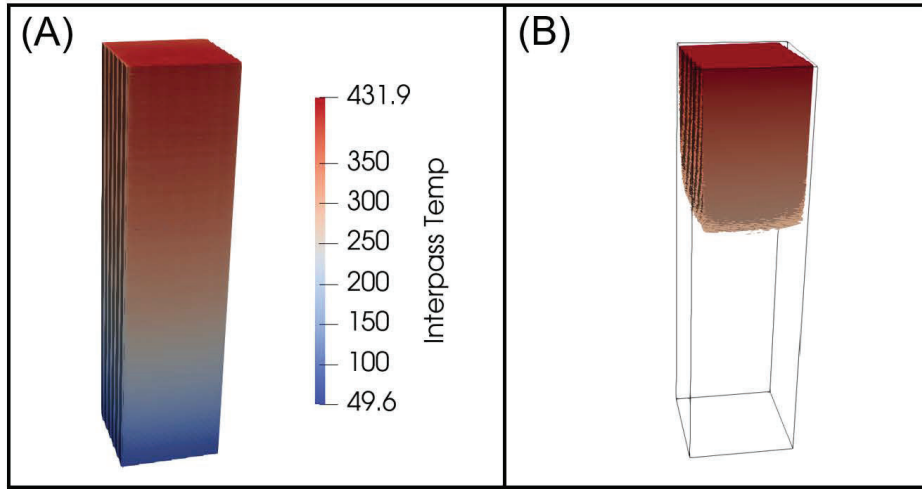


Figure 6: Interpass temperature of a tall brick structure in (A) and a threshold temperature of 350 °C shows particular locations of heat accumulation on the part.

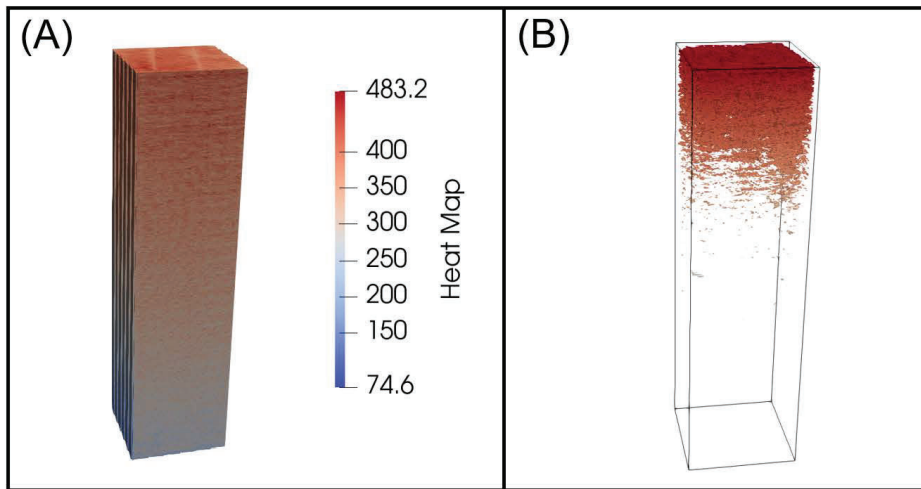


Figure 7: Heat map on the left (A) is the tall brick structure. (B) has a threshold of 425 to show the areas of the highest laser intensity to focus on for defects.

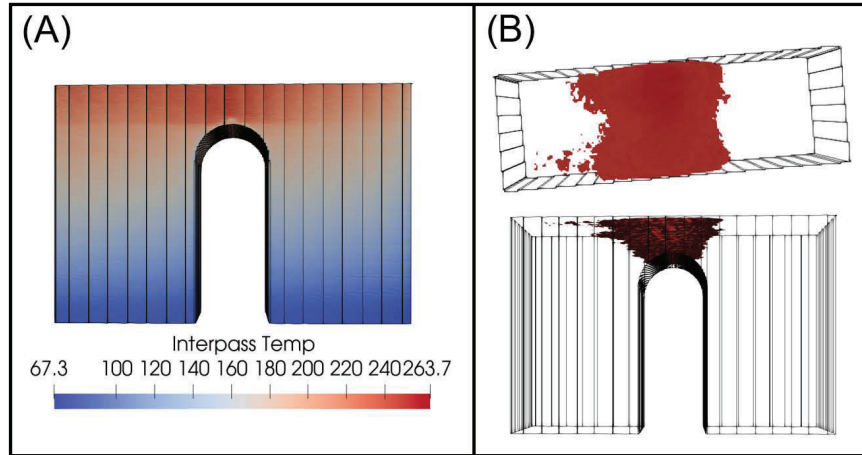


Figure 8: Interpass temperature of the arch structure in (A) and a threshold temperature of 250 °C shows particular locations of heat accumulation on the part.

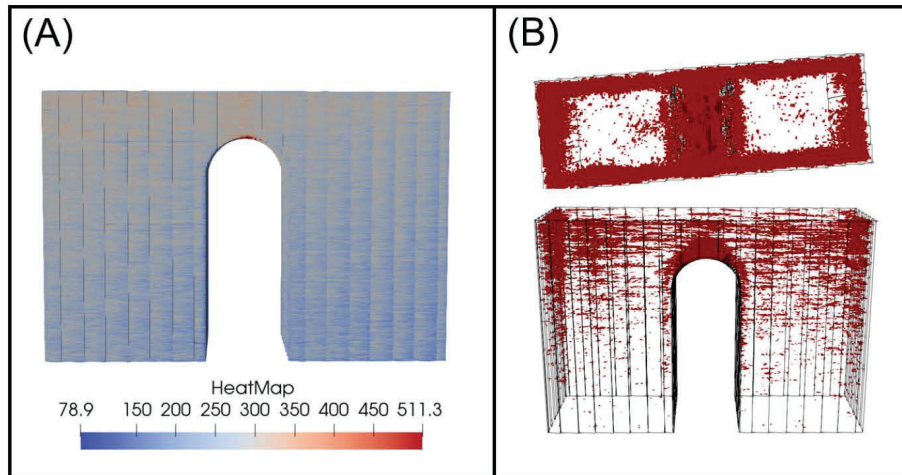


Figure 9: Heat map on the left (A) is the arch structure. (B) has a threshold of 350 to show the areas of the highest laser intensity to focus on for defects.

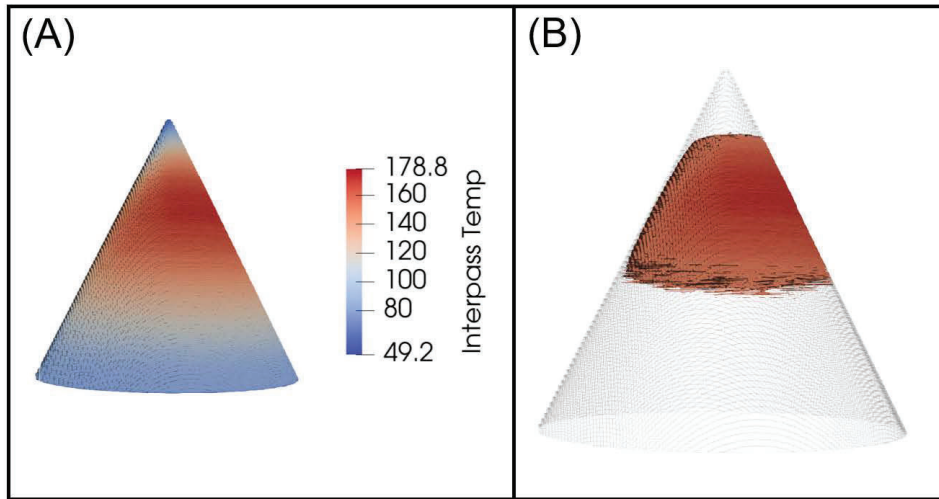


Figure 10: Interpass temperature of the cone structure in (A) and a threshold temperature of 150 °C shows particular locations of heat accumulation on the part.

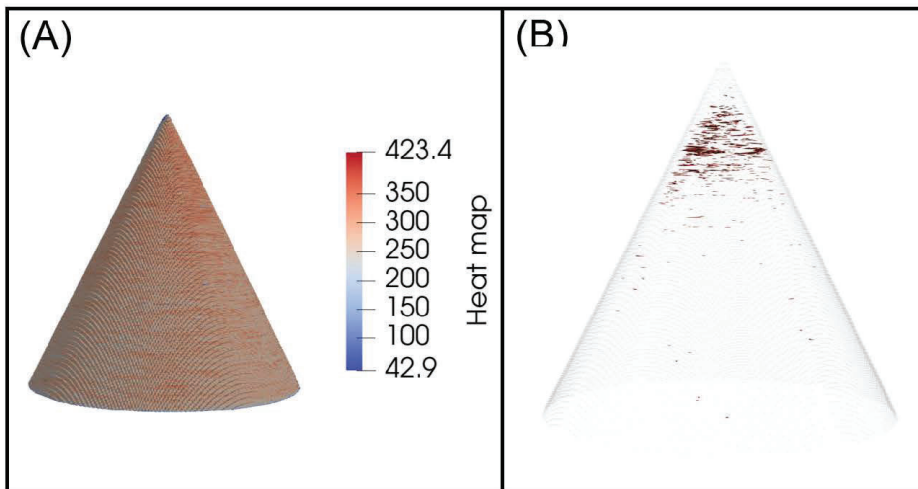


Figure 11: Heat map on the left (A) is the cone structure. (B) has a threshold of 375 to show the areas of the highest laser intensity to focus on for defects.

Process Simulations

This work utilizes an in-house computer code called the ‘‘Pittsburgh Additive Manufacturing Simulator’’ (PAMSIM) to perform process simulations to evaluate the temperature buildup. PAMSIM was built by combining matrix-free finite element modeling (FEM), adaptive remeshing, and graphical processing unit (GPU) computing, which allows simulations to run on relatively inexpensive computer with performance comparable to using a supercomputer. Table 2 lists the key features in the current version of PAMSIM.

Table 2: Key features of PAMSIM

Programming language	CUDA C/C++
Required hardware	GPU cards from NVIDIA with computational capabilities 6.0 or higher
Required libraries	OpenMP, CUDA 9.0 or newer
Analysis types	Transient thermal, Quasi-static structural analysis, Transient thermomechanical
Model inputs	Geometry file (stl, step, etc.), CLI file (containing all scan tracks information), Process parameters
Mesh generation	Mesh configurations with adaptive remeshing are generated using Python scripts.
Boundary conditions	Heat flux, convection, radiation, and/or constant temperature; displacement, stress
Solver	Conjugate gradient with Jacobi preconditioner, Newton-Raphson, line search
Parallelization	Embedded GPU parallelization on CUDA cores, parallelization across multiple GPUs
Output	Text files (analyzed by a developed python-based postprocessor) *.vtk files
Performance	1 GPU vs 1 CPU: 300x speedup Adaptive mesh refinement: 30-100x speedup

The thermal process simulation in PAMSIM solves the transient heat conduction equation:

$$\rho C_p \frac{dT}{dt} = \frac{\partial}{\partial x} \left(k \frac{\partial T}{\partial x} \right) + \frac{\partial}{\partial y} \left(k \frac{\partial T}{\partial y} \right) + \frac{\partial}{\partial z} \left(k \frac{\partial T}{\partial z} \right) + Q$$

$$T(x, t) = T_p \text{ on } \Gamma_D$$

$$k \frac{\partial T}{\partial x} = h(T(x, t)) - T_\infty \text{ on } \Gamma_{h,x}$$
(1)

where ρ , C_p , and k are the density, heat capacity, and thermal conductivity. The Dirichlet boundary condition is represented by Γ_D for the prescribed temperature of T_p . The heat transfer coefficient is h with T_∞ being the ambient temperature. The Robin boundary condition for the x component is represented by $\Gamma_{h,x}$. Only the x component is represented in Equation (1), but the y and z components follow the same principle.

The Stefan-Boltzmann law is implemented for radiation:

$$q_{rad} = \varepsilon \sigma (T_s^4 - T_{amb}^4)$$
(2)

where ε is the surface radiation emissivity, σ is the Stefan-Boltzmann constant, T_s is the surface temperature, and T_{amb} is the ambient temperature.

The layerwise simulation model consists of a layerwise element activation where a temperature is applied then removed and allowed to cool. The temperature is applied for a brief period of time, giving the area a thermal history comparable to that of laser scanning. Many models calculate the total power of the layer then apply it as an internal heat generation over the laser scanning process. When compared to the real printing process, this leads to lower peak temperatures. In this work, the applied temperature approach is utilized for high accuracy modeling. The applied temperature and time duration are calibration variables.

A modified flash heating approach was developed to improve the model accuracy by including two top surface convection coefficients. The recoat time on the EOS M290 machine is approximately nine seconds. A larger convection coefficient is applied for this recoat time (9 sec) to allow for a high cooling rate accounting for neglected physics. After the first cooling period, the convection coefficient is reduced for the laser scanning duration. This alteration in boundary condition provides a more robust model for geometries of various sizes and cross-sections as each part typically has a different convection coefficient. Part side convection coefficient is another calibration parameter included in this study. The substrate is preheated to 80 °C and is considered a fixed temperature. In previous trials with thermocouples, the substrate temperature is maintained. The substrate side and top surfaces is prescribed a convection coefficient of 5 W/(m² °C) based on past experience and is not considered a calibration parameter. A thermocouple captured the ambient build chamber temperature to be approximately 30 °C throughout the build. The boundary conditions applied to these five challenge geometries are illustrated in Figure 12.

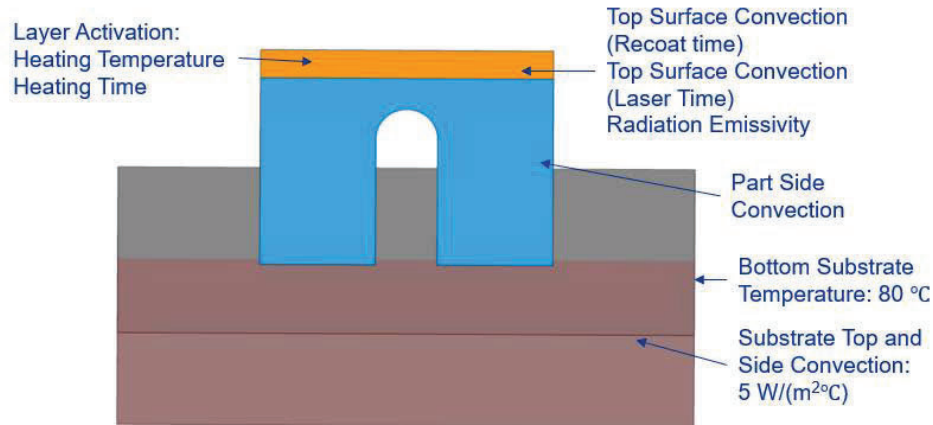


Figure 12: Boundary conditions for simulation modeling

Model calibration is a tedious process requiring hundreds of simulations. One often uses values from previous literature or a single calibration build since experiments are costly and time-consuming. This work shows the importance of why it is not accurate to use one build alone to calibrate the simulation model. This is because even though the calibrated model can closely match experimental data on one build, it can have an enormous error on another build, even with a similar shape. Although a GPU-accelerated FEM algorithm improves solution time, optimizing five parameters over several geometries is infeasible in that there will be too many simulations if the optimization is carried over the parameter space is divided uniformly by a relatively dense mesh grid. On the other hand, utilizing the Latin hypercube sampling (LHS) provides a reduced number of required simulations to sample the parameter space effectively. This workflow produces a highly parallelizable system where simulations are run simultaneously on different workstations, with the results combined at completion.

From our previous experience, Table 3 shows the model parameters with the range of values used in the calibration via the Latin hypercube sampling procedure. Radiation emissivity values greater than 0.4 makes the interpass temperatures much lower than in experiments, and thus, the values were reduced in the DOE. A wide range of applied temperature values and convection coefficients are selected in the design space for the LHS. Table 4 provides the element size in x and y direction with the z direction all the true layer thickness of 40 μm . Figure 13 shows an example of the 100 LHS for the stepped brick compared to the IR interpass temperature. The first 3 parts, brick, thin wall, and stepped brick are used for the simulation

calibration with the arch and cone left for the validation study. The results of all 5 geometries are shown in Figure 14 -Figure 18.

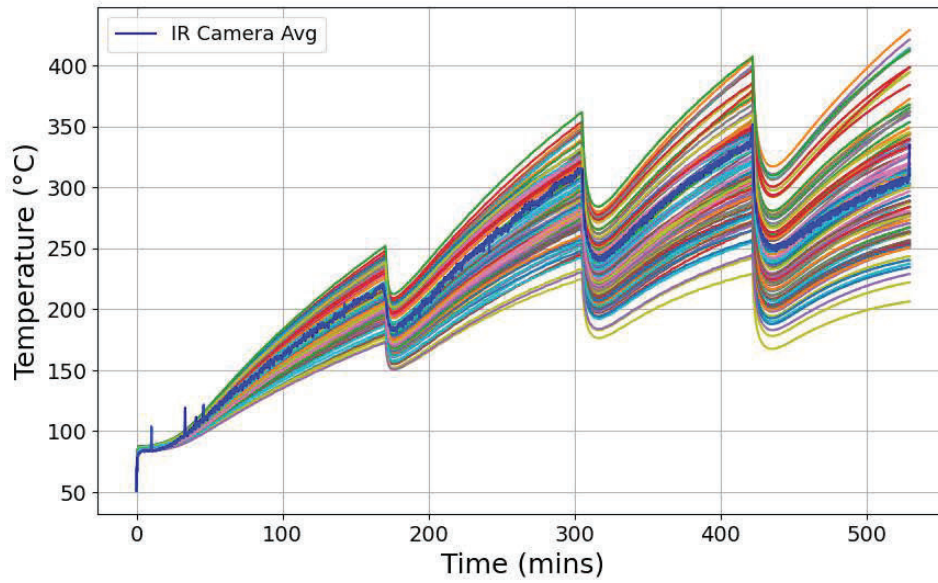


Figure 13: 100 Latin hypercube sampling simulation results for the stepped brick

Table 3: Modified flash heating process modeling parameters

	Range
Applied temperature	1300 – 1600 °C
Heating time	0.004 – 0.013 s
Radiation emissivity	0.1 – 0.3
Top surface recoat convection	40 – 70 W/(m ² °C)
Top surface laser convection	10 – 40 W/(m ² °C)
Part side convection	0 – 20 W/(m ² °C)

Table 4: Mesh element sizes in x and y direction.

	Element size (μm)
Cone	794
Arch	1,016
Stepped brick	1,586
Brick	1,587
Thin wall	250

Note: z-height of the element is kept constant at $40\ \mu\text{m}$.

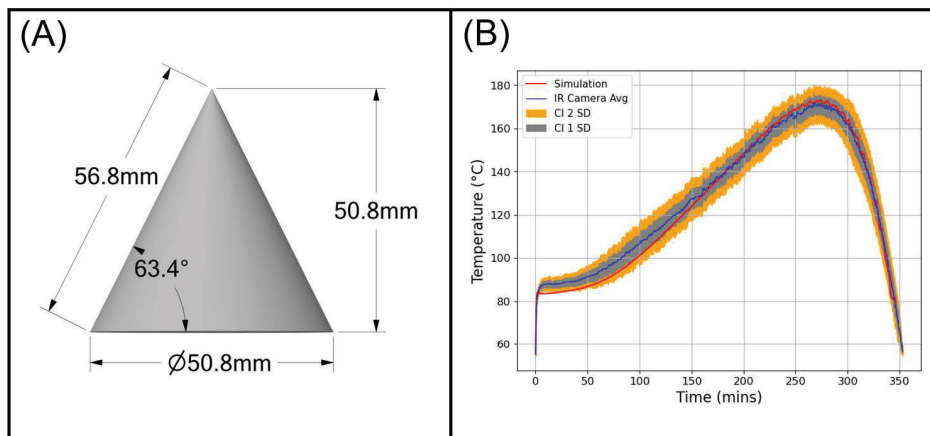


Figure 14: (A) Cone geometry dimensions. (B) Simulation results are superimposed on the IR interpass temperature surrounded by the standard deviation confidence interval and 2 standard deviation interval.

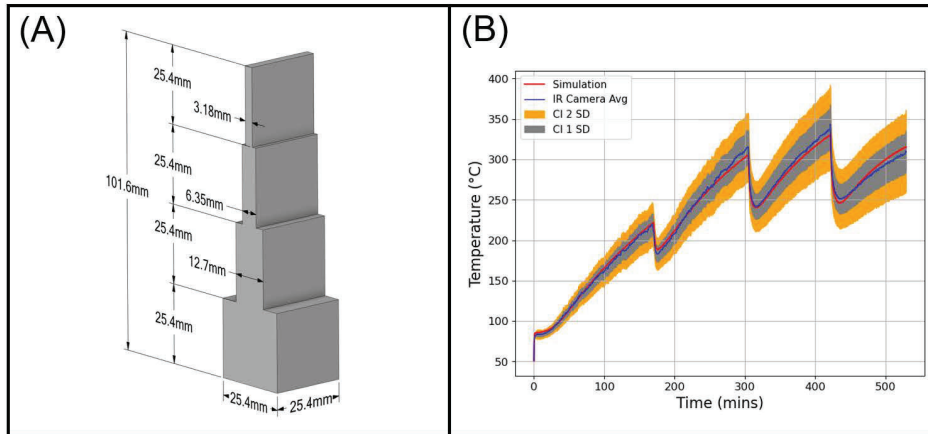


Figure 15: (A) Stepped Brick geometry dimensions. (B) Simulation results are superimposed on the IR interpass temperature surrounded by the standard deviation confidence interval and 2 standard deviation interval.

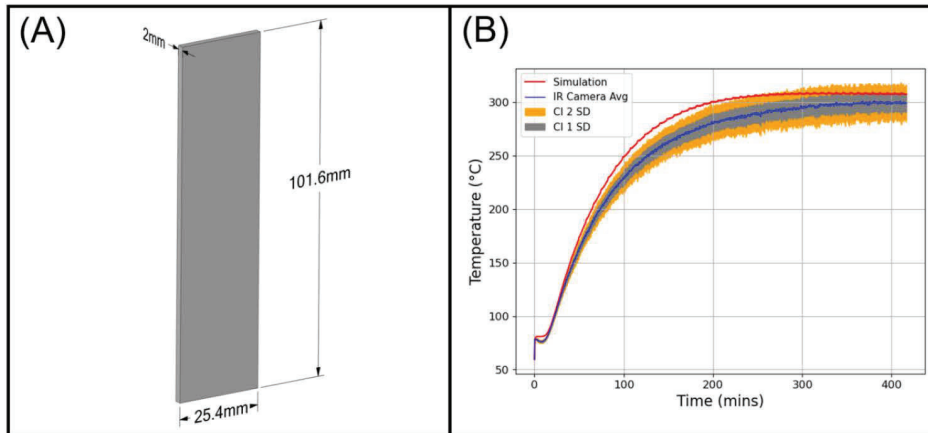


Figure 16: (A) Thin wall geometry dimensions. (B) Simulation results are superimposed on the IR interpass temperature surrounded by the standard deviation confidence interval and 2 standard deviation interval.

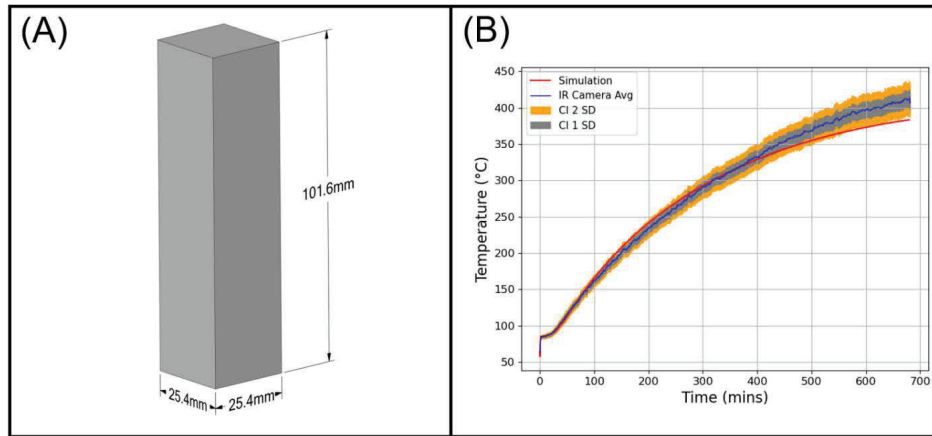


Figure 17: (A) Brick geometry dimensions. (B) Simulation results are superimposed on the IR interpass temperature surrounded by the standard deviation confidence interval and 2 standard deviation interval.

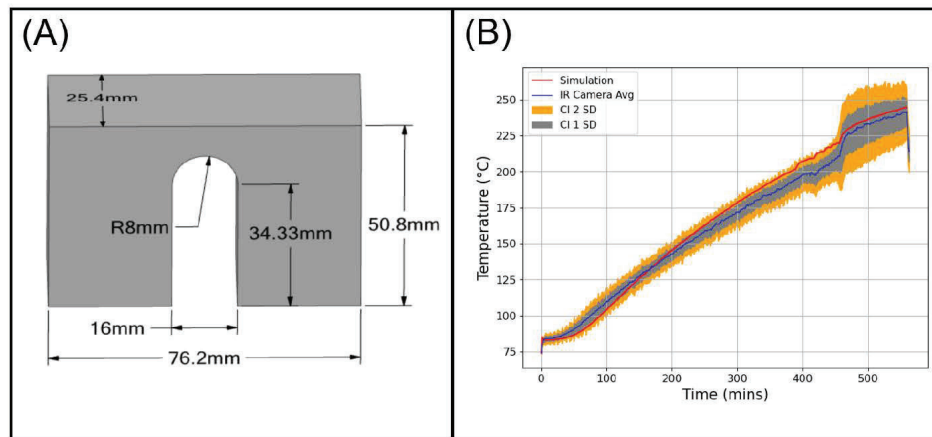


Figure 18: (A) Arch geometry dimensions. (B) Simulation results are superimposed on the IR interpass temperature surrounded by the standard deviation confidence interval and 2 standard deviation interval.

The new modified flash heating approach is employed in the process simulation model since it allows more flexibility in the simulations to melt, rapidly cool down, then cool down at a reduced rate, which is not considered in the standard flash heating method. As parts scan for a longer duration, high convection coefficient of 40-60 W/(m²°C) produces a significant error compared to parts or layers with shorter scanning times. Even with this new approach, multiple parts with various cross-sections are needed for calibration. For example, the lowest brick error

in the LHS is 20 °C with the same model parameters giving a 67 °C error for the thin wall structure. To find a generic calibration with high accuracy, multiple builds are required for a given parameter set. The optimal model parameters are listed in Table 5. The maximum absolute error and root mean squared deviation (RMSE) errors are listed in Table 6.

Table 5: Calibrated model parameters

	Value
Applied temperature	1420.3 °C
Heating time	0.011 s
Radiation emissivity	0.149
Top surface recoat convection	53.5 W/(m ² °C)
Top surface laser convection	27.3 W/(m ² °C)
Part side convection	11.3 W/(m ² °C)

Table 6: Geometry interpass temperature errors

Geometry	MAPE (%)	MAE	RMSE	Max Error (°C)
Brick	3.1	9.9	13.0	29.9
Stepped brick	1.5	3.7	4.4	12.8
Thin wall	5.7	14.1	15.2	23.8
Cone	3.2	3.7	4.5	15
Arch	3.2	5.1	5.9	14.2

Summary

The IR camera temperature and spatial calibration provide accurate temperature and spatial information for variation geometries through the mesh projection method. Through this process, the interpass temperature and heat map are generated for a full part reconstruction for post processing. IR data for some parts reach over 800 GBs which is reduced to a couple hundred megabytes with the main features for users to post process. With all 5 geometries monitored with the IR camera, calibration and simulation validation are completed with high accuracy.

Layerwise simulation calibration to a single part is highly inaccurate when extended to different geometries. Calibration with 3 parts using the new modified flash heating approach provides a very good interpass prediction validated against 2 additional geometries. All the predictions fell within 2 standard deviations of the experiments except for the thin wall. The thin wall has an increased error during the middle of the build. The heat transfer to the powder is expected to have a more considerable impact on the cooling rates compared to the other 4

geometries. In all 5 challenge geometries, the maximum error in any layer was less than 30 °C. Depending on the top surface location and scan strategy, the temperature can vary over 50 °C meaning the simulations still capture accurate predictions for layerwise heat accumulation.

REPORT DOCUMENTATION PAGE

Form Approved
OMB No. 0704-0188

The public reporting burden for this collection of information is estimated to average 1 hour per response, including the time for reviewing instructions, searching existing data sources, gathering and maintaining the data needed, and completing and reviewing the collection of information. Send comments regarding this burden estimate or any other aspect of this collection of information, including suggestions for reducing the burden, to Department of Defense, Washington Headquarters Services, Directorate for Information Operations and Reports (0704-0188), 1215 Jefferson Davis Highway, Suite 1204, Arlington, VA 22202-4302. Respondents should be aware that notwithstanding any other provision of law, no person shall be subject to any penalty for failing to comply with a collection of information if it does not display a currently valid OMB control number.
PLEASE DO NOT RETURN YOUR FORM TO THE ABOVE ADDRESS.

1. REPORT DATE (DD-MM-YYYY) 02/14/2024	2. REPORT TYPE Technical Memorandum	3. DATES COVERED (From - To)
--	---	-------------------------------------

4. TITLE AND SUBTITLE Agency Additive Manufacturing (AM) Certification Support Team (AACT) Risk Reduction – Safe Life Category: Fracture Control Framework for Un-inspectable Fracture Critical AM Parts	5a. CONTRACT NUMBER
	5b. GRANT NUMBER
	5c. PROGRAM ELEMENT NUMBER

6. AUTHOR(S) Park, Alison M.; tilson, William G.; Wells, Douglas N.; Lang, Christopher G.; Kantzos, Christopher A.	5d. PROJECT NUMBER
	5e. TASK NUMBER
	5f. WORK UNIT NUMBER 869021.01.23.01.01

7. PERFORMING ORGANIZATION NAME(S) AND ADDRESS(ES) NASA Langley Research Center Hampton, VA 23681-2199	8. PERFORMING ORGANIZATION REPORT NUMBER NESC-RP-21-01678
---	---

9. SPONSORING/MONITORING AGENCY NAME(S) AND ADDRESS(ES) National Aeronautics and Space Administration Washington, DC 20546-0001	10. SPONSOR/MONITOR'S ACRONYM(S) NASA
	11. SPONSOR/MONITOR'S REPORT NUMBER(S) NASA/TM-20240002004

12. DISTRIBUTION/AVAILABILITY STATEMENT
Unclassified - Unlimited
Subject Category Space Transportation and Safety
Availability: NASA STI Program (757) 864-9658

13. SUPPLEMENTARY NOTES

14. ABSTRACT
The NASA Engineering and Safety Center (NESC) was requested to support the development of a governing philosophy to provide a consistent and systematic approach for fracture control certification of additive manufacturing (AM) hardware that cannot be reliably inspected. The overall goal of the NESC assessment was to make progress toward a framework for general certification of un-inspectable fracture critical AM hardware and toward approaches for evaluating risks associated with these components. This report contains the results of the assessment.

15. SUBJECT TERMS
Additive Manufacturing; NASA Engineering and Safety Center; Risk Reduction; Fracture Critical

16. SECURITY CLASSIFICATION OF:			17. LIMITATION OF ABSTRACT	18. NUMBER OF PAGES	19a. NAME OF RESPONSIBLE PERSON
a. REPORT	b. ABSTRACT	c. THIS PAGE			STI Help Desk (email: help@sti.nasa.gov)
U	U	U	UU	110	19b. TELEPHONE NUMBER (Include area code) (443) 757-5802